Stony Brook University

Stony Brook University

3-D Shape Measurement Based on Fourier Transform and Phase Shifting Method

A Dissertation Presented

by

Hong Guo

to

The Graduate School

in Partial Fulfillment of the Requirements

for the Degree of

Doctor of Philosophy

in

Mechanical Engineering

Stony Brook University

December 2009

Stony Brook University

The Graduate School

Hong Guo

We, the dissertation committee for the above candidate for the Doctor of Philosophy degree, hereby recommend acceptance of this dissertation.

Dr. Peisen S. Huang – Dissertation Advisor
Professor, Department of Mechanical Engineering

Dr. Fu-pen Chiang – Chairperson of Defense
Professor, Department of Mechanical Engineering

Dr. Yu Zhou
Assistant Professor, Department of Mechanical Engineering

Dr. Hong Qin
Professor of Computer Science,
Department of Computer Science of Stony Brook University

This dissertation is accepted by the Graduate School.

Lawrence Martin
Dean of the Graduate School

Abstract of the Dissertation

3-D Shape Measurement Based on Fourier Transform and Phase Shifting Method

by

Hong Guo

Doctor of Philosophy

in

Mechanical Engineering

Stony Brook University

2009

Phase shifting method and the Fourier transform method are both fringe analysis methods. This dissertation research focuses on utilizing these two methods to extract 3-D shape information encoded in fringe patterns obtained from digital fringe projection technique and shadow moiré technique respectively. A modified Fourier transform method is developed for real-time 3-D shape measurement of dynamic objects based on the digital fringe projection technique. A phase shifting scheme is developed for the shadow moiré technique in effort to improve its resolution and accuracy. A novel face recognition method is proposed, which employs phase shifting method and the Fourier transform method to obtain an efficient spectral representation of 3-D face.

Digital fringe projection technique is a full-field, high-resolution, and high-speed 3-D shape measurement method. Real-time fringe pattern acquisition, processing, and 3-D display by use of 3-step phase shifting method has been previously achieved on a high-speed digital fringe projection system. However, measurement of

fast moving or changing objects remains difficult in that at least three fringe patterns taken over time are required. Although the Fourier transform method only needs one frame of fringe pattern, the measurement quality is limited when objects with complex shapes are measured. In this research, a modified Fourier method is proposed, which aims at measuring dynamic objects with complex shapes. The basic idea is to acquire a flat image in addition to a fringe image, which provides necessary information for overcoming the shortcomings of the conventional Fourier transform method. Two fringe projection schemes are proposed and compared. The experimental results demonstrated that the proposed method can be used for real-time 3-D shape measurement of complex shapes, and improved measurement quality over 3-step phase shifting method is achieved.

Shadow moiré is a traditional full-field optical 3-D shape measurement technique. By combining phase shifting method with shadow moiré technique, the resolution of the measurement can be greatly improved. Various phase shifting schemes have been previously proposed. However, none of them provides exact close-form phase solution for the phase shifting shadow moiré. In this research, we provide an elegant exact solution for phase shifting shadow moiré. Four phase-shifted fringe patterns are obtained by translating the grating vertically in equal steps. The Carré algorithm is applied to the phase-shifted fringe patterns to obtain an exact close-form phase solution. Simulation and experimental results verified the proposed method.

Face recognition is an intuitive and promising human biometrics method. 2-D and 3-D face recognition methods have been extensively studied. However, the performance of 2-D methods is greatly influenced by facial texture and illumination variations. 3-D methods require reconstruction of the 3-D face geometry which results in high computation and storage expenses. In this research, a face recognition method is proposed, which employs a spectral representation of 3-D face to perform face recognition without 3-D reconstruction. A high-speed digital fringe projection system captures three phase-shifted fringe patterns of a face. 3-step phase shifting method and the Fourier transform method are applied to face fringe patterns to remove facial texture and illumination variations and extract spectra related to the 3-D shape of the face. The eigenface algorithm is employed to analyze the face spectra database and

recognize the identity of the unknown face. The experimental and simulation results demonstrated promising recognition rates with reduced computation and storage expenses.

Dedicated to My Family

Contents

List of Figures

List of Tables

Acknowledgements

First of all, I would like to express my deepest gratitude to my advisor Professor Peisen Huang. This dissertation research could not be accomplished without his contributions of time and ideas. I benefited so much from his encouragements, guidance and help.

I am grateful to my committee members, Professor Fu-pen Chiang, Professor Yu Zhou, and Professor Hong Qin, for their precious time on reviewing and providing valuable feedbacks on this dissertation. I also thank Professor Qiaode Ge and Professor Goldie Negat for their valuable time on reviewing my dissertation proposal.

I would like to thank my colleague Mr. Xu Han in the Optical Metrology Laboratory for his help in my research. I also would like to thank former lab members Dr. Song Zhang, Dr. Jiahui Pan, Dr. Qingying Hu for their valuable advice and help.

My thanks also goes to Professor Goldie Negat and Dr. Zhe Zhang. It was a pleasure for me to work together them on the robotic search and rescue project. I would like to thank my colleague in ME department, Gunes Uzer, for his help on SEM operation.

My study at Stony Brook was enjoyable due to my friends Wenfei Liu, Yi Ding, Xiao Yun, Jian Yao, and Wei Zhao.

And last but not least, I thank my wife Yanxiao Zhao, my parents, and my brother. Their love and support carried me through the tough times in my PhD study.

Chapter 1

Introduction

Optical 3-D shape measurement technology plays an important role in manufacturing, medicare, biometrics, and entertainment industry, due to the non-contact nature of the measurement. Among various techniques, the structured light method has salient advantages of high-resolution, full-field measurement and fast data acquisition. In this dissertation research, two structured light 3-D shape measurement methods, namely digital fringe projection and shadow moiré, are studied. This research focuses on effectively generating fringe patterns and accurately extracting 3-D shape information from the fringe patterns obtained from digital fringe projection and shadow moiré technique respectively.

Digital fringe projection is a high-resolution, full-field, high-speed 3-D shape measurement technique, which is especially suitable for measuring free-form surfaces with high resolution. A novel fringe projection and analysis method is proposed for measuring the 3-D shape of moving or changing objects in real-time by use of a digital fringe projection technique. As an application of the digital fringe projection technique, a human face recognition method based on the digital fringe projection and fringe analysis is proposed, in which a spectral representation of the 3-D face is obtained by analyzing the face fringe patterns by the Fourier transform method and the phase shifting method. Shadow moiré technique is a traditional high-accuracy optical 3-D shape measurement technique. A phase shifting scheme is proposed for the shadow moiré setup to improve the measurement accuracy.

This chapter gives an overview of optical 3-D shape measurement technology and explains the motivation and objectives of this dissertation research. The rest of this chapter is organized as follows. Current optical 3-D shape measurement techniques related to this research are briefly reviewed in Sec.1.1. The motivation and objectives are given in Sec.1.2. The structure of this dissertation is outlined in Sec.1.3.

1.1 Overview of 3-D Shape Measurement Technology

With the fast development of computer and optical components in the past two decades, the optical 3-D shape measurement technology has achieved great improvements in terms of accuracy, speed and measurement range. Several widely employed optical 3-D shape measurement techniques are summarized as follows.

1.1.1 Laser triangulation

Laser triangulation technique utilizes the triangle formed by the laser light source, the laser spot on the object surface, and the image of the spot on the receiving sensor to acquire range information [1, 2]. The distance between the light source and the receiving sensor is calibrated. The direction of the incident laser beam is known. The beam is incident on a diffusely scattering surface and the light spot on the surface forms an image on the sensor. Based on the position of the image on the sensor, the angle between the incident and reflected laser beam can be calculated. The distance between the light source and the object surface can be calculated employing trigonometry. The principle of triangulation measurement has been widely used in other optical dimensional measurement techniques.

The laser light source can be a single point source or a linear source. Linear source laser scanners have larger field of view, usually in the order of 20 to 30 degree. Point source laser scanners have better depth resolution and immunity to ambient light. The measurement range of commercialized laser triangulation systems is 40-650 mm. The accuracy can reach 10 μm [3]. However, complicated scanning system is required in order to achieve full field measurement. The measurement speed is rather low for laser scanning.

1.1.2 Time-of-flight

Time-of-flight technique detects the time of a laser pulse traveled to the object surface and reflected back to the receiving sensor. Based on the speed of the light and the recorded time, the distance between the object and the sensor can be calculated. The technique demands high time resolution electronics, usually an avalanche photodiode. Besides timing laser pulse, different methods have been developed for the time-of-flight systems, such as amplitude modulation and frequency modulation methods. The 3-D surface is scanned point by point. The accuracy is in the order of 1 mm [4, 5]. Time-of-flight technique

is suitable for measuring large scale objects (e.g. airplane) and conducting landscape survey (e.g. building and plant).

1.1.3 Stereo vision

Stereo vision technique reconstructs 3-D geometry of an object using a pair of 2-D images captured from two different points of view [6]. In both images, pixel correspondences, which are the pixels that belong to the same 3-D points, are detected by image correlation techniques. The intrinsic and extrinsic parameters of the cameras are obtained by camera calibration. With the pixel correspondences and camera parameters, the 3-D coordinates of the 3-D points can be calculated based on the projective geometry [7]. Multiple images captured by one camera from different perspectives can also be used for camera calibration and 3-D geometry reconstruction [8]. As a passive optical technique, no light pattern projection is required and the setup of stereo vision technique is simple.

Due to the limited features that can be used for building pixel correspondence in the image pair, the resolution of the technique is usually much lower than that of the 2-D image. Although with the help of epipolar geometry, building pixel correspondences is the bottle neck of the speed performance of stereo vision technique. In order to assist building robust pixel correspondences, efforts such as mounting bright markers on the surface of the object are made [9]. Illumination, surface condition, object geometry, and camera calibration determine the measurement accuracy [10]. The accuracy of the technique could achieve 0.1 mm [11].

1.1.4 Coded pattern projection

Coded pattern projection techniques facilitate the building of pixel correspondences by projecting a single pattern or a set of light patterns onto the objects [12, 13]. The configurations of one camera and a projector or a pair of cameras and a projector are employed. The pixels in the pattern have their codewords. The camera captures the deformed pattern from an offset angle. The captured pattern is analyzed and the codewords are recognized, so that pixels on the pattern can find their correspondences located in the projected pattern or in another camera image.

There are different coding strategies, i.e. how to assign codewords to the pixels. Color coding utilizes different colors to code the pixels [14, 15]. Binary coding only uses two illumination levels, which are 0 and 1. Every pixel has a unique codeword formed by the combination of 0s and 1s [16, 17]. N-ary coding reduces the large number of patterns to be projected by the binary

coding by increasing the coding basis [18, 19]. Intensity ratio coding is based on linear changing gray levels [20, 21]. There are also hybrid techniques such as color N-ary Gray code [22].

For coded pattern projection techniques, the larger number of pixels that must be coded, the more complicated the coding is. Therefore pixel-by-pixel resolution for coded pattern projection is difficult to achieve especially for high-resolution images.

1.1.5 Interferometry

Interferometric techniques are usually employed for measuring simple object surface with high accuracy requirement, such as optical components. Most interferometers use laser as the light source. The laser beam is split into two beams and sent into different propagation paths. Then the beams are superposed on the object's surface to generate interference patterns, usually fringe patterns. The fringe patterns are analyzed by phase shifting methods or Fourier transform methods to obtain the phase map of the fringe pattern, which is related to surface topography [23, 24]. The surface profile is reconstructed by using the geometry of the setup and the phase map. Widely used interferometers includes: Fizeau interferometer, Twyman-Green interferometer, Mach-Zehnder interferometer, and Michelson interferometer [25, 26]. White-light interferometer that utilizes broad bandwidth light source is also used for optical metrology [27]. The accuracy of the interferometry measurement systems can achieve 1/1000 of a fringe [5]. Various fringe pattern analysis methods are developed to improve the resolution and accuracy of optical interferometry systems, especially phase shifting methods [28].

1.1.6 Moiré method

Moiré method acquires the contour of the object surface by the interference of two grating patterns, a reference grating pattern and the deformed reference grating pattern [26, 29, 30, 31]. Moiré method includes two kinds of techniques: shadow moiré and projection moiré. Shadow moiré uses a single grating placed over the object [32, 33]. A camera and a point light source are mounted over the grating. The grating produces a shadow that is cast on the object and deformed by the 3-D surface topography. When the object is viewed through the grating from a direction different from the light source, the moiré pattern is observed as a result of the interference of the shadow of the grating and the grating itself. Projection moiré technique projects the grating onto the object surface, and then observes the object through a second grating from a different point of view [34, 35, 36]. The distorted grating pattern on the

object surface interfere with the second grating to generate moiré pattern. The distance between the object and the gratings could be much larger than that of the shadow moiré setup.

The moiré pattern obtained from both techniques contains 3-D surface topography information. Analyzing the moiré pattern by the phase shifting method to obtain the phase map is a common practice. The height map between the grating and the object surface can be determined by using the phase map and the geometry of the setup. The typical measurement range of the phase shifting moiré method is from 1 mm to 0.5 m with the resolution at 1/10 to 1/100 of a fringe [5]. Moiré method is utilized for full-field non-contact 3-D shape measurement in industry. Compared with interferometry, the measurement range is larger and the optical setup is simpler.

1.1.7 Digital fringe projection

Digital fringe projection technique utilizes a liquid crystal display (LCD) projector or a digital light processing (DLP) projector to project single or multiple sinusoidal fringe patterns onto a diffuse object surface [5]. The fringe pattern is distorted by the 3-D shape of the surface. A camera mounted on an offset angle captures the deformed fringe patterns. The deformed fringe patterns are analyzed by the phase shifting or the Fourier transform method to obtain the phase map. The phase map along with the calibration parameters of the camera and projector are employed to calculate the 3-D shape of the surface.

Digital fringe projection is a fast and flexible full-field 3-D shape measurement technique. Phase shifts of the fringe patterns can be accurately introduced into the fringe pattern without mechanical errors. Other parameters can also be easily changed to satisfy the measurement requirements. High-speed digital fringe projection system based on the digital micromirror device (DMD) technology has been built [37]. Fig. 1.1 shows the principle of DLP display technology. DMD is an array of micro mirrors mounted on hinges that are individually controlled by the computer [38]. The grayscale of each pixel is controlled by adjusting the time that each micro mirror stays at "on" position. Color images are displayed by projecting the contents of color channels (R, G, B) sequentially at a high image refreshing rate.

In the digital fringe projection system, the phase-shifted fringe patterns are encoded in three color channels (R, G, B) and projected onto the object surface sequentially at a frequency of 180 Hz. The projector works at the black-and-white (B/W) mode. Therefore, the projected fringe patterns are all in grayscale. The synchronized B/W camera captures the fringe images. The 3-D shape measurement result is generated by analyzing the captured fringe patterns. Fig. 1.2 shows the system diagram of the high-speed digital fringe

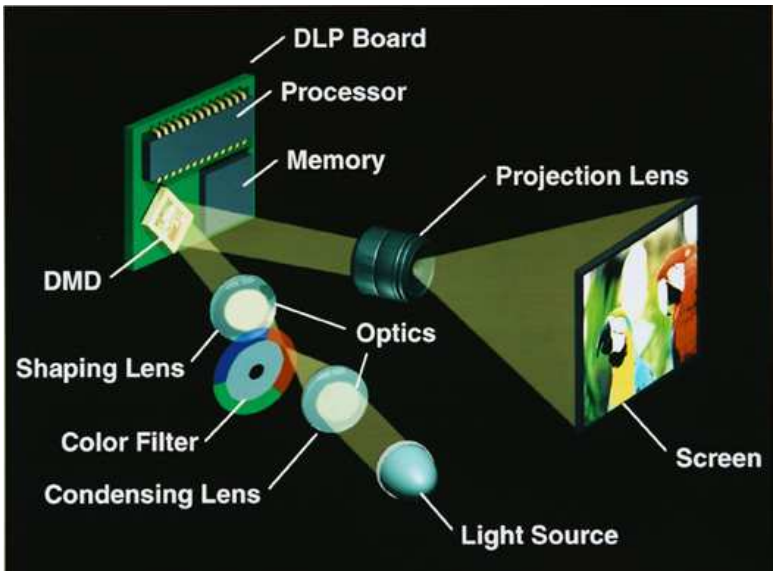

Figure 1.1: System diagram of a DLP projectior.

projection system.

Fringe analysis is an important task for the digital fringe projection technique. The fringe patterns are analyzed by phase shifting method or the Fourier transform method. Phase shifting method needs at least three phase-shifted fringe patterns to obtain the phase map [39]. The averaging effect of the phase shifting method makes the method robust to noises and background illumination variation. Also, solving phase map pixel by pixel renders phase shifting method the ability to handle complex shapes. Because multiple fringe patterns are needed, phase shifting method was considered less ideal for measuring moving or changing objects.

The Fourier transform method only needs a single fringe pattern in order to obtain the 3-D shape [40]. Therefore, Fourier transform method can be used for 3-D shape measurement of moving objects or dynamic processes. The disadvantage of the Fourier transform method is that the measurement quality for object with complex shapes is limited due to the problems of processing fringe pattern in spatial frequency domain, such as spectrum overlapping and spectral leakage.

Compared with the coded pattern projection technique, the main advantage of the digital fringe projection technique is pixel-by-pixel 3-D resolution. Meanwhile, the fringe analysis process is fully automatic and robust to noises.

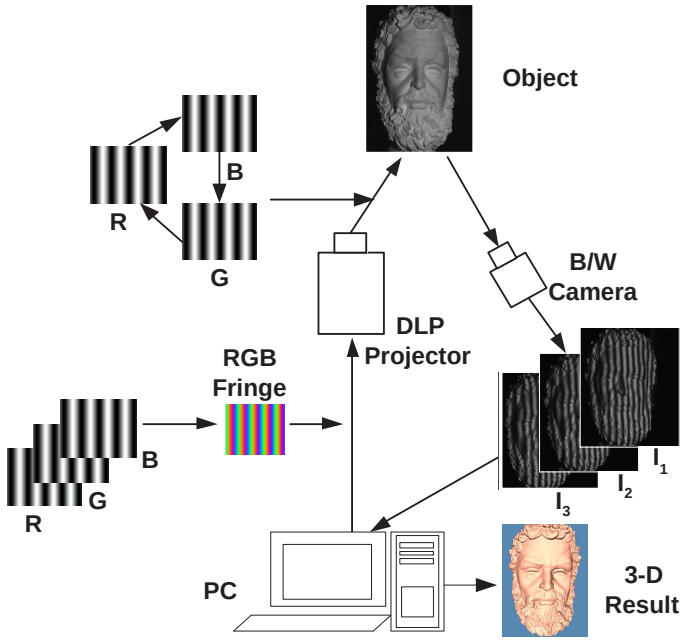

Figure 1.2: System diagram of the high-speed digital fringe projection system.

1.2 Motivation and Objective

1.2.1 3-D shape measurement of dynamic objects

Full-field high-resolution 3-D shape measurement has many applications, such as medical imaging, motion capture, online inspection and biometrics. In most of the above applications, moving or changing objects are involved and real-time data processing is required, therefore real-time 3-D shape measurement of moving or changing objects is of great research value.

Digital fringe projection technique is suitable for this task due to its high-speed fringe projection capability. Although real-time 3-D shape measurement system has been implemented on the digital fringe projection system using 3-step phase shifting method, the object movement during the acquisition of a sequence (a least three) fringe images causes measurement errors. On the other hand, the Fourier transform method only needs one fringe pattern, but its measurement results of objects with complex shapes are not satisfactory. 3-D shape measurement of moving or changing objects is a challenging task.

One way to improve the 3-D measurement result of fast moving or changing objects is to further increase the fringe pattern projection and acquisition speed, which mostly relies on the improvement of the hardware systems of pro-

jector and camera. Currently, as further increasing the pattern projection and capture speed meets the hardware bottleneck, improvement on the software side seems more practical. Developing a modified Fourier transform method to improve its ability of measuring complicated shapes can provide a solution for measuring moving or changing objects. This research can substantially improve the measurement results based on the current digital fringe projection hardware systems.

1.2.2 Phase shifting shadow moiré

Shadow moiré for 3-D shape measurement has been extensively studied since 1970's. By using phase shifting method to analyzing shadow moiré patterns, the phase calculation achieved automation, and the resolution has been greatly improved. However, generating phase-shifted moiré patterns with the shadow moiré optical setup is not an easy task, especially when the phase shifting algorithm employed demands uniform phase shift across the field of view.

During the past two decades, various procedures have been proposed in effort to introduce phase shifts into a shadow moiré setup. Mauvoisin *et al.* studied the methods that could possibly produce phase shifts, which include: changing the grating period, changing the distance between the light source and camera, changing the distance between the grating plane and camera-light source plane, changing the distance between object and the grating plane[32]. Their works showed that exact uniform phase shifts across the field of view is theoretically impossible due to the nonlinear nature of the height-phase relation. Therefore, typical phase shifting algorithms fail to produce accurate results.

Various techniques that introduce approximate uniform phase shifts in the field of view have been proposed. However, no exact close-form phase solution has been provided by these techniques. In this research, we aim to develop a phase shifting scheme for the shadow moiré method to provide exact close-form phase solution, in order to improve the measurement accuracy.

1.2.3 3-D human face recognition

During the past decade, human face recognition has been attracting more and more researchers because of the growing demands from security surveillance, law enforcement, information control, and entertainment industry [41, 42]. Face recognition is an intuitive biometrics. Face image acquisition require less subject cooperation and awareness to collect than those of fingerprints, irises, voice or signature. Based on the underlying face data, face recognition methods can be divided into two groups, 2-D methods and 3-D methods [43].

The performance of 2-D face recognition methods are greatly influenced by the illumination and facial skin texture variations. 3-D methods are not affected by illumination and texture variations, but the 3-D reconstruction of the facial geometry is not computationally efficient and the size of the 3-D data is huge.

We seek a more efficient facial representation that can utilize the underlying 3-D face geometry without reconstructing the 3-D coordinates. Since the digital fringe projection technique for 3-D shape measurement extracts the 3-D information by analyzing the deformed fringe patterns, it is possible to directly make use of the 3-D face information for recognition purpose by fringe analysis. The background illumination and surface texture can be solved from phase-shifted fringe patterns by the phase shifting method. The Fourier transform method extracts the 3-D shape related spectra in the spatial frequency domain. In this research we propose to employ a spectral face representation acquired by fringe analysis for face recognition.

1.2.4 Research objectives

The objectives of this dissertation research are listed as follows:

- Develop pattern projection schemes for the modified Fourier transform method.
- Develop an effective phase unwrapping method for the modified Fourier transform method.
- Develop absolute phase retrieval techniques for the modified Fourier transform method.
- Implement the modified Fourier transform method on the digital fringe projection system to achieve real-time 3-D shape measurement of moving or changing objects.
- Develop a phase shifting shadow moiré method to provide exact close-form phase solution.
- Verify the proposed phase shifting shadow moiré method by simulation and experiments
- Develop a face recognition method based on the digital fringe projection technique and fringe analysis.
- Design experiments and simulation to evaluate the face recognition method's performance.

1.3 Dissertation Structure

This dissertation includes five chapters. Chapter 1 is the introduction. The background, motivation, and the objectives of this dissertation are introduced.

Chapter 2 presents the proposed modified Fourier transform method for real-time 3-D shape measurement. The method adopts the hardware system of a previously built high-speed digital fringe projection system. Two pattern projection schemes are proposed in order to prevent the spectrum overlap. Both of the pattern projection schemes produce a flat image that does not contain fringe pattern. A binary mask is generated based on the grayscale histogram of the flat image. The windowing technique is applied to reduce spectral leakage. The phase map is calculated. A phase unwrapping method is proposed for the modified Fourier transform method which utilizes the fringe visibility as a quality index to guide the path-following unwrapping algorithm. Two absolute phase map retrieval methods are designed for the pattern projection schemes respectively. The 3-D reconstruction process is briefly introduced, in which the 3-D coordinates are computed based on the absolute phase map. Experiments demonstrated the real-time 3-D shape measurement results of face sequences while the subjects are speaking. Improvements over the 3-step phase shifting method are observed in the results.

Chapter 3 introduces a phase shifting shadow moiré technique based on the Carré algorithm. First, the recent research work related to phase shifting shadow moiré is reviewed. The principle of the shadow moiré technique is introduced. Then, the phase shifting scheme is proposed to obtain four phase-shifted moiré patterns. A grating pattern removal method is described. After removing the unwanted grating pattern, the Carré algorithm is applied to the phase-shifted moiré patterns to obtain the exact close-form phase solution. A simulation is designed using MatLab. The proposed method is verified by the simulation program. Experimental results of a NIST calibration block and a lens also demonstrated satisfactory measurement results.

Chapter 4 proposes a face recognition method based on digital fringe projection. Digital fringe projection technique has been successfully employed in Chapter 2 for real-time high-resolution 3-D shape measurement. This chapter presents a novel 3-D face recognition method that directly utilizes 2-D images generated by a structured light system without reconstructing the 3-D geometry. First the related research work is reviewed. Then the fringe pattern projection scheme is briefly introduced. Three phase-shifted sinusoidal fringe patterns are sequentially projected onto the subject's face. The distorted fringe patterns are captured by the camera and analyzed by the phase shifting method to remove texture and illumination. The resultant fringe pattern is transformed into frequency domain, where the spectra related to the 3-D

facial geometry are filtered out. The eigenface algorithm is applied to the face spectra to perform the recognition. In order to evaluate the proposed method, experiments are carried out using the digital fringe projection system. In order to compare the proposed method with the baseline 2-D method, a simulation is designed by use of the Face Recognition Grand Challenge 2.0 (FRGC2.0) face database. In the simulation, the fringe pattern is virtually projected on the 3-D face. Both the simulation results showed promising recognition rate.

Chapter 5 summarizes this dissertation research and outlines the future research work.

Chapter 2

Modified Fourier Transform Method for Real-time 3-D Shape Measurement

With the fast development of camera and projector technologies, the digital fringe projection technique for 3-D shape measurement is now capable of high-speed and high-resolution measurement. As successful as it has been proved on measuring still or slow-moving objects, the digital fringe projection systems utilizing phase shifting methods can only produce less satisfactory results when handling fast moving or changing objects. The main limitation for the phase shifting method is that a series of fringe patterns (at least three) taken in sequence are required. This chapter proposes a modified Fourier transform method for real-time 3-D shape measurement. The method is implemented on the digital fringe projection system introduced in the previous chapter. The proposed method greatly improved measurement results on moving or changing objects compared with 3-step phase shifting method, while maintaining high measurement speed and resolution.

This chapter is organized as follows. Section 2.1 introduces the conventional Fourier transform method for 3-D shape measurement and briefly reviews recent related research work. Section 2.2 presents the fringe projection schemes of the modified Fourier transform method. Section 2.3 presents the quality-guided phase unwrapping method. Section 2.4 introduces the absolute phase map retrieval. Section 2.7 shows the experimental results. Section 2.8 summarizes this chapter.

2.1 Introduction

The Fourier transform method (FTM) for 3-D shape measurement, which is also referred to as Fourier transform profilometry (FTP), is a widely used full-field optical method for 3-D shape measurement [26, 44]. FTM was originally developed for the analysis of simple fringe patterns generated by interferome-

try [40]. Later, it was successfully applied to 3-D shape measurement [45, 46]. Conventional FTM only needs one frame of fringe pattern to obtain the phase map. Therefore it is much less sensitive to motion, compared to the phase shifting methods, such as 3-step method, 4-step method, or Carré algorithm, which needs multiple (at least 3) fringe patterns. However, the shortcomings of the FTM prevent it from directly being applied in the digital fringe projection system for real-time 3-D shape measurement. To facilitate further discussion of those shortcomings, the principle of the conventional FTM for 3-D shape measurement is briefly reviewed as follows.

2.1.1 Principle of the Fourier transformed method

A sinusoidal fringe pattern can be expressed as follows,

$$g(x,y) = a(x,y) + b(x,y)\cos[2\pi f_0 x + \phi(x,y)]\,, \tag{2.1}$$

where $\phi(x,y)$ is the phase that contains the shape information, $a(x,y)$ relates to the background illumination, $b(x,y)$ represents the local amplitude of the cosine function and relates to the surface reflectivity. f_0 is the carrier frequency. Applying Euler's formula to Eq. 2.1,

$$g(x,y) = a(x,y) + c(x,y)e^{i2\pi f_0 x} + c^*(x,y)e^{-i2\pi f_0 x}\,, \tag{2.2}$$

where

$$c(x,y) = 1/2b(x,y)e^{i\phi(x,y)}\,, \tag{2.3}$$

and $*$ denotes a complex conjugate. By taking 1-D Fourier transform with respect to x, Eq. 2.2 gives

$$G(f_x,y) = A(f_x,y) + C(f_x - f_0,y) + C^*(f_x + f_0,y)\,, \tag{2.4}$$

where $A(f_x,y)$ and $C(f_x - f_0,y)$ are the 1-D Fourier transforms of $a(x,y)$ and $c(x,y)$ respectively. Assume $\phi(x,y)$, $a(x,y)$, and $b(x,y)$ vary very slowly compared to the carrier frequency f_0. The three terms in Eq. 2.4 are separated in the spatial frequency domain. The Fourier spectra are shown in Fig. 2.3. A properly designed filter is applied to isolate the $C(f_x - f_0,y)$ term. Then $C(f_x - f_0,y)$ is taken inverse Fourier transform. The phase $\phi(x,y)$ can be extracted by computing the logarithm of $c(x,y)$, and then isolating the imaginary part.

$$\phi(x,y) = \mathrm{Im}\left[\log[c(x,y)]\right] = \mathrm{Im}\left[\log\left[\frac{1}{2}b(x,y)\right] + i\phi(x,y)\right], \tag{2.5}$$

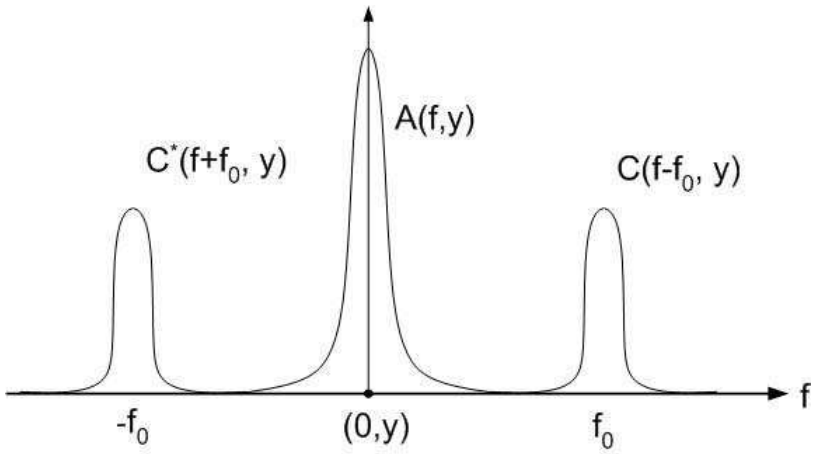

Figure 2.1: Fourier spectra $|G(f_x, y)|$.

The phase thus obtained is wrapped in the range of $-\pi$ to π. To remove the 2π discontinuity, a phase unwrapping process can be applied. The unwrapped phase map is a continuous phase map. A reference plane is utilized to retrieve the 3-D shape based on the geometry of the optical setup [45]. This reference phase map is subtracted from the unwrapped phase map. The resulting phase map $\Delta\phi(x, y)$ is converted to coordinates according to the geometric setup shown by Fig. 2.2. The height of the surface point $D(i, j)$ is $\overline{DB}$. Since $\overline{DB}$ is much smaller than the distance between the system and the object in practice, the height of of point $D(x, y)$ is calculated by the following equation,

$$Z(i,j) = \overline{DB} \approx \frac{l}{d}\overline{AC} = \frac{pl}{2\pi d}\phi_{AC} = K_z \Delta\phi(i,j)\,, \tag{2.6}$$

where l is the distance between the reference plane and the line connecting the optical centers of DMD and CCD, and d is the distance between the above two centers. p is the fringe pitch of the reference plane. K is a calibrated constant. $\Delta\phi(i, j)$ is the phase value at point $D(i, j)$. The X and Y coordinates are calculated by use of two calibrated constants K_x and K_y.

$$X(i,j) = K_x i\,, \tag{2.7}$$

$$Y(i,j) = K_y j\,. \tag{2.8}$$

Conventional FTM's salient advantage is that only one frame of fringe image is needed. It is ideal for 3-D shape measurement of fast moving or changing objects. However, the Fourier transform method has the following limitations that affect the measurement quality when measuring object with complex

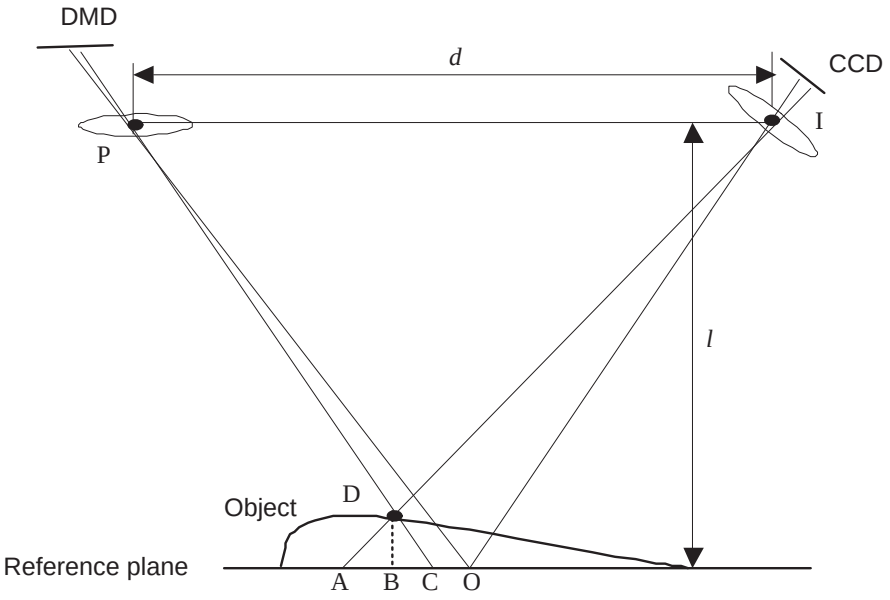

Figure 2.2: Phase-to-coordinate conversion in the conventional Fourier transform method.

shapes, such as steep slopes and holes.

First, spectral overlapping. The overlapping of the background terms and the terms containing phase information occurs in the spatial frequency domain when measuring complex 3-D shapes [44]. Steep slopes will dramatically change the carrier frequency from the camera's point of view. The spectra around the carrier frequency sometimes overlap with the spectra around the zero frequency.

Second, spectral leakage. Discrete Fourier transform (DFT) will generate spectral leakage when discontinuity occurs at the ends of the signal [47]. The length of the sinusoidal fringe pattern is finite. The 1-D discrete Fourier transform assumes the fringe pattern is a part of an infinite repetitive fringe pattern. Therefore, if the two ends of the fringe pattern can not be connected smoothly, sharp discontinuities will generate broad band frequency components and spread over the spectrum. Also, edges of the holes and shadows in the fringe pattern are discontinuities that causes spectral leakage. The spectral leakage produces phase errors.

Third, robustness of phase unwrapping. The only fringe pattern used by the conventional FTM is usually corrupted by noises. Therefore, unwrapping process is difficult due to lack of reliable information that could be used to guide the phase unwrapping process.

Fourth, the accuracy of the 3-D coordinate reconstruction. The conventional FTM used a reference plane and assuming small surface height variation from the reference plane and approximation is used in the phase-to-height conversion, as shown in Eq. 2.5. The coordinate conversion model is not suitable for applications requiring large height measurement range. Also, the lens distortions of the camera and projector were not considered in the coordinate calculation. Accurate phase-to-coordinate conversion requires the absolute phase map retrieval to be used with the more sophisticated camera and projector calibration model.

2.1.2 Related work

In order to improve the conventional FTM, different fringe projection schemes were studied [48, 49, 50]. Chen *et al.* proposed to use a bicolor fringe pattern to obtain two recorded fringe patterns with a 180° phase shift to each other [48]. The unwanted background term is removed by subtracting one of the fringe patterns from the other. The zero frequency terms in the spatial frequency are eliminated; and as a result, the spectrum overlapping is prevented. Also, the noise level is reduced in the resulting high contrast fringe pattern. The main disadvantage is that the object surface color significantly affect the accuracy in that the color pattern is employed. Yue *et al.* proposed a novel technique that uses a fringe pattern modulated from two 180° phase-shifted gray level fringe pattern [49]. The modulated fringe pattern is first projected onto the object, then the recorded deformed fringe pattern is demodulated into two 180° phase shifted fringe patterns. Finally the unwanted zero frequency components are removed. The disadvantage of this technique is that the two phase-shifted fringe patterns are decoded by filtering in the frequency domain, and then by inverse Fourier transform. Thus the final recovered phase is obtained by two times of fast Fourier transform (FFT) and inverse fast Fourier transform (IFFT), which are not only computationally expensive but also degrades the accuracy. In this research, more effective fringe pattern projection schemes for Fourier transform method are proposed.

Phase unwrapping is a common yet difficult task for fringe analysis methods, especially when noises and geometric discontinuities exist in the phase map. Various phase unwrapping techniques have been proposed to solve the phase unwrapping problems in various applications [51]. Branch cut algorithms connect nearby residues by branch cuts and unwrap the phase map by integrating the phase difference around the branch cuts [52, 53, 54]. Quality-guided algorithms first generate a quality map that indicates the goodness of the phase, and then unwrap the pixels with good quality first [55, 56, 57]. Minimum discontinuity approach identifies the loops of discontinuities and add

appropriate multiples of 2π to the pixels in the loops [58]. Minimum Lp-norm method and weighted least-squares method minimize the wrapped phase difference between the wrapped phase map and the unwrapped phase map [59, 60]. Temporal phase unwrapping method utilizes a series of fringe patterns with changing pitches to accomplish phase unwrapping [61]. Depending on the applications, every algorithm has its own advantages and disadvantages. The phase unwrapping algorithm needs to be selected based on the requirements of the system and the characteristic of the wrapped phase map.

As to the phase unwrapping problem specific to the Fourier transform method, Takeda *et al.* proposed to use frequency-multiplex fringe pattern to improve the phase unwrapping process [46]. Burton *et al.* proposed multichannel Fourier fringe analysis to aid the unwrapping process [62]. Those two techniques need more than one fringe patterns to be projected onto the object, and the same number of wrapped phase maps need to be calculated. This is computationally expensive because FFT and inverse FFT operations are repeatedly used for each fringe pattern. Zappa and Busca compared eight of the above-mentioned phase unwrapping algorithms used for unwrapping the phase map generated by the Fourier transform method for 3-D shape measurement [63]. Among them, the quality-guided algorithm achieved a better result with reasonable execution time. Phase unwrapping method proposed by Su *et al.* used data modulation of the recorded fringe pattern as a quality index to guide the unwrapping process [62]. The data modulation is defined as the peak-to-peak amplitude of the sinusoidal fringe pattern, which is closely related to the local reflectivity of the object surface. The algorithm achieved satisfactory unwrapping results. In this research, we will develop quality-guided phase unwrapping algorithm for the proposed fringe projection schemes.

The 3-D reconstruction in the previously proposed Fourier transform methods utilized a reference plane [48, 49]. Hu and Harding's recent work showed specifically that the phase shifting method with the absolute phase map concept was significantly more accurate than the Fourier transform method with the reference plane approach [64]. The drawbacks of the phase-to-coordinate conversion algorithm using the reference plane include: (1) The optical system setup is complicated and requires high accuracy calibration. (2) The conversion of coordinates is only accurate when the measured surface is very close to the reference plane. (3) The algorithm itself cannot take the camera and projector lenses distortion into account.

2.2 Modified Fourier Transform Method

We seek to utilize additional information to solve the existing problems of the conventional FTM. The influence of the background illumination can be removed if we could obtain image that exactly describes the background illumination of the fringe pattern:

$$g_0(x, y) = a(x, y)\,, \tag{2.9}$$

where $a(x, y)$ is the same term in Eq. 2.1 representing the background illumination. Subtracting Eq. 2.9 from the captured sinusoidal fringe image expressed in Eq. 2.1, and then performing the 1-D Fourier transform with respect to x, we have

$$G'(f_x, y) = C(f_x - f_0, y) + C^*(f_x + f_0, y)\,. \tag{2.10}$$

With the background illumination removed, the zero frequency terms are out of the equation before the Fourier transform, and the overlapping in the frequency domain can be prevented or at least alleviated. The magnitude of the Fourier spectra are shown in Fig. 2.3.

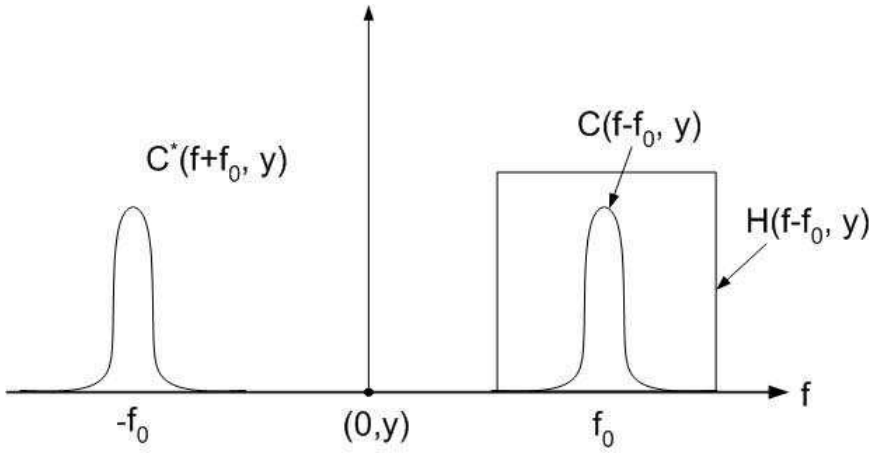

Figure 2.3: Fourier spectrum

We propose to obtain the background illumination term by taking advantage of previously developed high-speed digital fringe projection system. The working principle of the system has been introduced in Chapter 1. The system consists of a digital video projector based on digital micro-mirror device (DMD) and a high-speed black-and-white (B/W) camera. Three different fringe patterns can be encoded in three color channels (R, G, and B), and the fringe patterns are captured sequentially at a frequency of 90 frame/second or

higher. There is great flexibility of designing fringe pattern for each color channel. Based on this fringe projections system, two fringe projection schemes are proposed. The first one directly projects one flat pattern and a fringe pattern. The other one projects three phase-shifted fringe patterns. The details of the two schemes are introduced as follows.

2.2.1 Flat pattern + fringe pattern

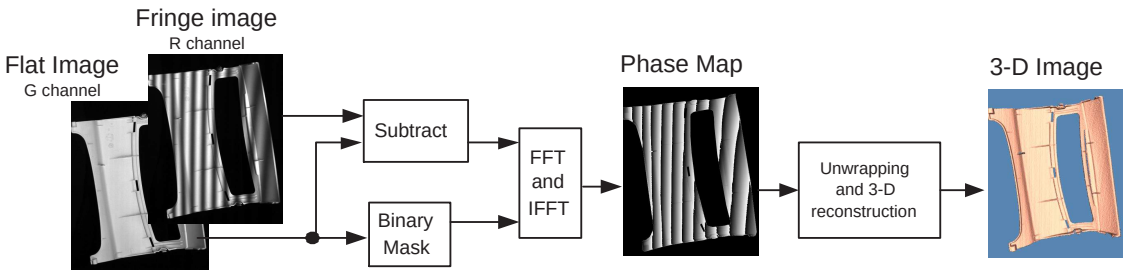

Figure 2.4: Schematic system diagram for the modified Fourier transform.

In the first scheme, a flat pattern and a sinusoidal fringe pattern are employed. The schematic diagram of the method is shown in Fig. 2.4. Flat pattern means a uniform grayscale pattern whose intensity value is the average of the sinusoidal fringe pattern. A fringe pattern and a flat pattern are encoded in the color channels (R, G and B). When the fringe and flat patterns are projected onto the object, the synchronized camera captures the fringe image $g_0(x, y)$ and flat image $g(x, y)$ sequentially.

2.2.2 Three phase-shifted fringe patterns

In the second scheme, the system projects three phase-shifted fringe patterns with $2\pi/3$ phase shift between neighboring fringe pattern. Averaging three captured fringe images can generate a flat image. Three phase-shifted fringe patterns are expressed as follows.

$$p_1(x, y) = a_p + b_p \cos\left[2\pi f_0 x - \frac{2\pi}{3}\right], \tag{2.11}$$

$$p_2(x, y) = a_p + b_p \cos\left[2\pi f_0 x\right], \tag{2.12}$$

$$p_3(x, y) = a_p + b_p \cos\left[2\pi f_0 x + \frac{2\pi}{3}\right], \tag{2.13}$$

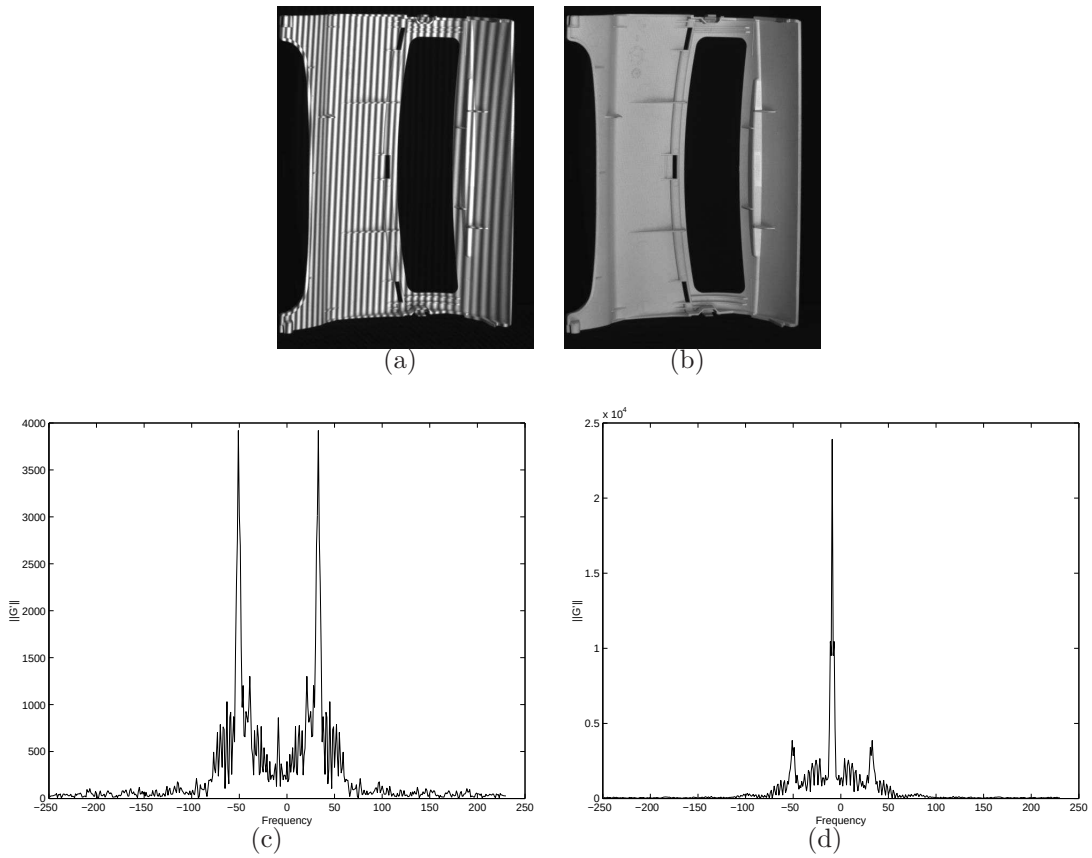

Figure 2.5: Flat+fringe pattern projection. (a)Fringe image; (b)Flat image; (c)Spectrum of 320th row with the flat image subtracted; (d)Spectrum of 320th row of the fringe image.

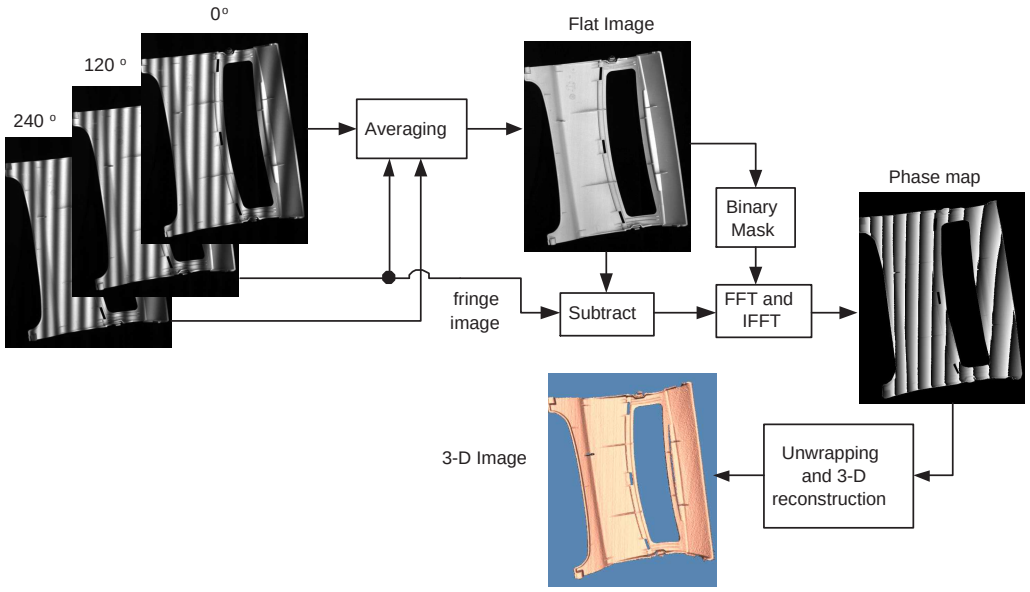

Figure 2.6: Schematic diagram for the modified Fourier transform using 3 fringe images.

where a_p is the bias and b_p is the amplitude of the fringe pattern. The fringe patterns represented by Eq. 2.11 $\sim$ Eq. 2.13 are encoded into three color channels of a DLP projector and projected onto the object. The captured fringe images have the following forms,

$$g_1(x,y) = a(x,y) + b(x,y)\cos\left[2\pi f_0 x + \phi(x,y) - \frac{2\pi}{3}\right], \tag{2.14}$$

$$g_2(x,y) = a(x,y) + b(x,y)\cos\left[2\pi f_0 x + \phi(x,y)\right], \tag{2.15}$$

$$g_3(x,y) = a(x,y) + b(x,y)\cos\left[2\pi f_0 x + \phi(x,y) + \frac{2\pi}{3}\right], \tag{2.16}$$

where $\phi(x,y)$ is the phase that contains the shape information, $a(x,y)$ represents the background illumination, $b(x,y)$ is related to the surface reflectivity, and f_0 is the carrier frequency of the fringe pattern. The background term is solved by averaging the three fringe patterns,

$$a(x,y) = \frac{g_1(x,y) + g_2(x,y) + g_3(x,y)}{3}. \tag{2.17}$$

The background $a(x,y)$ is the flat image of the object without the fringe pattern. In every three consecutive captured fringe images $g_1(x,y)$, $g_2(x,y)$,$g_3(x,y)$,

the background is calculated and subtracted from $g_2(x, y)$. Then the Fourier transform is followed to obtain the phase map.

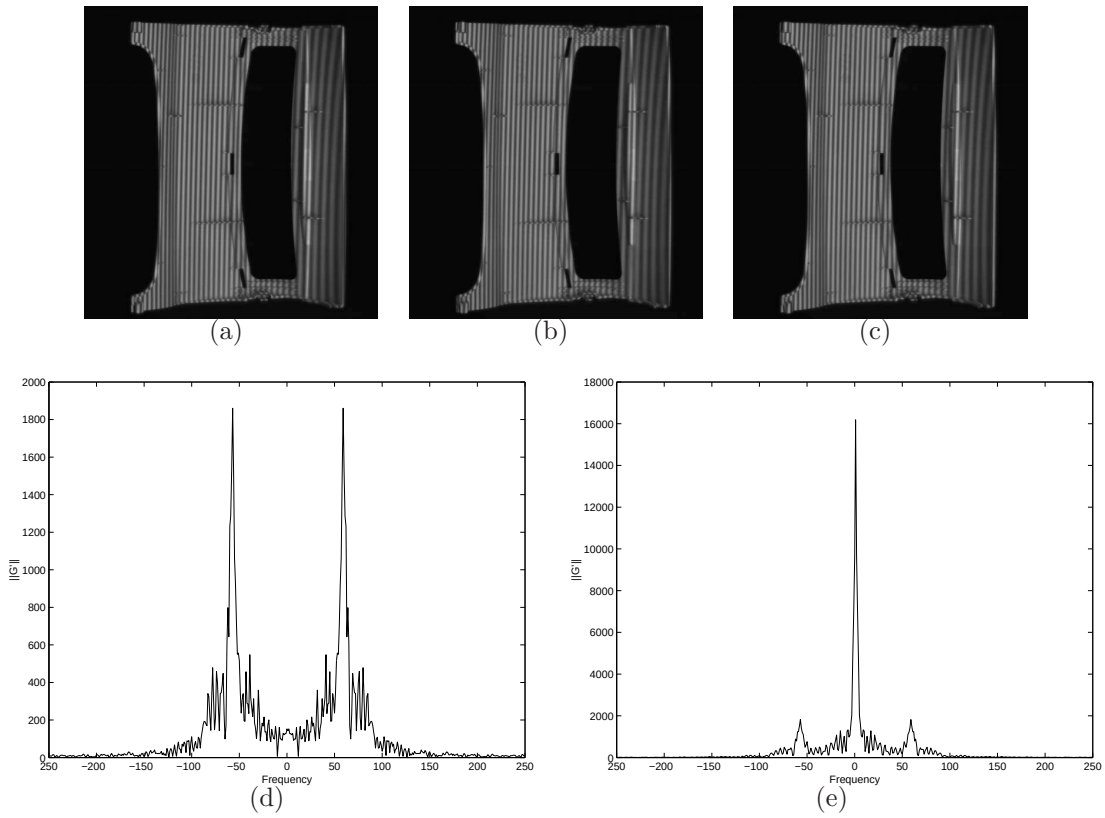

Figure 2.7: Three phase-shifted pattern projection. (a)-(c)Fringe images; (d)Spectrum of 320th row with the flat image subtracted; (e)Spectrum of 320th row of the second fringe image.

Comparing the two fringe projection schemes, the "flat+fringe" scheme needs less patterns. Therefore it is more suitable for measuring fast moving or changing objects. However, the disadvantages include (1) The grayscale of the flat pattern needs to be calibrated in order to compensate for the grayscale error of the projector. (2) The system needs to differentiate the captured fringe image from the flat image. The advantages of using three phase-shifted fringe patterns to generate the flat image include: (1) No grayscale calibration is needed. (2) The averaging effect helps to reduce random intensity noises. (3) The order of the phase-shifted fringe pattern does not affect the phase calculation. Any three consecutive fringe patterns can be used to generate the flat image. The disadvantage is that three fringe patterns are needed

to calculate one 3-D image. It needs more time to capture fringe images and defects caused by motion are more likely to occur. Therefore, flat+fringe pattern projection is preferred when measuring fast moving objects. For slowly moving or changing objects, three phase-shifted pattern projection scheme can achieve better results.

2.2.3 Binary mask generation

In order to reduce the spectrum leakage, various of "windows" can be applied to the data. Shadows and holes need to be detected in the fringe patterns before the windows can be applied. The shadows and holes are detected in the flat image based on an intensity threshold. The object was put in front of a black background when capturing the images. Shadows and holes appear to be the dark areas in the captured flat image. The intensity threshold is generated based on the grayscale histogram of the flat image. In the histogram, the intensity value corresponding to the valley between the two peaks formed by the foreground and background is selected as the intensity threshold. For different surfaces such as, plastic workpiece and human face, new thresholds need to be determined by this process. A binary mask is generated based on the threshold to indicate the shadows and holes. Fig. 2.2.3 shows the histogram and the binary mask for the free-form workpiece used in previous examples. Windows will be applied based on the boundaries marked by the binary mask. 1-D forward and inverse FFT will be performed within each continuous valid fringe pattern area indicated by the binary mask. Thus the computation time is greatly reduced.

2.2.4 Spectral leakage reduction

For an undistorted sinusoidal fringe pattern with a constant carrier frequency f_0, there should be only one non-zero frequency component f_0 in the corresponding spatial frequency spectrum. However, when using FFT to transform such a sinusoidal fringe pattern with non-integer number of periods into spatial frequency domain, the spectrum will spread to all frequency components instead of concentrated on the carrier frequency of the fringe pattern. This is known as spectral leakage. The spectral leakage will decrease the signal to noise ratio in that it causes a given spectral component to contain not only its own signal energy, but also the energy from the rest of the spectrum. In FTM for 3-D shape measurement, the phase term is obtained by forward and inverse FFT. Spectral leakage in FFT will introduce phase errors.

An effective means to reduce spectral leakage is to modulate the amplitude of the signal to make the signal fit into one period, which is called windowing.

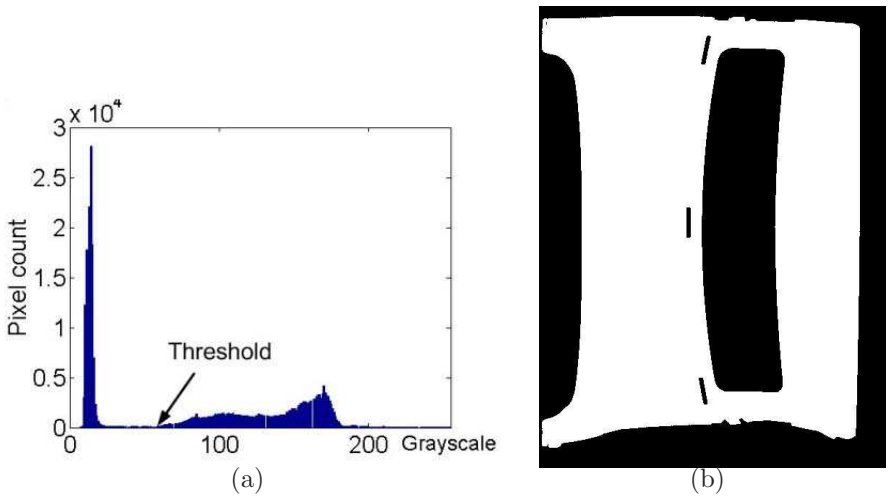

(a) (b)

Figure 2.8: Binary mask generation. (a) Histogram of the flat image; (b) Binary mask.

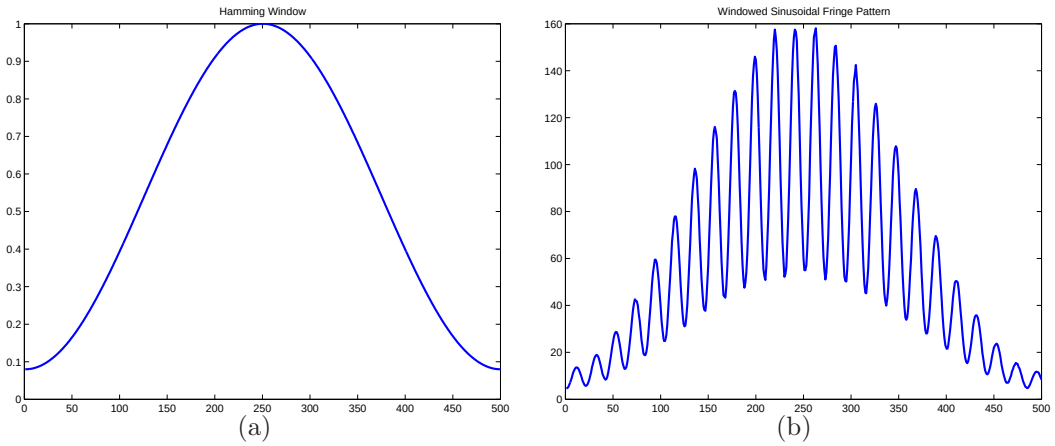

(a) (b)

Figure 2.9: Window function. (a)Hamming window; (b)Windowed sinusoidal fringe pattern.

A window function is multiplied with the data to achieve windwoing. In order to reduce spectral leakage, various windows can be applied to the signal data before performing FFT [47]. Both ends of a 1-D signal are compressed to a value near zero to make sure they are approximately continuous. Some of the widely used windows are Hamming window, Hanning window, Blackman window, and Kaiser window. Berryman *et al.* studied the effectiveness of the windowing functions on the FTM [65]. The research shows that the windowing can improve the measurement quality when the fringe pattern is not dense and noise level is low. The disadvantage of the windowing is that windowing functions compress the data close to both ends are close to zero. The compression of amplitude degrades the quality of the phase values in those areas. Fig. 2.9 shows the windowing of a sinusoidal fringe pattern. The period of the fringe pattern is 20 pixel/cycle.

Extension of the boundaries of the fringe pattern has been proved effective on reducing error [66]. In this research, in order to reduce spectral leakage while preserving measurement qulaity, the data is extended at both ends with zeroes, before a 1-D Hamming window is applied. After the inverse FFT, the extended data are discarded. A white plane cardboard is employed to demonstrate the spectral leakage reduction by windowing. Three phase-shifted fringe patterns projected onto the cardboard are captured. The period of the fringe pattern is 20 pixel/cycle. The 3-D measurement results are shown in Fig. 2.10. When no window function is applied, spectral leakage causes "ripples" on the plane, especially on both edges. When Hamming window is applied without extending the boundary of the fringe pattern, the ripple error is reduced. When both boundaries in the X direction are extended by 10% of the width of the plane before applying the Hamming window, the ripple error is further reduced. Fig. 2.10(d) - Fig. 2.10(f) show the cross sections of the measurement results. A fitted straight line is shown in the cross section plot. The root mean square (RMS) error of the data against the fitted line is calculated. The measurement result without windowing has an RMS error of 0.5537 mm. Windowing the fringe pattern directly reduced the ripples but errors on the borders are still high (RMS=0.6539 mm). Windowing with the extension of the boundaries generates a much lower error (RMS=0.3402 mm).

2.3 Phase Unwrapping

The wrapped phase maps obtained by the above methods are in the range of $-\pi$ to π. The process of removing the 2π discontinuities is called phase unwrapping. The phase unwrapping process is important for acquiring the accurate 3-D shape of the object.

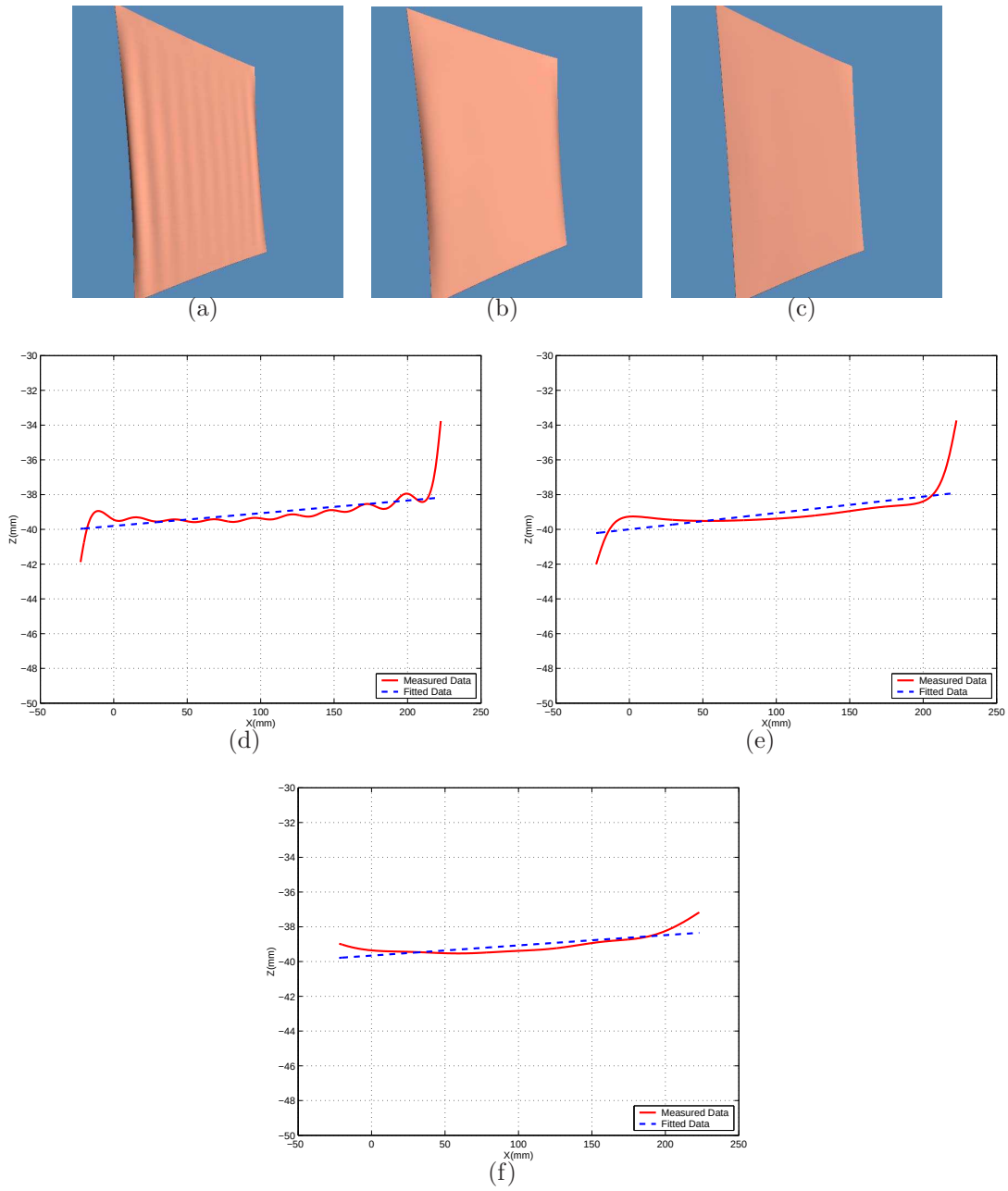

Figure 2.10: Windowing effect on the results of MFTM. (a)-(c) 3-D images of a white plane cardboard affected by windowing; (d)-(e)Cross sections at the same row from (a)-(c).

Phase unwrapping for the phase map produced by FTM is a difficult task when noise level is high and less information is available, compared to phase shifting methods. Meanwhile, the real-time 3-D reconstruction requires high processing speed. The quality-guided can produce robust unwrapping results with reasonable speed for high-speed applications. In this section, a quality-guided unwrapping algorithm using fringe visibility as quality index is proposed for the modified FTM. First, two quality indexes are introduced. Then, the path following algorithm is introduced. The unwrapping results are shown at the end of this section.

2.3.1 Quality index

Quality index plays an important role in quality-guided path following algorithms. It is the information recovered from the wrapped phase map or from the fringe images, which can be used to determine the goodness of the phase quality. In this research, phase gradient and fringe visibility are employed to assist the quality-guided phase unwrapping process and their results compared.

Phase Gradient

Phase gradient is calculated from the wrapped phase map. It is defined as follows.

$$\Delta(i,j) = \sqrt{(\Delta^x_{i,j})^2 + (\Delta^y_{x,y})^2}\,, \tag{2.18}$$

where,

$$\Delta^x_{i,j} = W\{\phi(i+1,j) - \phi(i,j)\}\,, \tag{2.19}$$

$$\Delta^y_{i,j} = W\{\phi(i,j+1) - \phi(i,j)\}\,, \tag{2.20}$$

Here $W\{\}$ is a wrapping operator, $\phi(i,j)$ is the wrapped phase map, and $\Delta^x_{i,j}$ and $\Delta^y_{i,j}$ are the wrapped phase difference in the horizontal and vertical directions. Phase gradient is a quality measure that indicates the variation of the phase in both X and Y direction. It has been successfully used as a quality index for phase unwrapping in the phase shifting method [67]. Low phase gradient value indicates high phase quality. For the Fourier transform method, higher carrier fringe frequency helps to preserve details in the 3-D measurement result. Unfortunately, when the pitch of the fringe pattern is small (high carrier frequency), the phase variation is large in the areas even without geometric discontinuities. In the modified Fourier transform method, a higher carrier frequency is preferred because it allows for finer details of an object to be measured. As a result, the ability of phase gradient for classifying phase quality is greatly limited. The resulting high phase gradient in the wrapped

phase map poses a problem for the quality-guided unwrapping algorithm using only phase gradient as the quality index to distinguish noises.

In the proposed method, phase gradient is employed in the preprocessing step. A threshold of phase gradient is set to eliminate pixels with abnormally high phase gradient values.

Visibility

Visibility is a measure of the contrast of the fringe pattern. Its value is in the range of $[0, 1]$ with 0 indicating zero visibility of the fringes. In a digital fringe projection system, geometric discontinuities typically create shadow areas because of the offset angle between the light source and the camera. Low visibility value means low signal-to-noise ratio, which usually implies poor phase quality [68]. In colored surface areas, although the modulation value of the pixel is low, the phase quality can be good if contrast is high enough. Visibility map has better discrimination power than modulation map in such cases. The visibility map of the sinusoidal fringe pattern is expressed as

$$\gamma(x, y) = \frac{b(x, y)}{a(x, y)}, \tag{2.21}$$

where $a(x, y)$ and $b(x, y)$ have the same meanings as those in Eq. 2.1. The visibility map is difficult to obtain in the conventional Fourier transform method. In the proposed modified Fourier transform method, the visibility map can be calculated by using the flat image as $a(x, y)$. Based on Eq. 2.10,

$$b(x, y) = 2|C(f_x - f_0, y)|, \tag{2.22}$$

In this research, visibility map and phase gradient map are employed as the quality maps to guide the unwrapping process.

2.3.2 Quality-guided path following

A masking operation is performed before the unwrapping process begins. First, an intensity threshold is generated to identify areas with shadows and holes based on the grayscale values of the flat image, and to exclude pixels with intensity values close to zero. The threshold is chosen based on the intensity histogram of the flat image. Then, the phase gradient map is calculated based on Eq. 2.18-Eq. 2.20 and a threshold is selected to eliminate pixels with higher phase gradient values than the threshold. Also, a threshold of visibility is set to eliminate pixels with poor phase quality from the unwrapping process.

The quality-guided path-following phase unwrapping process is performed using the flood-fill algorithm [57]. The visibility map is employed as the quality map. The algorithm utilizes an adjoin list to store sorted pixels to be unwrapped. In our method, the adjoin list is formed by N queues, which are corresponding to N quality levels. Phase unwrapping is an iterative process. Our quality-guided phase unwrapping process is illustrated in Fig. 2.11. At the

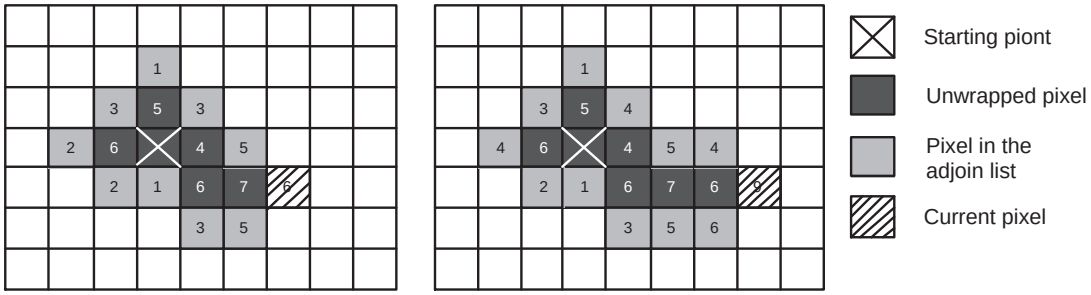

Figure 2.11: Flood-fill algorithm.

beginning of the process, a starting pixel close to the image center is selected, whose quality is over a pre-set threshold, and is marked as "unwrapped" Then the four neighboring pixels of the starting pixel are examined. If they are not masked out, then they are pushed into queues corresponding to their quality values. In the next step, queues are checked from high quality to low quality. If the queue of highest quality pixels is not empty, a pixel is popped out, and its phase value is unwrapped by use of Eq. 2.23 or Eq. 2.24, depending on the relative position with the unwrapped neighboring pixel:

$$\varphi(i,j) = \varphi(i-1,j) + \Delta^x_{i,j}\,, \tag{2.23}$$

$$\varphi(i,j) = \varphi(i,j-1) + \Delta^y_{i,j}\,, \tag{2.24}$$

where $\varphi(i,j)$ is the unwrapped phase and $\Delta^x_{i,j}$ and $\Delta^y_{i,j}$ are the wrapped phase difference along the X and Y directions respectively. Once this is done, the pixel is then marked as "unwrapped". Its four neighboring pixels are then examined in the same way. The process continues until all the queues are empty.

The proposed phase unwrapping method for modified FTM is tested using a plaster sculpture with complex shape. The fringe and flat images at a resolution of 532×500 pixels. Each pair of images has two identical fringe images and one flat image. The flat pattern's intensity is calibrated to compensate for the grayscale error of the projector, so that the captured flat image represents the average intensity of the fringe image. Fig. 2.12 shows the fringe image and

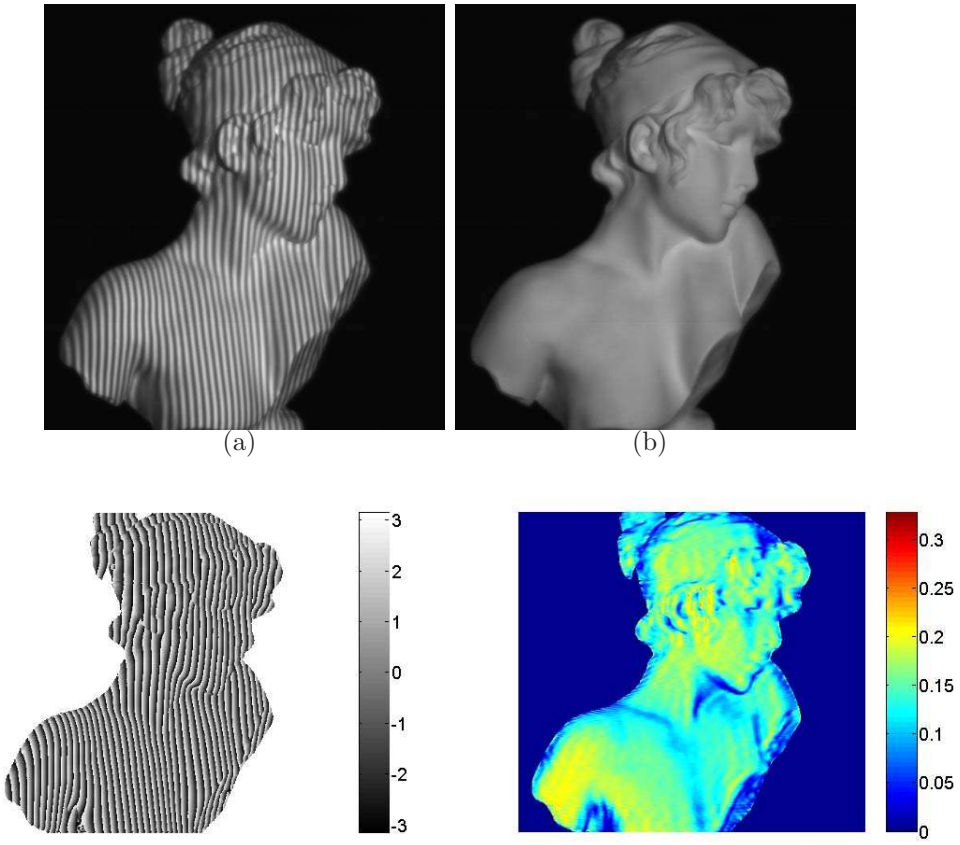

Figure 2.12: Phase unwrapping result of a model. (a) Fringe image. (b) Flat image. (c) Wrapped phase map. (d) Visibility map.

the flat image. The fringe pattern used in the experiment has a pitch of 9 pixels/fringe. The surface of the statue is white. The visibility variation is caused mainly by the surface shape. In the visibility map shown in Fig. 2.12(d), low visibility values are seen in the areas of shadows or geometric discontinuities.

In Fig. 2.13, the four intermediate steps in the quality-guided unwrapping process are shown. The unwrapping process starts from a pixel close to the center of the image. Pixels with high phase quality are unwrapped first. The flood-fill algorithm successfully grows the unwrapped region until it has completely unwrapped the phase map, as shown in Fig. 2.13(d).

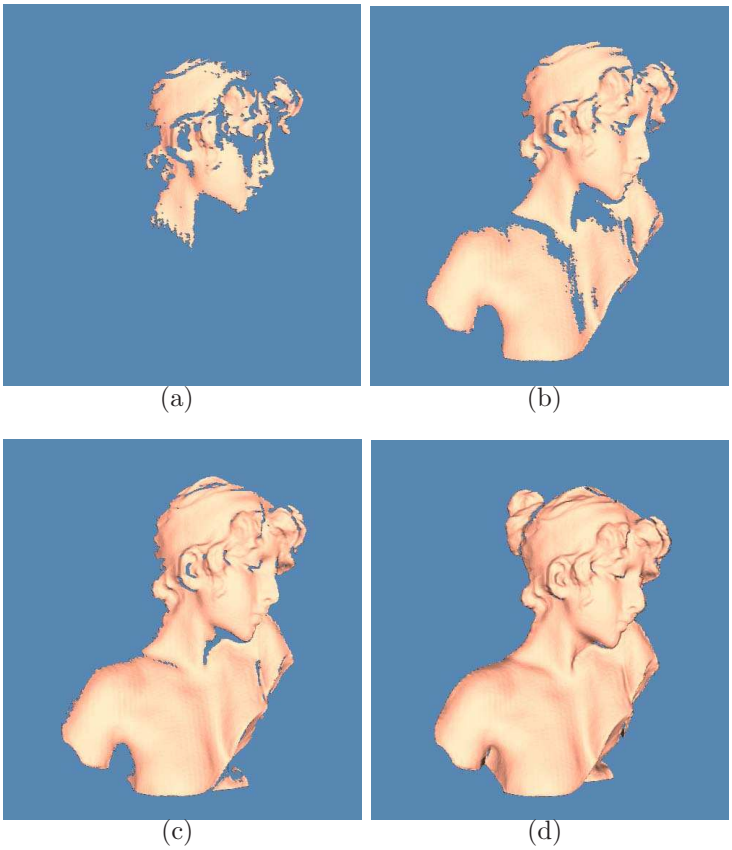

Figure 2.13: Quality-guided phase unwrapping process. (a) Intermediate step 1. (b) Intermediate step 2. (c) Intermediate step 3. (d) Final result.

2.4 Absolute Phase Retrieval

The resulting continuous phase map is a relative phase map $\phi(x, y)$, whose value depends on the starting point of the unwrapping process. An absolute phase map is required by the 3-D reconstruction process. The phase value distribution in an absolute phase map does not depend on the start point of the unwrapping process. The phase values in the absolute phase map can be used to build the correspondence between the projector and the camera pixels. Based on the correspondence, the 3-D coordinates can be calculated by triangulation.

The absolute phase map retrieval is achieved by embedding markers in the projected patterns and then detected its positions in the captured images. For the "flat+fringe" fringe projection scheme, two cross-shaped markers with distinguishable grayscale patterns are embedded in the flat pattern and the fringe pattern. For the three phase-shifted fringe pattern projection scheme, three cross-shaped markers with different visibility patterns are embedded into three fringe patterns.

2.4.1 Marker detection

Flat pattern + fringe pattern

The embedded markers are shown in Fig. 2.14(a) and Fig. 2.14(b). The intensity distribution on the marker in the fringe pattern is uniform and the intensity value is that of the flat pattern. The captured marker intensity distribution is the same as that expressed as in Eq. 2.9. In the flat image, the intensity on the marker is sinusoidal with a π phase difference with the fringe pattern. The captured marker intensity distribution in the flat image is expressed as,

$$g_m(x, y) = a(x, y) + b(x, y) \cos[2\pi f_0 x + \phi(x, y) + \pi] , \tag{2.25}$$

The marker is detected in the flat image by use of a template that has the same intensity distribution with the fringe marker. The template is shown in Fig. 2.14(c). The template matching is performed. For each location, the squared intensity differences between each pixel on the template and the pixel on the captured flat image are summed up. The center of the marker is located by minimizing the sum of the squared intensity difference. The marker is designed to be projected onto a flat area on the object in order to reduce detection error. Fig. 2.15 shows a marker detection result of a workpiece. The template matching result is normalized into the grayscale intensity interval of $[0, 255]$ for visualization purpose. Each pixel in the image represents the sum

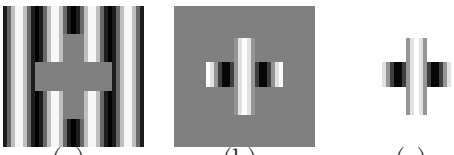

(a) (b) (c)

Figure 2.14: Markers and template. (a) Marker embedded in the fringe pattern; (b) Marker embedded in the flat pattern; (c) Template.

of the squared difference at that point. The marker's center is successfully detected in this example.

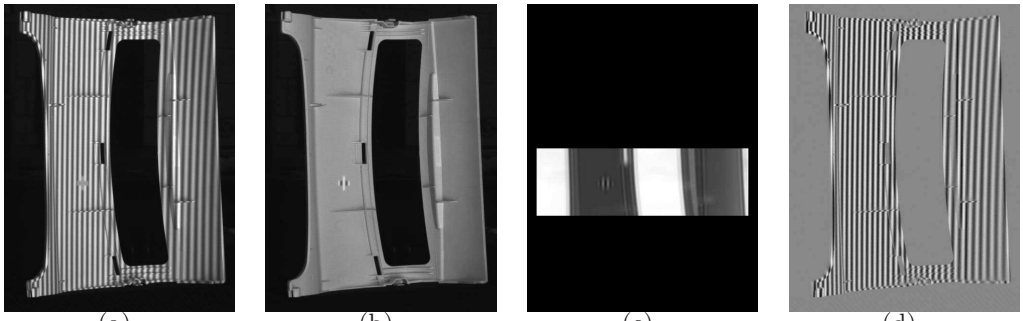

(a) (b) (c) (d)

Figure 2.15: Marker detection and removal example. (a) Fringe image; (b)Flat image; (c) Template matching result; (d)Marker removal result.

Three phase-shifted fringe pattern

The three phase-shifted fringe patterns expressed in Eq. 2.14∼Eq. 2.16 have the same visibility map as defined in Eq. 2.21. A one-pixel wide cross-shaped marker is embedded in the same position in three fringe patterns. The marker is visible in the visibility map, because the visibility values on the marker are set to be lower than other pixels. The marker's position is detected in the visibility map by template matching in the visibility map. A marker detection example is shown in Fig. 2.16. The location of the marker in the fringe pattern to be projected is known and fixed in the patterns to be projected. According to the principle of epipolar geometry [6], the marker's locations in the captured images for different object distances form a straight trajectory if lens distortion is ignored. Therefore, the search area is set to be a narrow strip centered at

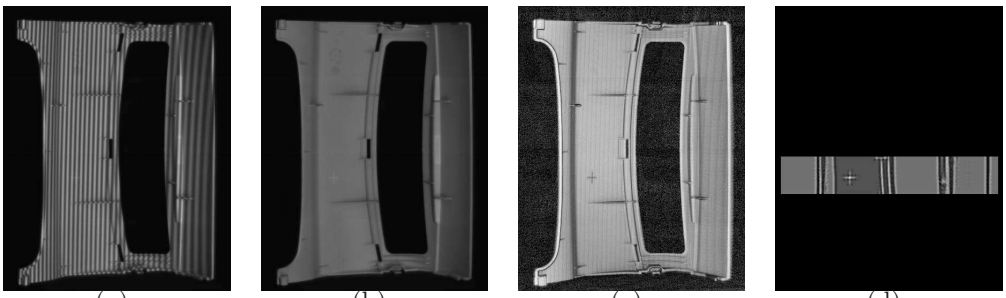

(a) (b) (c) (d)

Figure 2.16: Marker detection example for the 3 phase-shifted fringe patterns. (a) One of three fringe images; (b)Flat image; (c) Visibility map; (d)Template matching result.

the calibrated marker trajectory. With this approach, the search time and error rate are significantly reduced.

The absolute phase map retrieval relies on the detection of the location of the marker's center. Assume the relative phase of the center pixel of the marker is ϕ_0, and the absolute phase value of that pixel is 0. The absolute phase map $\Phi(x, y)$ is given by

$$\Phi(x, y) = \varphi(x, y) - \varphi_0 \,. \tag{2.26}$$

2.4.2 Marker removal

When subtracting Eq. 2.9 from Eq. 2.1, the result only contains the sinusoidal term. Therefore, the marker is completely removed during the subtraction of the flat image from the fringe image. Because the two markers are on the same position in the images, the blurring effect on both markers cancel each other completely. Therefore, the marker removal does not affect the phase extraction. A marker removal example for the "flat+fringe" pattern scheme is shown in Fig. 2.15(d).

For the three phase-shifted fringe pattern scheme, the width of the marker arm is one or two pixel in the captured fringe image. Therefore, the marker is left in the fringe image and it is removed in the final 3-D result by interpolating the 3-D surface in the marker area.

The absolute phase map builds a constraint between the camera pixels and projector pixels. With this correspondence and projector and camera calibration parameters, an absolute phase map is converted in to 3-D coordinates. This process is called phase-to-coordinate conversion or 3-D reconstruction.

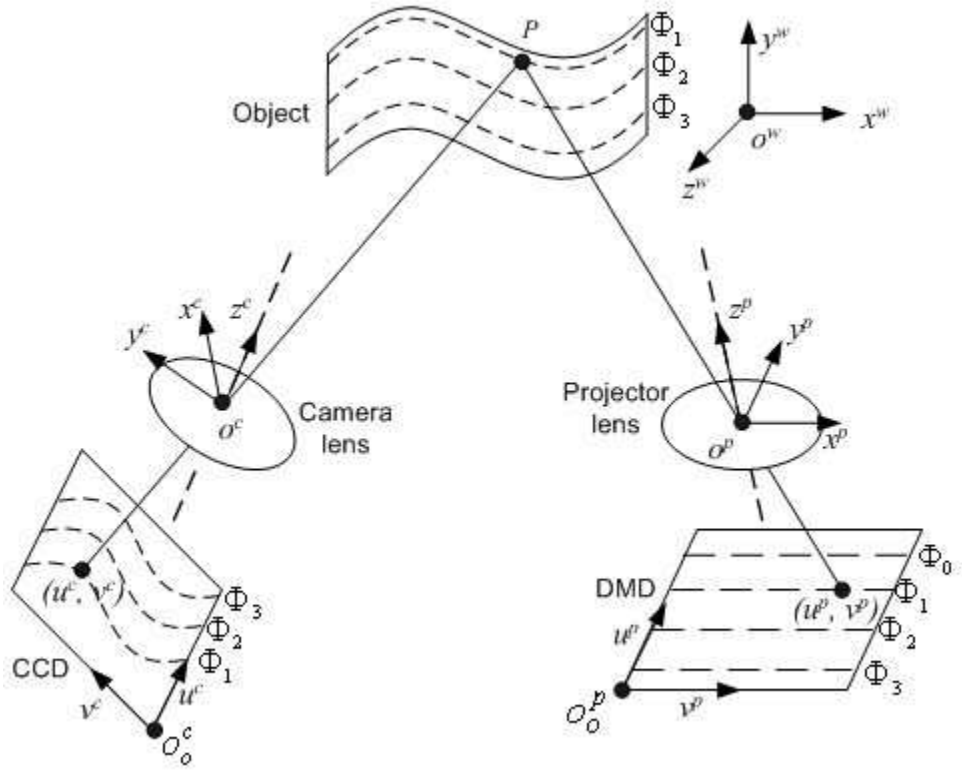

Figure 2.17: Coordinate systems used for 3-D reconstruction.

2.5 3-D Reconstruction

In Fig. 2.17, an arbitrary pixel (u^c, v^c) on the CCD has an absolute phase value Φ_1. The corresponding pixel on the DMD can be found on a line $u^p = \Phi_1$, on which all the pixels have the same absolute phase Φ_1. This pixel correspondence allows the sophisticated camera and projector calibration model to be applied to obtain accurate 3-D coordinate reconstruction results [69]. The coordinate systems used for the 3-D reconstruction is shown in Fig. 2.17. The camera camera (CCD) and projector (DMD) coordinate systems are $\{o^c; x^c, y^c, z^c\}$, and $\{o^p; x^p, y^p, z^p\}$ respectively. The camera image pixel coordinate system and projector image pixel coordinate system are $\{o_0^c; u^c, v^c\}$ and $\{o_0^p; u^p, v^p\}$ respectively. The world coordinate is $\{o^w; x^w, y^w, z^w\}$.

An arbitrary point on P the object surface has the homogeneous coordinate $\{x^w, y^w, z^w, 1\}^T$. The camera image of P is $I^c = \{u^c, v^c, 1\}^T$. The corresponding pixel projector on the projector side is $I^p = \{u^p, v^p, 1\}^T$. The camera and projector are calibrated separately [70]. A^c and $[R^c, T^c]$ are the intrinsic and extrinsic parameters for the camera respectively. A^p and $[R^p, T^p]$

are the intrinsic and extrinsic parameters for the projector respectively. Applying the pinhole model to the camera and projector, we have the following two equations.

$$s^c I^c = A^c[R^c, T^c]P\,, \tag{2.27}$$

$$s^p I^p = A^p[R^p, T^p]P\,, \tag{2.28}$$

where s^c, s^p are the scaling factors for the camera and projector respectively. Observing Eq. 2.27 and Eq. 2.28, we have 7 unknowns, namely (x^w, y^w, z^w), u^p, v^p, s^c, s^p, and 6 equations. From the absolute phase constraint, we can obtain another equation:

$$u^p = f(\Phi(u^c, v^c))\,, \tag{2.29}$$

where function f takes the absolute phase value as input and returns a pixel index, which represents a line on the DMD with the same absolute phase value. Solving Eq. 2.27, Eq. 2.28, and Eq. 2.29 simultaneously, the 3-D coordinates of P in the world coordinate system (x^w, y^w, z^w) can be solved.

2.6 Software Implementation

A C++ program is created to implement the proposed MFTM and to provide a graphic user interface (GUI). A snapshot of the GUI of the program is shown in Fig. 2.18. The program implements multiple document interface (MDI). It can display the 3-D measurement result in real time, while display 3-D snapshots in multiple windows. Other implemented functions include: record a sequence of fringe images, off-line processing a sequence of fringe images, export 3-D point cloud into ASCII format files, save 3-D snapshots, and modifying the projected fringe pattern. Multi-threaded programming is employed to implement the real-time 3-D display.

The FFT operations used in the program is implemented by FFTW library [71]. FFTW is a C subroutine library for discrete Fourier transform (DFT). The FFT functions in the library can perform 1-D or 2-D FFT of arbitrary input size.

2.7 Experimental Results

The proposed modified FTM has been implemented on the digital fringe projection system introduced in Chapter 1. The fringe pattern and the flat pattern are sequentially projected by a digital-light-processing (DLP) projector working in black-and-white (B/W) mode. The fringe and flat patterns are respectively encoded into RGB channels of the DLP projector. A B/W cam-

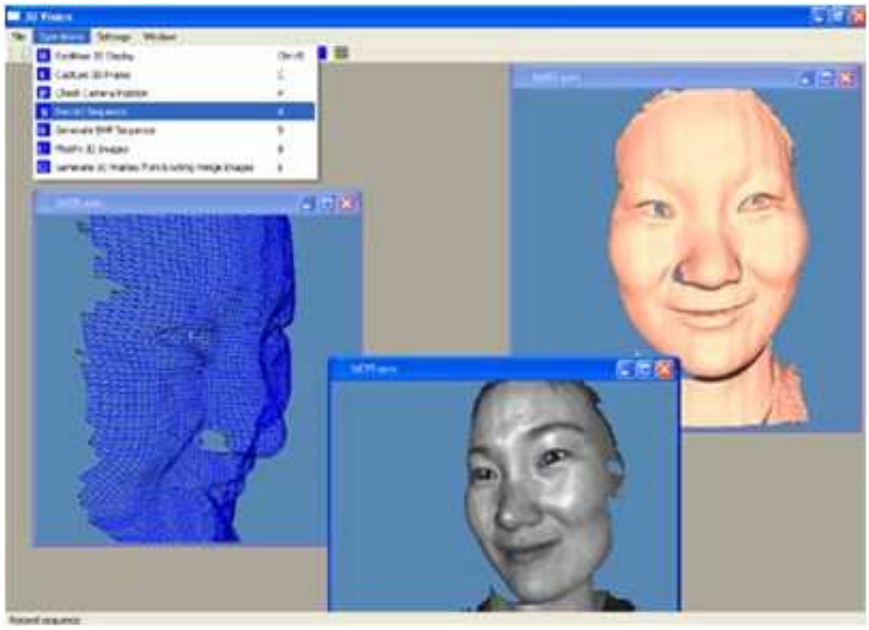

Figure 2.18: Software interface.

era synchronized with the projector's projection timing continuously captures fringe pattern images. Captured flat images and fringe images are differentiate by comparing the intensity differences of two pixels separate by half fringe cycle. The camera and projector are calibrated respectively using a nonlinear calibration method [69].

2.7.1 Projector grayscale calibration

For the flat+fringe pattern projection scheme, the grayscale of the projector needs to be calibrated. Theoretically, if the sinusoidal fringe pattern varies in the range of $[0, 255]$, the intensity of the uniform grayscale pattern should be set to 127 or 128 in order to obtain a flat image that could approximately cancel the zero order terms in the frequency domain. In other words, the mean intensity value of the captured flat image should be approximately equal to that of the fringe image. However, due to the difference between the two color channels of the projector and the nonlinearity of the projector's output, the digital video projector used in our experiment has a small difference between the two mean values. The projector's grayscale output error needs to be compensated in order to make the flat image represent the zero frequency terms.

The following measures are taken to compensate the projector's grayscale

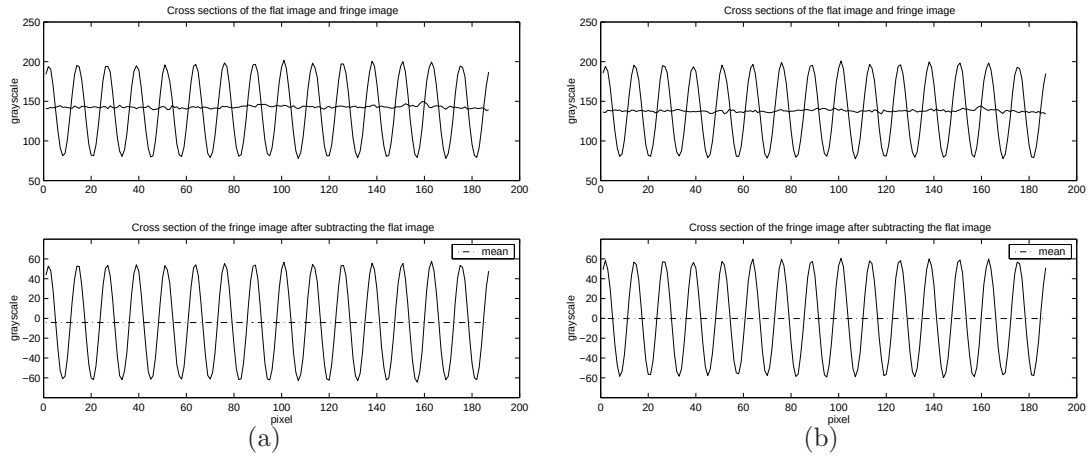

Figure 2.19: Projector grayscale error compensation. (a) Before compensation; (b) After compensation.

error. A white plane board is used. The plane board fills the camera's field of view. First, adjust the projector's bias and contrast until the nonlinearity response between the intensity input and output is minimized. Then, adjust the flat pattern's intensity until the difference between the mean intensity value of the captured flat image and that of the captured fringe image is minimized. The fringe pattern and the flat pattern are projected onto the white board sequentially. The initial intensity value of the flat pattern is set to 128. A single row of pixels with the length of 15 cycles is taken from the same location of the fringe image and and the flat image respectively. The mean intensity values are calculated. Adjust the intensity of the flat pattern based on the previous result to reduce the difference.

In order to lower the influence of the background noise and electronic noise, the average of 10 sets of fringe and flat images are used. Repeat the above process until the two mean values are close enough. The grayscale compensation result is shown in Fig. 2.19. In Fig. 2.19(a), the upper part shows the cross sections of the flat image and the fringe image. The lower part shows the cross section of the fringe image after subtracting the flat image, in which the dashed line indicates the mean value before compensation. The difference of mean values is 4.20 when the intensity of the flat pattern is 128. Fig. 2.19(b) shows the same cross sections after compensation. The mean value of the fringe image after subtracting flat image is reduced to 0.14 after adjust the intensity of the flat pattern to 126.

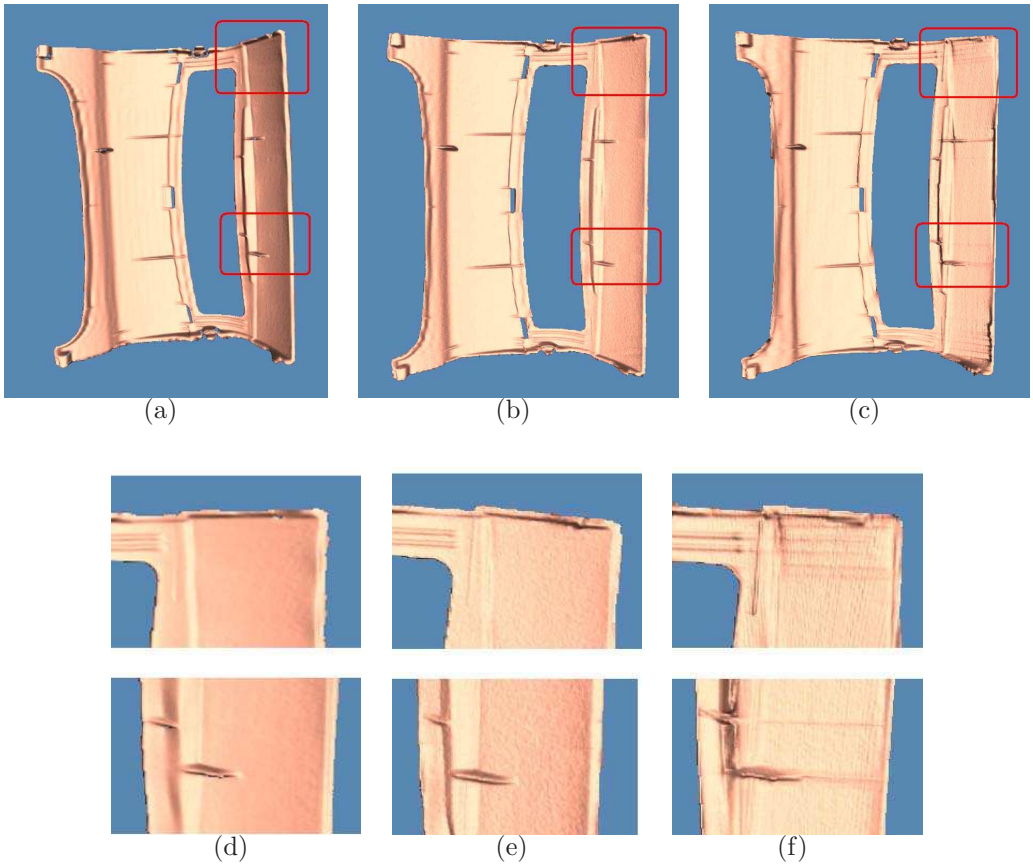

Figure 2.20: 3-D measurement results of a free-form part. (a) Flat+fringe pattern scheme; (b) Three phase-shifted fringe pattern scheme; (c) Conventional FTM method; (d) Zoom-in view of (a); (e) Zoom-in view of (b); (f) Zoom-in view (c).

2.7.2 Measurement of still object with complex shape

In order to compare the proposed MFTM with the conventional FTM, the 3-D shape of the free-form workpiece is measured by use of both fringe projection schemes. Fig. 2.20 shows the 3-D measurement results by use of the flat+fringe pattern scheme, three phase-shifted scheme, and conventional FTM.

Notice that there are slopes on both sides of the part. The zoom-in views of the result from the conventional FTM by use of the same fringe pattern shows the defects caused by the spectrum overlapping and spectrum leakage. Both MFTM fringe projection schemes show significant improvement. Detailed features are preserved in the 3-D results.

2.7.3 Measurement of moving object and changing face sequence

In order to evaluate the performance of the proposed method, the 3-D shape of a moving plaster cylinder is captured by use of the 3-step phase shifting method and MFTM respectively. The cylinder is moving in the horizontal direction at approximately 0.5m/s. The results are shown in Fig. 2.21.

The defects caused by motion are examined on cross sections of the 3-D results. Each cross section is a row in the middle of the along the horizontal direction. The cross sections are fitted into arcs, and the root mean square (RMS) errors on the cross sections are calculated. The difference between the measured data and the fitted data are plotted in Fig. 2.21. The RMS error of 3-step phase shifting method 0.1896 mm. RMS error of flat+fringe patterns 0.0394 mm. RMS error of 3 phase-shifted fringe patterns 0.0477 mm. There is no texture on the cylinder. The ripple-like defects in the results from phase shifting method and MFTM by use of three fringe patterns are caused by the motion. During the capture of 3 fringe patterns, the movement of the cylinder causes misalignment of the fringe pixels, and therefore phase error occurs.

Fig. 2.22 shows two facial expression sequences measured by the proposed method and 3-step phase shifting method respectively. Two sequences are captured by the same fringe projection system. The camera resolution is 640×480 pixels. The face occupies about 1/3 of total image pixels. The subject is speaking with a normal speed. The proposed modified Fourier transform method achieved 3-D frame rate of 25 frame/sec.

Obvious improvements can be observed in the MFTM result. Because there are only two patterns needed for the proposed method, the defects caused by the motion around the mouth area are reduced, compared to the ripple-like defects in the result from 3-step phase shifting method. Also, the periodic vertical lines, which are caused by projector intensity errors, do not appear in the MFTM result. The periodic noise is filtered out in the frequency domain.

Our experimental results show that for the worst case, that is when all image pixels are occupied, the 3-D frame rate achieved 13 frame/second for the camera with resolution of 532×500 pixels. The computer used to obtain the result is Dell Precision 690. The bottleneck for further improving the frame rate is the computational load of FFT. With more advanced fast FFT algorithm and hardware computing power, the frame rate could be further improved.

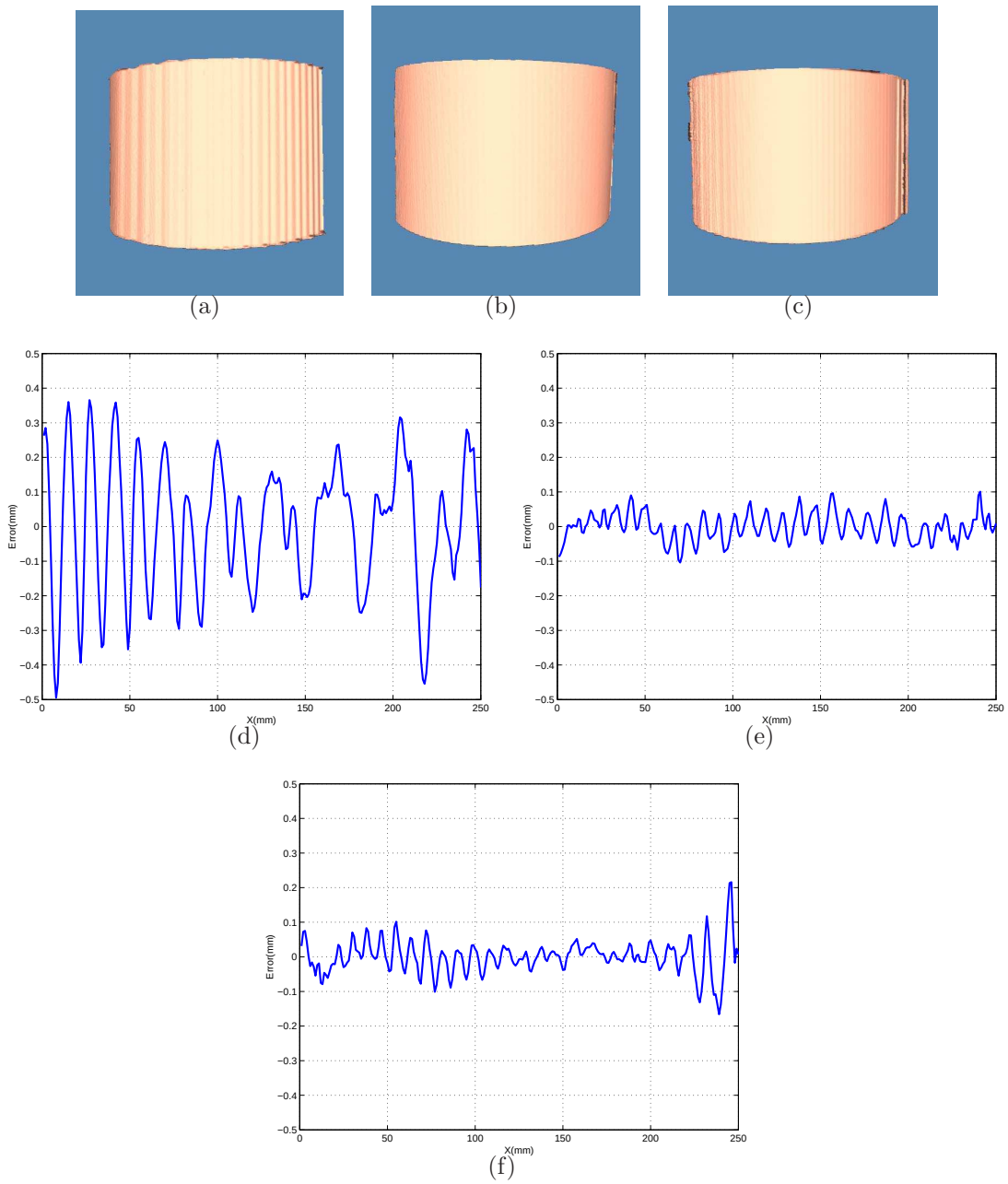

Figure 2.21: A moving cylinder. (a) 3-step phase shifting; (b) MFTM with flat+fringe patterns; (c) MFTM with 3 phase-shifted fringe patterns; (d)-(e)Error on the cross sections of (a)-(c) in the middle of the cylinder along X direction.

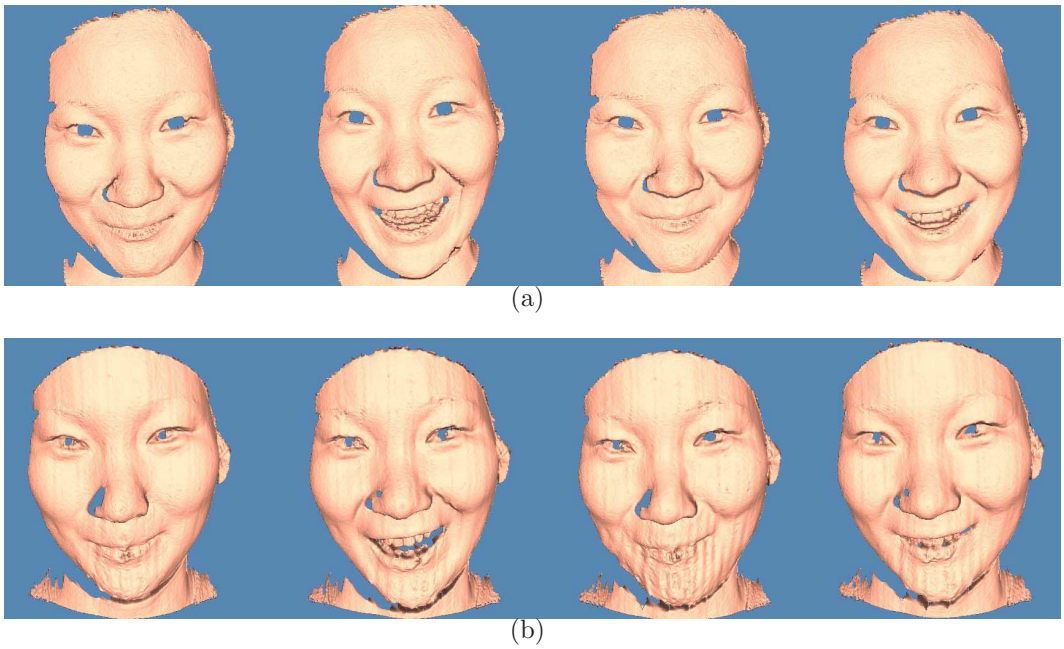

(a)

(b)

Figure 2.22: Facial expression sequences. (a) Result from the proposed method. (b) Result from the 3-step phase shifting method.

2.8 Summary

This chapter has proposed a modified Fourier transform method for real-time 3-D shape measurement. Two fringe projection schemes are proposed to prevent the spectrum overlapping and facilitate the absolute phase retrieval. The forward and inverse 1-D FFT are performed within the areas indicated by the binary mask. The computational load is reduced, and the spectral leakage is alleviated by first extending then windowing the data. The proposed method is implemented on a high-speed digital fringe projection system. The experimental results showed that the proposed method produced better measurement results when measuring object with complex shapes than the conventional Fourier transform method. The system demonstrated substantial improvement on measuring moving and changing objects compared to phase shifting method.

Chapter 3

Phase Shifting Shadow Moiré by use of Carré Algorithm

In this chapter, a novel phase-shifting shadow moiré technique is proposed. The proposed technique has the potential of significantly improving the measurement accuracy and extends the measurement range. The phase shifts are generated by translating the grating in equal steps in the direction perpendicular to the grating plane. Nonuniform phase shifts in the field of view are generated. The Carré algorithm is utilized to process the resulting fringe patterns. The method provides a close form exact solution of the phase map for the first time.

In this chapter, Section 3.1 introduces the principle of shadow moiré technique, and several phase shifting algorithms for fringe pattern analysis. Section 3.2 reviews previous related research work of combining the phase shifting method with shadow moiré technique. Section 3.3 explains the grating removal method. Section 3.4 proposes a novel phase-shifting shadow moiré method. Section 3.5 describes the phase-to-coordinate conversion. Section 3.6 presents the simulation results. Section 3.7 shows the experimental results. Section 3.8 draws the conclusion.

3.1 Introduction to Phase Shifting Shadow Moiré Technique

3.1.1 Principle of shadow moiré technique

Moiré pattern is a beat pattern that appears, for example, when one looks through two identical straight line gratings rotated by a small angle to each other.

The moiré method for 3-D shape measurement utilizes an optical setup to generate a grating pattern that is projected onto the 3-D surface. When a camera observes the 3-D surface from a different perspective through an-

other grating, a moiré pattern is observed as the result of superposing of the straight grating and the deformed grating pattern on the surface. Combined with the optical geometry, the moiré pattern can be analyzed to retrieve 3-D information.

Shadow moiré and projection moiré are two techniques to generate moiré patterns. The application of moiré method to optical shop testing and surface topography has a long history [30, 31]. Shadow moiré has been extensively studied since 1970's, because it has wide applications due to its simple setup and high accuracy. Shadow moiré uses a grating placed above the object. The optical setup is shown in Fig. 3.1. The light source and the camera are at the same distance to the grating plane. When the camera looks though the grating, the shadow of the grating cast onto the object geometrically interferes with the grating itself, and the moiré pattern is observed. The light source does not have to be coherent. The grating can be either binary or sinusoidal pattern. The image captured by the camera is a shadow moiré pattern.

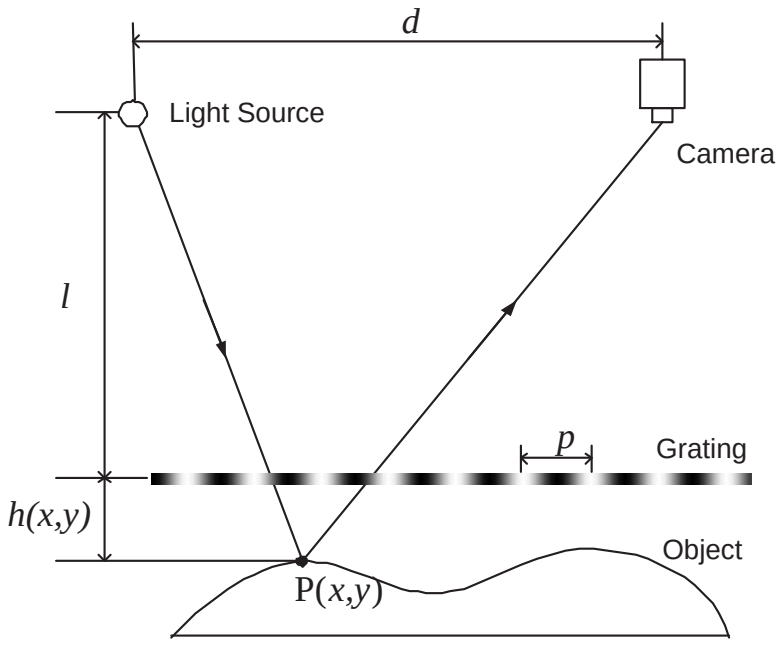

Figure 3.1: Schematic setup of shadow moiré.

Fig. 3.2 shows a shadow moiré pattern generated by computer simulation, in which the grating has sinusoidal intensity distribution and the object is a sphere. The moiré pattern includes the sinusoidal grating pattern itself and the fringe pattern generated by the moiré effect. The fringe pattern contains

useful topography information while the grating pattern is unwanted. After removal of the grating pattern, the fringe pattern can be analyzed by phase shifting or the Fourier transform method.

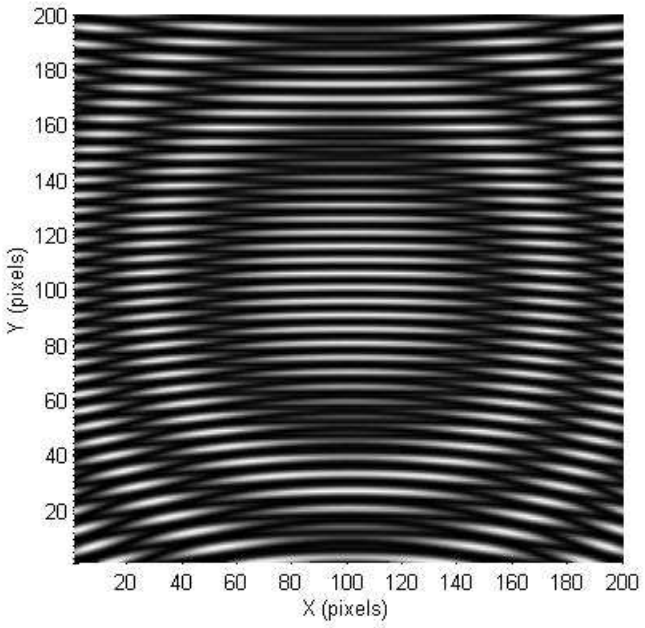

Figure 3.2: Shadow moiré pattern on a sphere.

The 3-D shape of the sphere in Fig. 3.2 can be obtained by first calculating the phase map of the moiré pattern in Fig. 3.1. In Fig. 3.2 the fringe contours contain useful geometric information of the object's surface, while the high frequency grating pattern is useless and is considered as noises. The removal of the unwanted grating patterns will be introduced in Section 3.3. After the unwanted grating pattern being removed, the fringe contour pattern can be expressed as,

$$I(x,y) = I'(x,y) + I''(x,y)\cos[\phi(x,y)]\,, \tag{3.1}$$

where,

$$\phi(x,y) = \frac{2\pi d h(x,y)}{p[l + h(x,y)]}\,. \tag{3.2}$$

In Eq. 3.1, $\phi(x,y)$ is the phase term, $I(x,y)$ is the measured intensity, $I'(x,y)$ is the background intensity, and $I''(x,y)$ is the intensity modulation. In Eq. 3.2, p is the pitch of the sinusoidal grating, d is the distance between light source and the camera, l is the distance from the grating plane to the

light source or camera, and $h(x, y)$ is the surface height measured from the grating plane. The surface height can be solved from Eq. 3.2 pixel by pixel. Note that the phase-height relation is nonlinear.

In order to solve for the height, phase map have to be retrieved first. Among the fringe analysis methods, the phase shifting method is usually employed to obtain the phase map. By combining phase shifting method with shadow moiré, the measurement resolution and accuracy can be greatly improved.

3.1.2 Phase shifting algorithms for fringe analysis

Given a series of phase-shifted fringe patterns, phase shifting algorithms can be used to solve the phase. In order to illustrate the concept of phase-shifting algorithm, several widely phase shifting algorithms are introduced as follows: 3-step algorithm, 4-step algorithm, 5-step algorithm, and Carré algorithm [68, 72].

3-step algorithm is a typical phase shifting algorithm, which handles uniform phase shifts across the whole field of measurement. In 3-step algorithm, three recorded fringe patterns are expressed as

$$I_1(x, y) = I'(x, y) + I''(x, y) \cos[\phi(x, y) + \alpha_1] , \tag{3.3}$$

$$I_2(x, y) = I'(x, y) + I''(x, y) \cos[\phi(x, y) + \alpha_2] , \tag{3.4}$$

$$I_3(x, y) = I'(x, y) + I''(x, y) \cos[\phi(x, y) + \alpha_3] , \tag{3.5}$$

where $\alpha_i = -2\pi/3, 0, 2\pi/3$ are the phase shifts. By solving Eq. 3.3-Eq. 3.5 simultaneously, we have the phase at each pixel,

$$\phi(x, y) = \tan^{-1}\left(\sqrt{3}\frac{I_1 - I_3}{2I_2 - I_1 - I_3}\right) . \tag{3.6}$$

In 4-step algorithm, four fringe patterns (I_1, I_2, I_3, and I_4) are recorded [28, 73]. The phase shifts are $\alpha_i = 0, \pi/2, \pi, 3\pi/2$. The phase term is calculated as

$$\phi(x, y) = \tan^{-1}\left(\frac{I_4 - I_2}{I_1 - I_1 - I_3}\right) . \tag{3.7}$$

In 5-step algorithm, five fringe patterns (I_1, I_2, I_3, I_4, and I_5) are recorded. The phase shifts are $\alpha_i = -\pi, -\pi/2, 0, \pi/2, \pi$ [74, 75]. The phase term is calculated as

$$\phi(x, y) = \tan^{-1}\left(\frac{7(I_2 - I_4)}{-4I_1 + I_2 + 6I_3 + I_4 - 4I_5}\right) . \tag{3.8}$$

The Carré algorithm needs four frames of fringe patterns with constant phase shifts for the same pixel between neighboring frames [76]. The phase shift can be unknown. To solve the phase term, assume the phase shift $\alpha_i = -3\alpha/2, -\alpha/2, \alpha/2, 3\alpha/2$. the phase and phase shift can be solved as

$$\phi(x,y) = \tan^{-1} \frac{\sqrt{[(I_1 - I_4) + (I_2 - I_3)]\,[3(I_2 - I_3) - (I_1 - I_4)]}}{(I_2 + I_3) - (I_1 + I_4)}\,, \tag{3.9}$$

$$\alpha = 2\tan^{-1}\left(\sqrt{\frac{3(I_2 - I_3) - (I_1 - I_4)}{(I_2 - I_3) + (I_1 - I_4)}}\right). \tag{3.10}$$

3.2 Related Work

During the past two decades, various techniques have been proposed to implement the phase shifting method for shadow moiré technique. Most of the previous works employed phase shifting algorithms that require uniform phase shifts across the field, such as the 4-step algorithm. However, for every pixel in the field of view, if the surface height value $h(x, y)$ is not constant, uniform phase shifts in the field of view cannot be obtained by changing any parameter in Eq. 3.2. In that case, the n-step phase shifting algorithms will generate phase error theoretically. However, approximate uniform phase shifts in the field of view can be achieved in practice.

Dirckx *et al.* [77] proposed a phase shifting shadow moiré method by translating the object in the direction perpendicular to the grating plane. The assumption in the method is that with small translation steps, the phase shifts across the whole field-of-view are approximately uniform.

Yoshizawa and Tomisawa [33] proposed a phase shifting shadow moiré technique, in which the light source is translated in the direction parallel to the grating plane and grating is shifted perpendicularly to its own plane, in order to create uniform phase-shifts across the field. The results showed that the phase shifts are approximately uniform within certain fringe orders.

Xie *et al.* [78] proposed a phase shifting shadow moiré scheme by rotating the grating to obtain variation in grating pitch in the observer's point of view. However, the underling assumption was that the measurement range was much less than the distance between the observer and the grating plane ($h(x, y) \ll l$ in Fig. 3.1).

Jin *et al.* [79] proposed to first move the grating vertically and then rotate it. It was still an approximate method and the measurement range was restricted by the pitch of the grating and the rotation angle.

The results of the above-mentioned methods showed improved accuracy.

However, the results have inherent measurement error because the phase shifting algorithms employed all assume uniform phase-shifts across the field. Mauvoisin *et al.* [32] studied possible methods that could produce phase shifts in a shadow moiré setup, which included: changing period of the grating, translating the grating, translating the object, changing the distance between the light source and camera. Their work showed that the uniform phase shifts across the whole field of view for a shadow moiré setup was impossible due to the nonlinearity nature of the height-phase relation, as can be seen later in Eq. 3.2. However, if assuming the depth of measurement to be much less than the distance h between the camera and the grating plane, the phase shifts introduced by object translation perpendicular to the grating plane was shown to be almost uniform.

Degrieck *et al.* [80] proposed a digital implementation of the phase shifting shadow moiré that took into account the non-linearity of height-phase relation. The phase shift is produced by calculating a reference grating image iteratively. The calculation is expensive and depends on an initial guess of the height value.

Until now, no exact close-form solution of height has been proposed for phase shifting shadow moiré method.

3.3 Grating Pattern Removal

Allen and Meadows [81] had shown that translating the grating horizontally in four positions, where neighboring positions are separated by one quarter of the grating period, could remove the unwanted patterns without changing the useful fringe patterns. The proposed technique removes the unwanted grating patterns by translating the grating in its own plane two times. The grating is translated one third of the pitch each time. Suppose the intensity modulation of the grating $T_1(x)$ is given by

$$T_1(x) = \frac{1}{2} + \frac{1}{2}\sin\frac{2\pi x}{p}\,. \tag{3.11}$$

The intensity of the moiré pattern observed by the camera is

$$I_{g1}(x,y) = I_0\left[\frac{1}{2} + \frac{1}{2}\sin\frac{2\pi xl}{p(l+h(x,y))}\right]\left[\frac{1}{2} + \frac{1}{2}\sin\frac{2\pi}{p}\left(\frac{xl+dh(x,y)}{l+h(x,y)}\right)\right], \tag{3.12}$$

where I_0 is the background illumination intensity. Let

$$\theta_0 = \frac{2\pi xl}{p(l+h(x,y))}\,. \tag{3.13}$$

Based on Eq. 3.13, Eq. 3.12 could be rewritten as

$$I_{g1}(x,y) = \frac{I_0}{4}\left[1+\sin\theta_0\right]\left[1+\sin(\phi(x,y)+\theta_0)\right] . \tag{3.14}$$

When translating the grating by $p/3$, intensity modulation of the grating and the moiré pattern intensity are

$$T_2(x) = \frac{1}{2}+\frac{1}{2}\sin\left(\frac{2\pi x}{p}+\frac{2\pi}{3}\right) . \tag{3.15}$$

After applying the new grating modulation, the moiré pattern observed by the camera is rewritten as

$$I_{g2}(x,y) = \frac{I_0}{4}\left[1+\sin\left(\theta_0+\frac{2\pi}{3}\right)\right]\left[1+\sin(\phi(x,y)+\theta_0+\frac{2\pi}{3})\right] . \tag{3.16}$$

Further translating the grating for the third time by $p/3$, intensity modulation of the grating and the moiré pattern intensity are

$$T_3(x) = \frac{1}{2}+\frac{1}{2}\sin\left(\frac{2\pi x}{p}+\frac{4\pi}{3}\right) . \tag{3.17}$$

$$I_{g3}(x,y) = \frac{I_0}{4}\left[1+\sin\left(\theta_0+\frac{4\pi}{3}\right)\right]\left[1+\sin(\phi(x,y)+\theta_0+\frac{4\pi}{3})\right] . \tag{3.18}$$

Averaging the three moiré patterns I_{g1}, I_{g2}, I_{g3}, we have

$$I(x,y) = \frac{I_0}{4}\left(1+\frac{1}{2}\cos\phi(x,y)\right) . \tag{3.19}$$

In Eq. 3.19, the unwanted grating pattern is removed, and only the fringe pattern related to the object surface shape is retained.

Fig. 3.3 shows the grating removal result of a moire pattern generated by simulation. The object is a sphere. The grating has sinusoidal intensity modulation distribution. When the grating is translated one third of the grating pitch in the horizontal direction, the grating pattern is shifted 120° in the moiré pattern, while the moiré pattern (contour pattern) is unchanged. Three moiré patterns are shown in Fig. 3.3(a)-Fig. 3.3(c). After averaging the three images, the grating removal result is shown in Fig. 3.3(d).

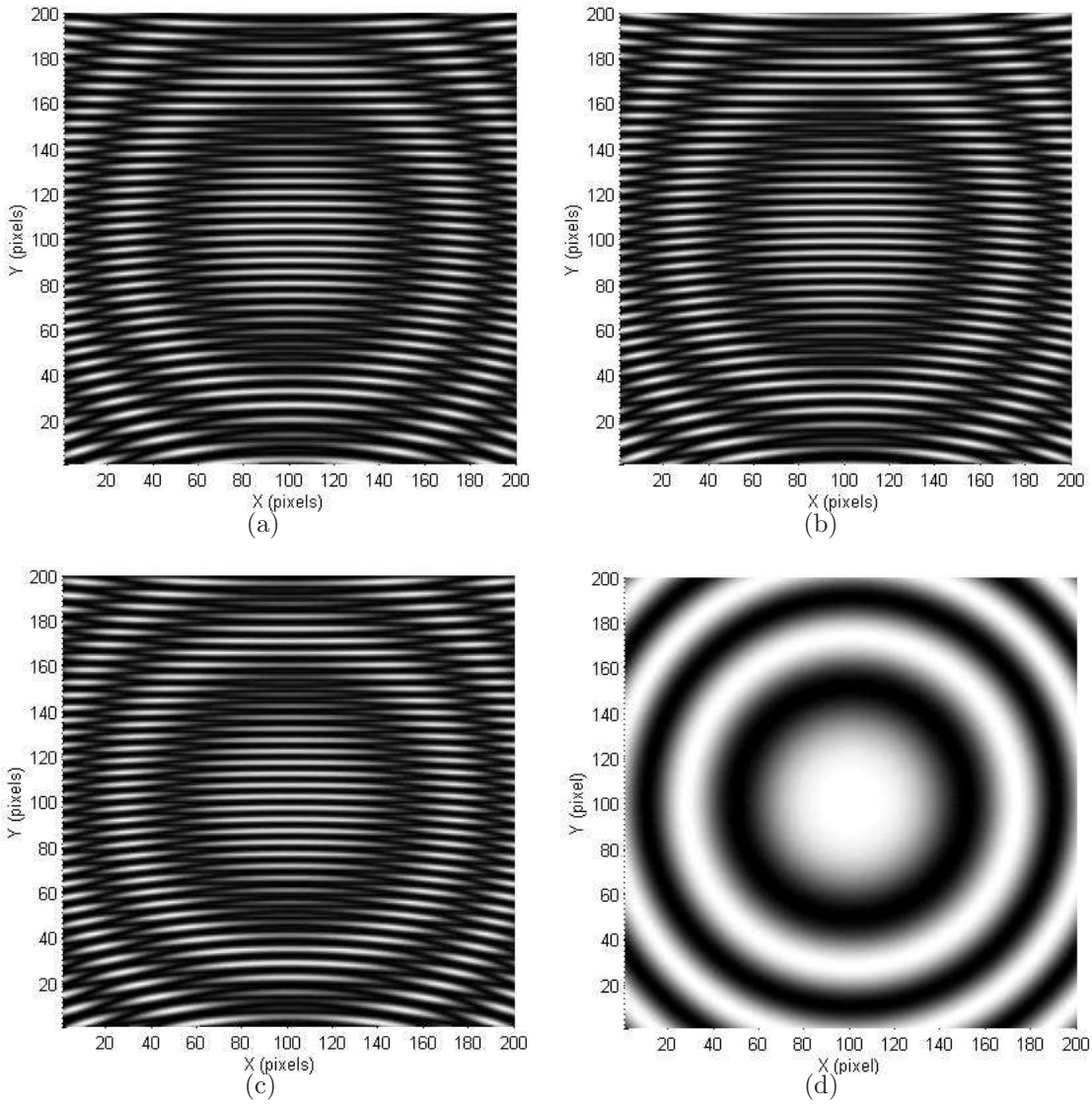

Figure 3.3: Remove grating pattern from the shadow moiré pattern. Grating horizontal translations: (a) 0°; (b) 120°; (c) 240°; (d) Grating removal result.

3.4 Phase Shifting Scheme and Carré Algorithm

The Carré algorithm only requires uniform phase shifts for each individual pixel between frames. Carré algorithm was originally developed to eliminate the need of knowing the exact amount of phase shift in the calculation of the phase map. As long as the phase shift is fixed at each pixel, the phase term can be accurately calculated. Thus it effectively removes the requirement for uniform phase shift across the field. Previous analysis suggests the possibility that the Carré algorithm could be utilized to provide an exact close-form solution of the phase in a shadow moiré setup.

3.4.1 Phase shifting scheme

In the proposed phase shifting scheme for shadow moiré technique, the phase shift is introduced by vertical translation of the grating in equal steps. The schematic diagram of the optical setup is shown in Fig. 3.4. Arrow 1 and 2 indicate the vertical and horizontal grating translation directions. Arrow

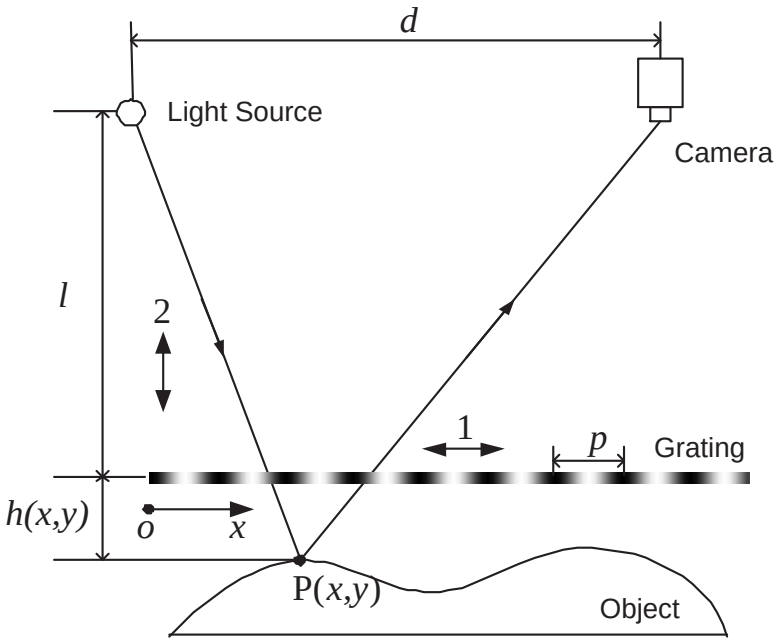

Figure 3.4: Schematic setup of the proposed phase shifting shadow moiré method.

1 indicates the direction of horizontal grating translation, which is for the purpose of removing unwanted grating pattern. The intensity modulation of the grating in Fig. 3.4 is sinusoidal. Two horizontal translation of the grating with one third of the pitch each time generates three moiré patterns with grating the pattern. Based on the grating pattern removal technique introduced in Section 3.3, averaging those three moiré pattern can remove the unwanted grating pattern.

Arrow 2 indicates the horizontal grating translation direction. Translating the grating in the direction perpendicular to the grating plane in equal steps generates uniform phase shifts for each pixel. Suppose there are four different moiré patterns generated at different vertical grating positions (relative to the light source or the camera) $l_i, i = 1, 2, 3, 4$. The phase shift between two neighboring patterns is expressed as

$$\alpha(x, y) = \frac{2\pi d l_{i+1}}{p\left[l_{i+1} + h_{i+1}(x, y)\right]} - \frac{2\pi d l_i}{p\left[l_i + h_i\right]} . \tag{3.20}$$

3.4.2 Carré algorithm

According to Fig. 3.4, for arbitrary point $P(x, y)$, we have

$$l_{i+1} + h_{i+1}(x, y) = l_i + h_i(x, y) . \tag{3.21}$$

Therefore Eq. 3.20 can be simplified as

$$\alpha(x, y) = \frac{2\pi d(l_{i+1} - l_i)}{p\left[l_i + h_i(x, y)\right]} . \tag{3.22}$$

Let the step of the vertical grating translation to be Δl. Then $l_i = l, l + \Delta l, l + 2\Delta l, l + 3\Delta l (i = 1, 2, 3, 4)$. The phase shift can be rewrite in the form of

$$\alpha(x, y) = \frac{2\pi d \Delta l_i}{p\left[l + h(x, y)\right]} . \tag{3.23}$$

In this way, the unform phase shifts for each point are introduced. Applying Carré algorithm to the phase-shifted moiré patterns, the phase term and phase shift are solved by Eq. 3.9 and Eq. 3.10 respectively.

The proposed phase shifting scheme only involves vertical and horizontal translation of the grating. The phase shifts need not to be accurate as long as they are equal. The exact solution of the phase map can be obtained.

3.4.3 Phase unwrapping

The phase values obtained from Eq. 3.9 are wrapped in the range of $[-\pi, \pi]$. Phase unwrapping has to be performed before the height map can be retrieved. The quality-guided path following unwrapping algorithm introduced in Section 2.3.2 is employed here again, in which the phase gradient is selected as the quality index.

The pixels are put in a queue according to the phase gradient from low to high. The one with the smallest gradient is unwrapped first and put into the solution array. And its four neighbors' phase gradients are computed, ranked, and put into the queue. Then, the top pixel in the queue is unwrapped. The unwrapping process in this way until the queue is empty. At the end of the process, the remaining pixels are in the completely isolated areas, caused by shadow or holes. The successful unwrapping process produces a continuous phase map, which is ready to be converted into coordinates.

3.5 3-D Reconstruction

The 3-D surface is reconstructed based on the phase map and the geometry of the shadow moiré setup. The surface height can be determined from Eq. 3.2 and Eq. 3.9 as follows,

$$h(x, y) = \frac{pl\phi(x, y)}{2\pi d - p\phi(x, y)} . \tag{3.24}$$

In order to reconstruct the object's 3-D surface, the X and Y coordinate also need to be calculated. The coordinate systems used in phase shifting shadow moiré is shown in Fig. 3.5. O_c is the optical center of the camera lens. o_c, x_c, y_c, z_c is the coordinate system on the imaging plane of the camera. o_w, x_w, y_w, z_w is the world coordinate system. f is the focal length of the camera. O_c, o_c and o_w are collinear. An arbitrary point on the object surface $P(x, y)$ has an image on the imaging plane $p(x_c, y_c)$. Based on geometry of similar triangles, the X and Y coordinate of P are:

$$x = \frac{x_c(l + h(x, y))}{f} . \tag{3.25}$$

$$y = \frac{y_c(l + h(x, y))}{f} . \tag{3.26}$$

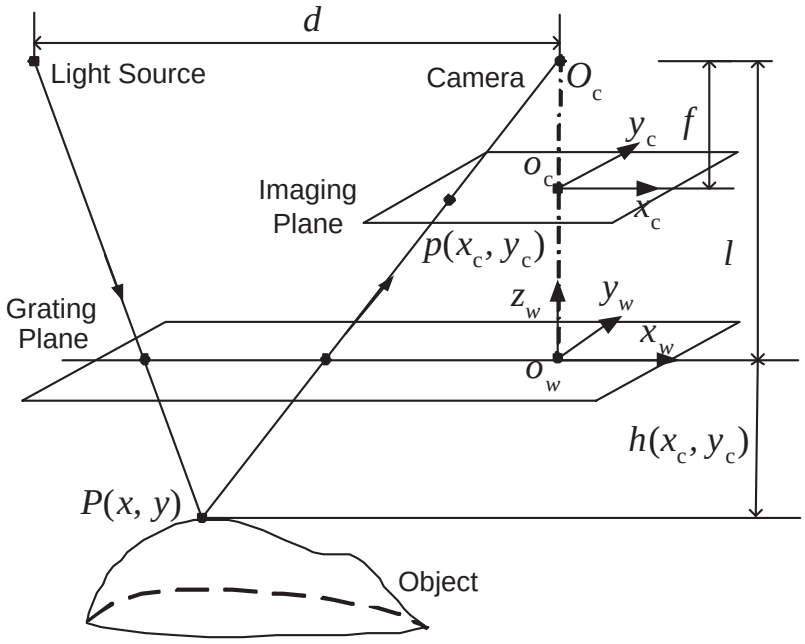

Figure 3.5: Coordinate systems in shadow moiré setup.

3.6 Simulation Results

The principle of the proposed phase shifting shadow moiré technique is verified by a simulation program using MATLAB. The input 3-D model is obtained by the digital fringe projection system introduced in Section 1.1.7. The 3-D image is shown in Fig. 3.6.

The MATLAB simulation program assumes the 3-D model has a diffuse reflection surface and uniform reflectivity. The light source is a point source and the camera has ideal pinhole imaging model. The grating has sinusoidal intensity modulation. We have the shadow moiré patterns shown in Fig. 3.6(b) - Fig. 3.6(d). They are obtained by translating the grating horizontally two times. By averaging three patterns, the unwanted grating pattern is removed. Image without grating pattern is shown in the first picture of Fig. 3.7.

Then, vertically translate the grating in three steps and repeat the above grating removal procedure at each step. We have four phase shifted fringe patterns shown in Fig. 3.7.

The Carré algorithm is applied to the four phase-shifted fringe patterns. The wrapped phase map $\phi(x, y)$, unwrapped phase map and phase shift map $\alpha(x, y)$ are obtained, as shown in Fig. 3.8.

Although Carré algorithm does not require the phase shifts to be known,

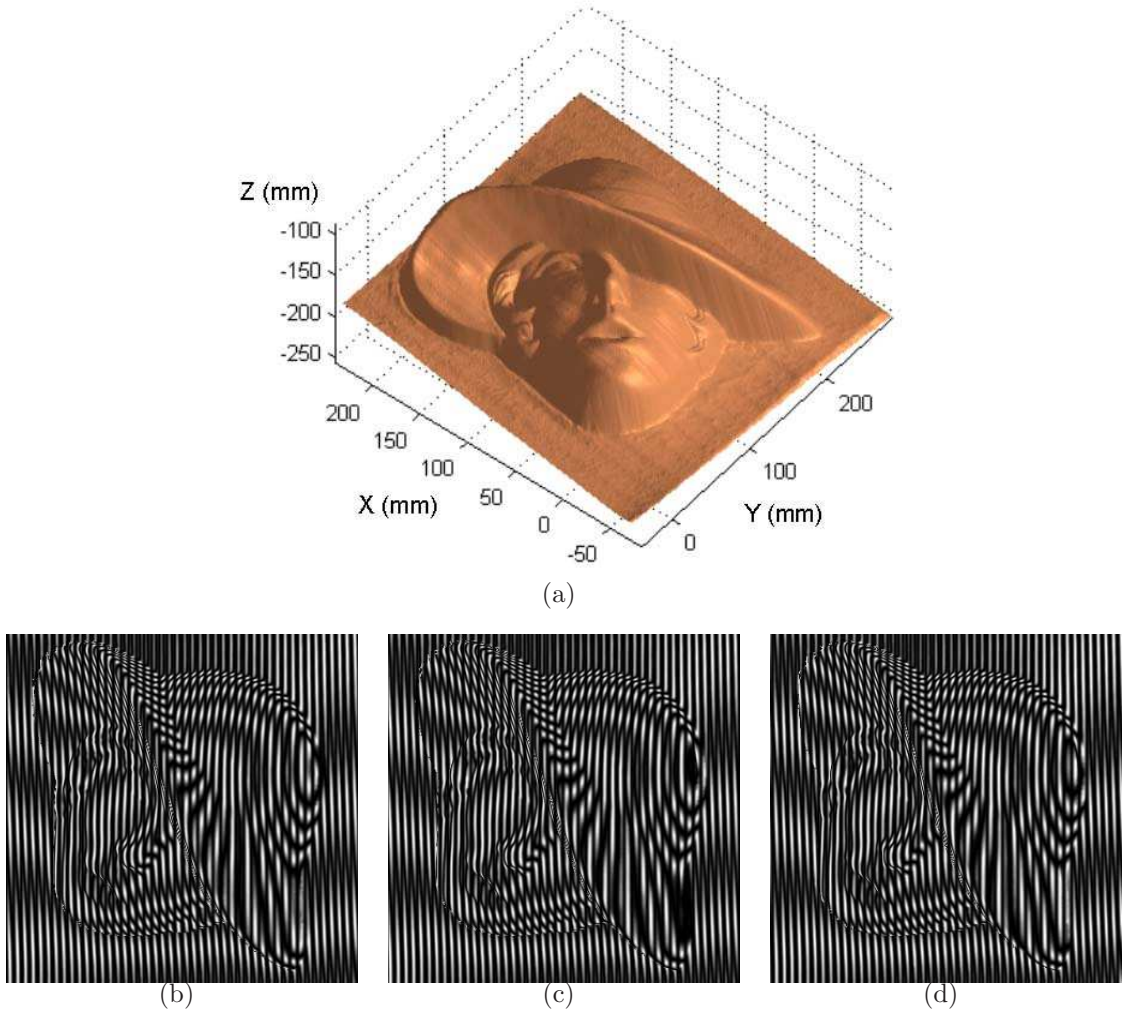

Figure 3.6: Shadow moiré patterns. (a) Input 3-D model; Grating horizontal translations: (b) 0°; (c) 120°; (d) 240°

.

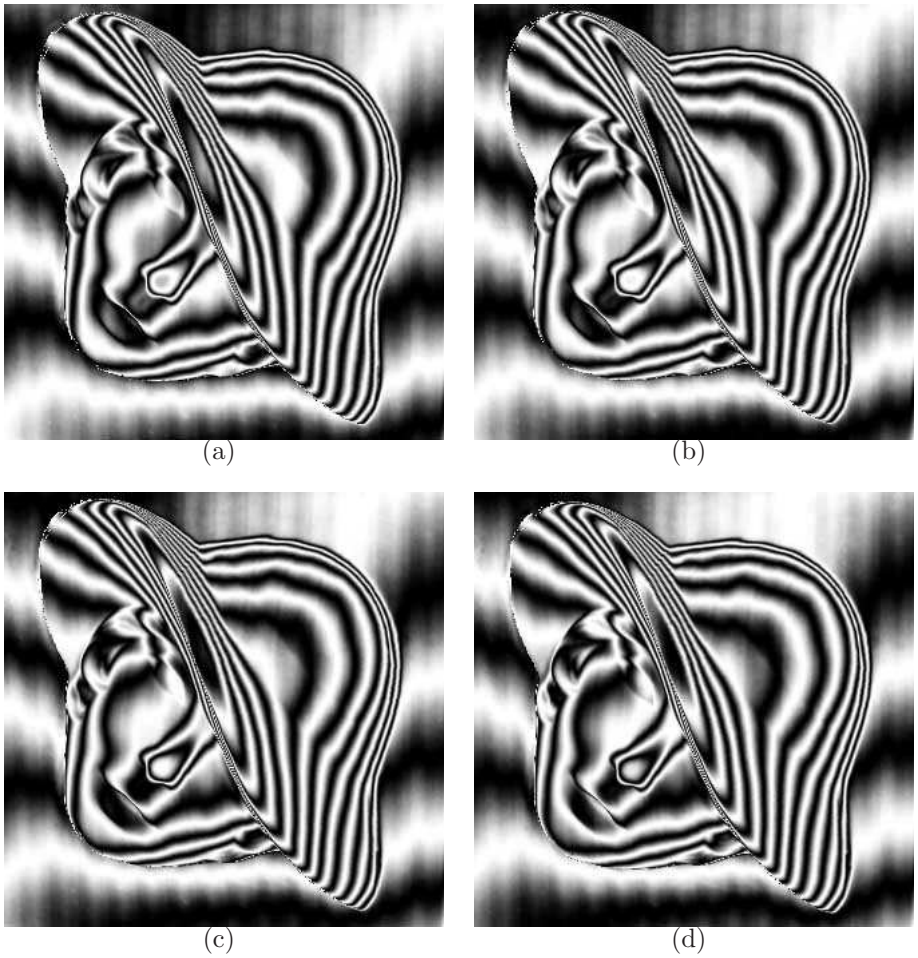

Figure 3.7: Phase-shifted moire patterns with grating pattern removed. (a)-(d) Four phase-shifted fringe patterns.

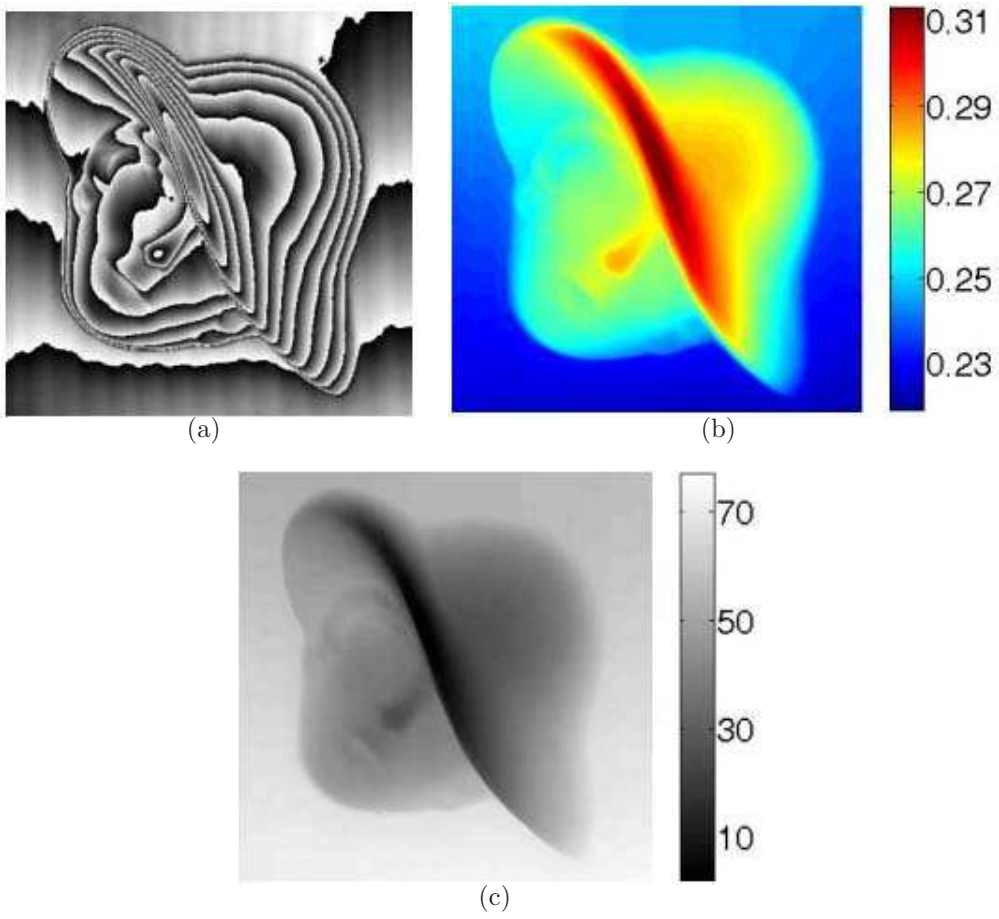

Figure 3.8: Simulation results. (a) Wrapped phase map; (b) Phase shift distribution $\alpha/2$ (rad); (c) Unwrapped phase map (rad).

a range of phase shift is preferred for minimizing the phase error. Theoretically, the phase term can be calculated for any phase shift step by Eq. 3.9. However, when systematic error and random error occur in the fringe images, $[(I_1 - I_4) + (I_2 - I_3)]\,[3(I_2 - I_3) - (I_1 - I_4)]$ could be a negative number and result in complex phase value.

Carefully selected phase shift steps can reduce the risk of complex phase value when systematic and random errors are inevitable. The relation between phase error and phase shift step has been studied in previous literature [82, 83, 84]. Phase error of phase shifting shadow moiré is generated by systematic phase shift error, systematic intensity error, and random intensity error. Phase shift steps between 90°-120° have been proved to reduce the influence of systematic and random errors.

In the proposed phase shifting scheme for the shadow moiré setup, each pixel's phase shift step is determined by the height value of that pixel. Most pixels should have phase shift steps in the range of 90°-120°. Fig. 3.8(b) shows the $\alpha/2$ value distribution (phase shift step of the Carré algorithm is α).

With the unwrapped phase map, the 3-D reconstruction is performed. The 3-D image is shown in Fig. 3.9. The 3-D shape of the input model is accurately reconstructed. The simulation successfully verified the proposed phase shifting shadow moiré method.

3.7 Experimental Results

Experiments were conducted on a NIST (National Institute of Standards and Technology) calibration block and a concave lens respectively. The grating employed is dense enough (100 lines/inch), so that the grating pattern is not visible in the moiré pattern. d and l in Eq. 3.24 are both 787.4 mm. The vertical grating translation step is 69.6 μm. Four phase-shifted moiré patterns were obtained, which are shown in Fig. 3.10 and Fig. 3.12 respectively.

The vertical translation step of the grating and the height of the objects are very small compared to l. Therefore, according to Eq. 3.23, the phase shift variation across the field of view is relatively small. The phase shifts in both experiments are about 90° in the field of view. The wrapped phase maps, unwrapped phase map, and reconstructed 3-D surfaces of the calibration block and the concave lens are obtained are shown in Fig. 3.11 and Fig. 3.13. The NIST calibration block is 2 inch square. The height of the step on the block is calibrated as 209.04 μm. The calculated step height by the proposed method is 205.78 μm. The error is 3.26μm.

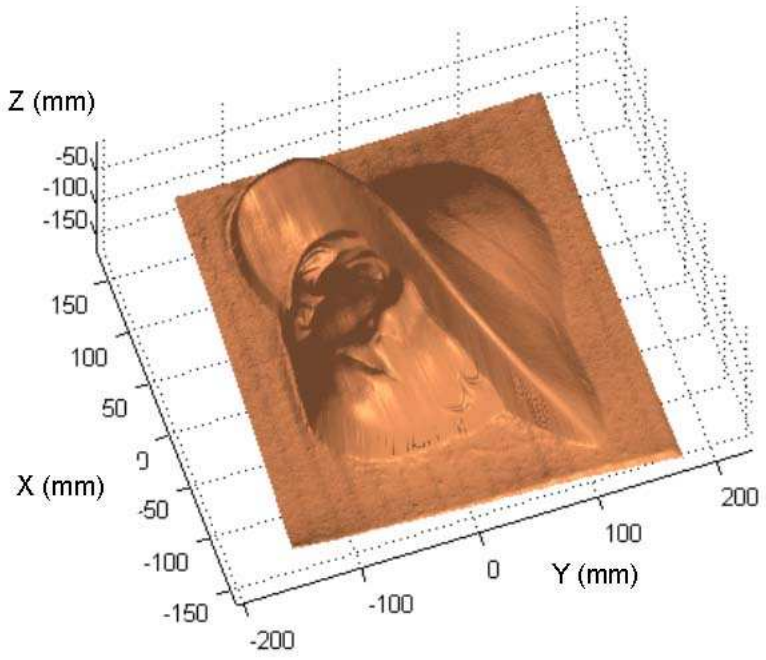

Figure 3.9: 3-D surface obtained by the proposed phase shifting shadow moiré method

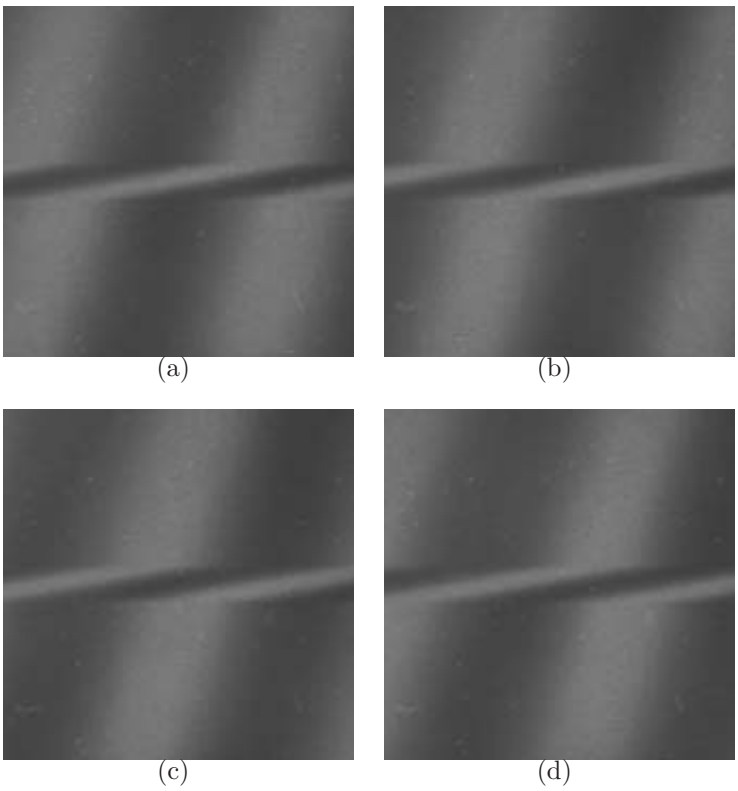

Figure 3.10: Phase-shifted moiré patterns of a NIST calibration block.

3.8 Summary

Due to the nonlinearity relation between the phase and geometry parameters of the optical setup, it has been difficult to apply phase shifting method in the shadow moiré technique for 3-D shape measurement. In this paper, a phase shifting shadow moiré method is proposed to provide a simple phase shifting scheme and an exact close form solution for the phase map. In our proposed method, the grating is translated in equal steps in the direction perpendicular to the grating plane to introduce phase shifts. It is demonstrated that the phase shifts are uniform for each pixel, while they are nonuniform across the field of view. The proposed method takes advantage of the Carré algorithm's ability of handling nonuniform phase shifts across the field to provide an exact close-form 3-D shape measurement result for the shadow moiré setup. The phase value at each point is determined by the Carré algorithm. The proposed method is successfully verified by computer simulation and the experimental results.

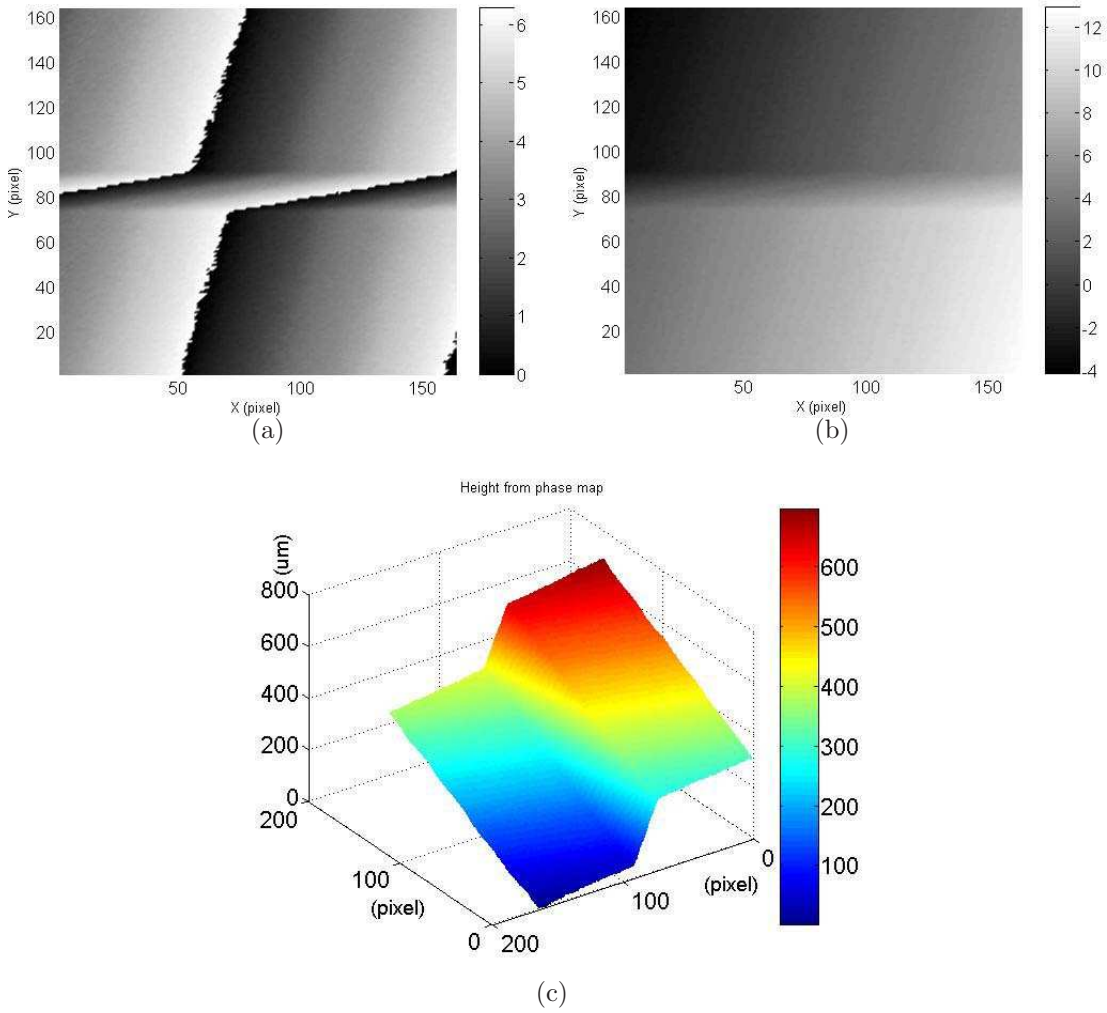

Figure 3.11: Measurement results of a NIST calibration block. (a) Wrapped phase map (rad); (b) Unwrapped phase map (rad); (c) Height map (μm).

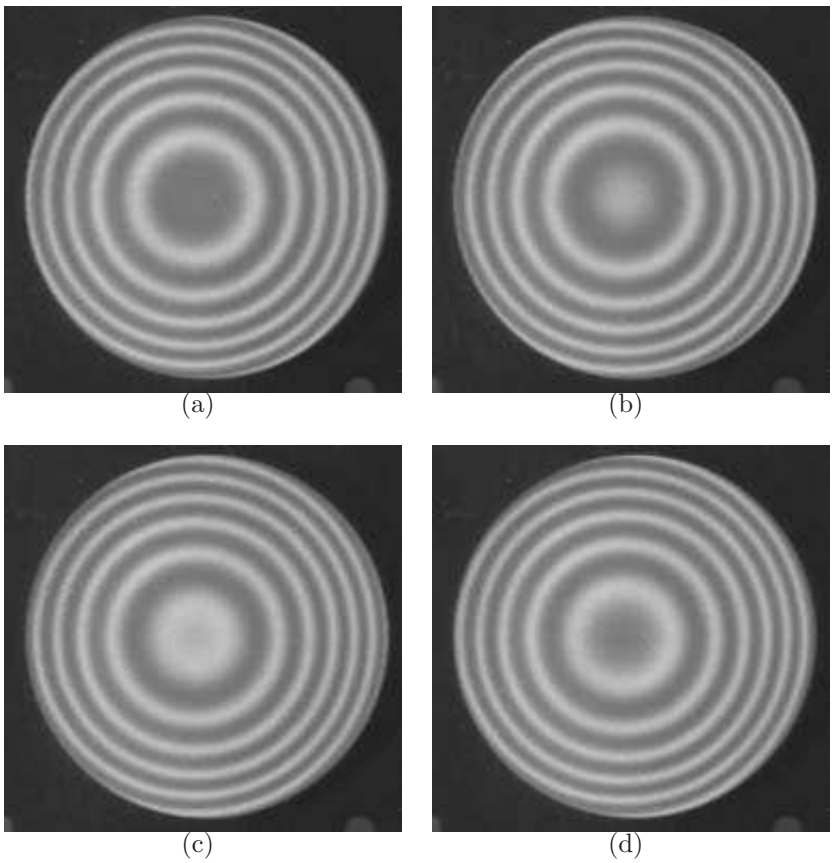

Figure 3.12: Phase-shifted moiré patterns of a lens.

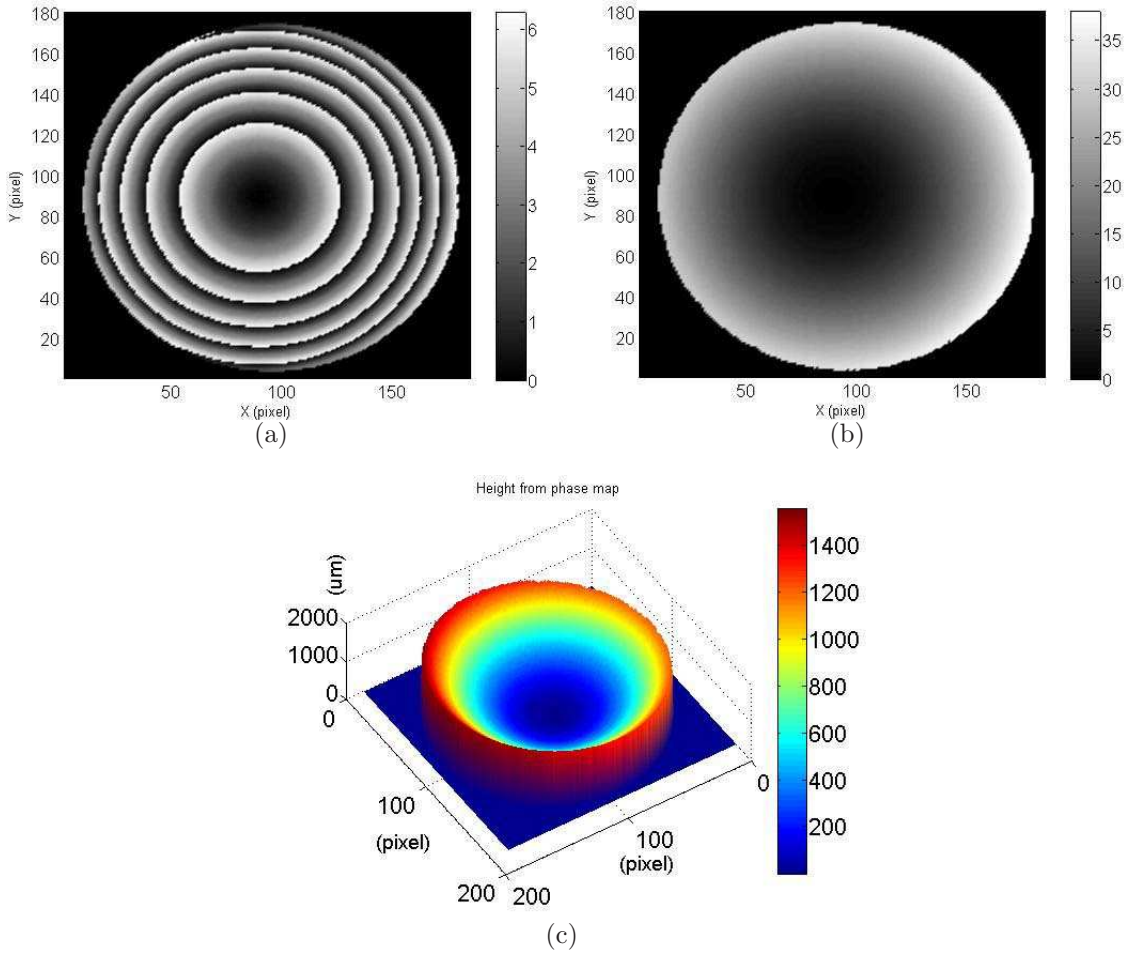

Figure 3.13: Measurement results of a lens. (a) Wrapped phase map (rad); (b) Unwrapped phase map (rad); (c) Height map (μm).

Chapter 4

Face Recognition Based on Fringe Pattern Analysis

This chapter introduces a novel face recognition method that takes advantage of the 3-D information of the face without reconstructing the 3-D coordinates. Two fringe pattern analysis methods, namely phase shifting method and the Fourier transform method, are employed. Three phase-shifted fringe images are analyzed and the background illumination and texture are removed. The resulting fringe pattern contains only 3-D facial geometry related information. Fourier transform is applied to the resulting fringe pattern and the filtered Fourier spectrum of the resulting fringe pattern is generated. Principal component analysis (PCA) is applied to the face spectra to perform face recognition. The proposed method is robust to background illumination and skin texture variation and has reduced computation and storage expenses compared to 3-D face recognition algorithms.

4.1 Introduction

Human beings recognize faces not long after they were born. However, face recognition has never been an easy task for machines. In recent years, human face recognition has been attracting more and more researchers because of its wide applications in security surveillance, law enforcement, information control, and entertainment [43]. Compared with other human biometrics, collecting face images requires less subject cooperation and awareness than those of fingerprints, irises, voice or signature.

Face recognition techniques based on 2-D intensity images have been extensively studied [41, 85, 86, 87, 88]. The recognition performance of 2-D techniques significantly relies on the consistency of the illumination and the skin texture for the same person. The cause of facial skin texture variation can be facial makeup, tanning, or aging. The illumination variation is caused by different lighting conditions, such as outdoor, indoor, or controlled lighting

environments. Even in an indoor controlled lighting environment, different cameras or the same camera with changed settings can produce face images with considerable intensity variations. Although preprocessing such as histogram equalization is usually performed, maintaining intensity consistency is difficult for 2-D face recognition techniques. The influence of skin texture and illumination variation can be eliminated by use of 3-D face data [89, 90, 91, 92]. Facial 3-D geometry is represented in the form of point cloud, profiles, or mesh. However, apart from the computational complexity of 3-D recognition algorithms, the reconstruction and storage expenses of the 3-D surface geometry are high.

In this chapter, a face recognition method based on fringe pattern analysis is proposed, which directly utilizes 2-D images generated by a structured light system without reconstructing the 3-D geometry. A high-speed digital fringe projection system is employed to project three phase-shifted sinusoidal fringe patterns onto the subject's face. First, the face fringe patterns are analyzed by the phase shifting method to generate one fringe pattern without any texture or background illumination. Then, the resultant fringe patterns are transformed into the spatial frequency domain. The spectra related to the 3-D facial geometry are extracted. Finally, the eigenface algorithm is applied to the face spectra to perform face recognition. The advantages of the proposed method include immunity to skin texture and background illumination variations; and the reduced computation and storage expenses compared to 3-D face recognition algorithms.

This chapter is organized as follows. In Section 4.2, the digital fringe projection technique is briefly introduced and the related work is reviewed. Section 4.3 presents digital fringe projections system and the proposed face fringe pattern analysis method. Section 4.4 describes the face normalization. Section 4.5 introduces the eigenface algorithm employed for to accomplish the recognition task. Section 4.6 shows the experimental and simulation results. The conclusion is drawn in Section 4.7.

4.2 Background and Related Work

The digital fringe projection technique has been studied as a structured light method for 3-D shape measurement of freeform surfaces. A digital video projector sequentially projects phase-shifted sinusoidal fringe patterns onto the object surface. When observed from a different perspective by the camera, the fringe pattern is distorted by the 3-D shape of the object. The captured fringe image contains 3-D shape of the object along with the surface reflectance and background illumination. The phase term in the sinusoidal function is

directly related to the 3-D shape information. Therefore, phase shifting or the Fourier transform method is applied to solve the phase map of the sinusoidal fringe pattern [68]. The 3-D reconstruction process includes three steps. First, the phase map is unwrapped to remove the 2π ambiguities [51]. Then the unwrapped phase map is used to solve the correspondence between the camera pixels and the projector pixels [70, 93]. With the intrinsic and extrinsic calibration parameters of the camera and projector, 3-D coordinates are reconstructed for each pixel [70]. The virtues of the digital fringe projection technique include non-contact, fast and high-resolution measurement.

The digital fringe projection technique has been successfully employed for 3-D face data acquisition [94, 95]. Much research has been done to utilize the 3-D face data obtained from various other structured light techniques for face recognition, such as laser scanning [96, 97], binary stripe pattern projection [98, 99], and rainbow camera [100]. Comparatively little research work has been done about utilizing the 3-D information encoded in the 2-D image captured by a structured light system without reconstructing the 3-D geometry. Andrade *et al.* proposed a electronic-optical 3-D face recognition system that matches the moiré patterns by use of optical technqiues [101]. The unknown subject's face is structurally illuminated and a moiré pattern is observed, which encodes the 3-D information of the face. The known reference moiré pattern is mixed with the unknown one and processed by the electronic-optical system. The recognition decision is made based on the output of the matching. Esteve-Taboada *et al.* proposed a 3-D object recognition method that examines the correlation of the grating patterns[102]. The method projects a grating pattern onto the object surface and records the distorted grating pattern. The distorted grating pattern and a reference pattern is processed by a modified joint transform correlation (JTC) technique to achieve 3-D object recognition. Both methods demonstrated fast recognition speed by directly utilizing 3-D information in the 2-D images. However, the disadvantages of the above techniques are that the hardware system is complicated and the one by one recognition process is not suitable for large database.

In this research, we propose to utilize the 3-D information encoded in the fringe patterns by use of the fringe analysis methods without going through the 3-D reconstruction process. Phase shifting method solves the phase map from a series of sequentially captured fringe patterns with known phase shifts. The background illumination and texture terms of the fringe pattern can be explicitly solved. Therefore, one of the advantages of phase shifting method is the robustness to illumination and texture variations. The Fourier transform method takes on a different perspective on how to solve the phase map. The fringe pattern is transformed into the spatial frequency domain, where the

phase terms is modulated by the surface reflectivity and are separated from the background illumination by the fringe frequency. The phase terms are extracted by filtering and then taken inverse Fourier transform. The phase map is the imaginary part of the result. Only a single fringe pattern is needed by the Fourier transform method. The drawback of the Fourier transform method is that the background illumination and surface texture severely affect the resulting phase map. For the purpose of face recognition, combining both fringe analysis methods provides a means to represent the the 3-D face in the spatial frequency domain without the influence of the background illumination and texture variations.

4.3 Principle

4.3.1 Digital fringe projection system

The digital fringe projection system utilized in this research has been introduced in Chapter 1. It consists of a digital video projector and a black-and-white (B/W) camera. The schematic system diagram is shown in Fig. 4.1. The projector is based on the digital light processing (DLP) technology. The projected pattern is formed on a digital-micromirror-device (DMD). Three phase-shifted sinusoidal fringe patterns are generated by computer and encoded in the red, green, and blue (RGB) color channels of a color image. Based on the working principle of DMD, the contents of the three color channels are projected sequentially at a high frequency (180 Hz). Because the projector works in B/W mode, three fringe patterns are sequentially projected onto the subject's face. The camera, which is synchronized with the projector, captures the fringe pattern from an offset angle at a speed of 90 frames/second. The data acquisition time for a set of 3 phase-shifted fringe pattern is 33 ms. Therefore, subjects do not have to sit still for several seconds for the data acquisition.

4.3.2 Texture and illumination removal

Three-step phase shifting method is employed to analyze the fringe patterns. Three phase-shifted sinusoidal fringe patterns could be written in the following forms:

$$I_R(x,y) = 255[1 + \cos(2\pi f_0 x - 2\pi/3)]\,, \tag{4.1}$$

$$I_G(x,y) = 255[1 + \cos(2\pi f_0 x)]\,, \tag{4.2}$$

$$I_B(x,y) = 255[1 + \cos(2\pi f_0 x + 2\pi/3)]\,, \tag{4.3}$$

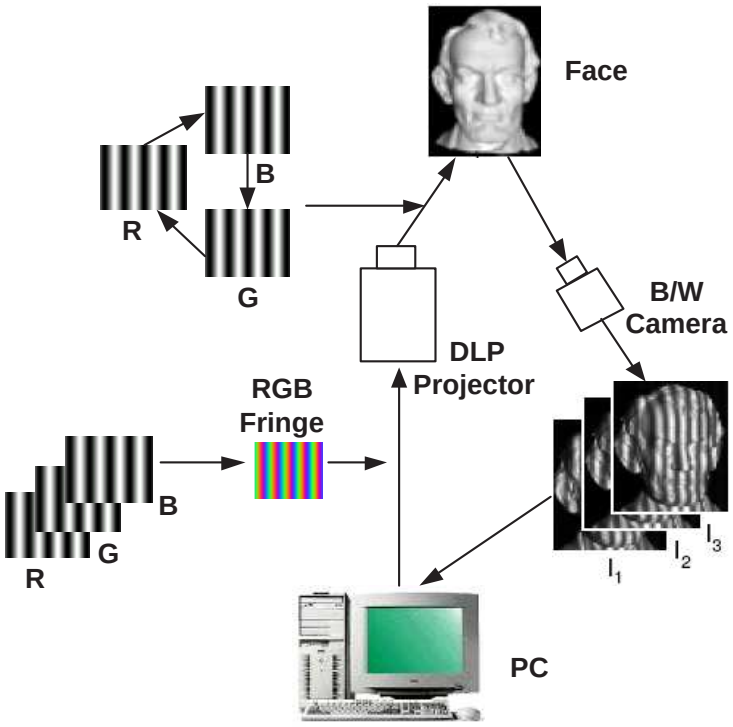

Figure 4.1: System diagram of the digital fringe projection system.

in which, x and y are the pixel indexes, f_0 is the frequency of the sinusoidal pattern, and the phase shift is $2\pi/3$. The three deformed fringe patterns captured by the synchronized camera are expressed as:

$$I_1(x,y) = I'(x,y) + I''(x,y)\cos[2\pi f_0 x + \phi(x,y) - 2\pi/3]\,, \tag{4.4}$$

$$I_2(x,y) = I'(x,y) + I''(x,y)\cos[2\pi f_0 x + \phi(x,y)]\,, \tag{4.5}$$

$$I_3(x,y) = I'(x,y) + I''(x,y)\cos[2\pi f_0 x + \phi(x,y) + 2\pi/3]\,, \tag{4.6}$$

where $I'(x,y)$ represents the background illumination or ambient light illumination. $I''(x,y)$ relates to the facial skin texture reflectivity. $\phi(x,y)$ is the phase information that contains the 3-D facial geometry. We could solve the background illumination and facial texture by solving Eq. 4.4, Eq. 4.5 and Eq. 4.6 simultaneously,

$$I'(x,y) = \frac{I_1 + I_2 + I_3}{3}\,, \tag{4.7}$$

$$I''(x,y) = \frac{\sqrt{3(I_1 - I_3)^2 + (2I_2 - I_1 - I_3)^2}}{3}\,. \tag{4.8}$$

The texture and illumination can be removed from one of the fringe image $I_2(x,y)$, resulting in a fringe image $I_f(x,y)$,

$$I_f(x,y) = \frac{I_2(x,y) - I'(x,y)}{I''(x,y)} = \cos[2\pi f_0 x + \phi(x,y)]\,. \tag{4.9}$$

The result in Eq. 4.9 is an image that only contains the 3-D face profiles. The intensity values of the pixels are in the range of $[-1,1]$. To visualize the result, it is normalized into the grayscale range of $[0,255]$ in Eq. 4.10.

$$I_{fn}(x,y) = \frac{255}{2}\{1 + \cos[2\pi f_0 x + \phi(x,y)]\}\,. \tag{4.10}$$

When the surface reflectivity is too low (e.g. shadow, black hair or beard), $I''(x,y)$ will be too close to zero. A threshold is set for $I''(x,y)$ to prevent Eq. 4.9 from generating unstable result. Fig. 4.2 shows the phase-shifted fringe patterns and the fringe pattern after texture and illumination removal. The resulting fringe pattern contains only the distorted fringe lines which represents the 3-D geometry related information. The skin texture is completely removed. The grayscale intensity of the pixels on eyes, hair and eyebrows are set to zero by the reflectivity threshold.

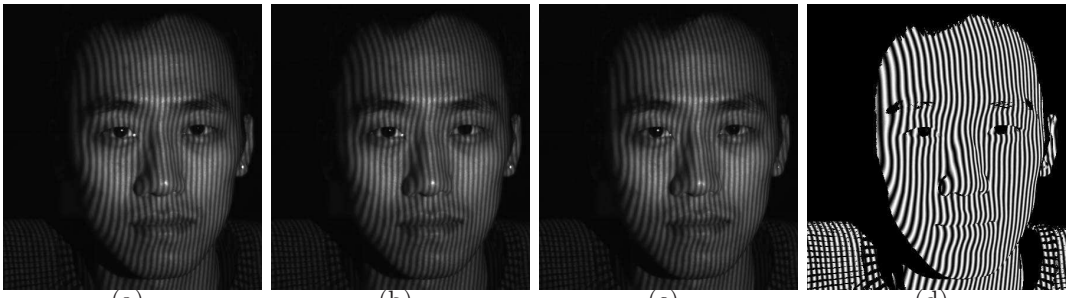

(a) (b) (c) (d)

Figure 4.2: Skin texture and illumination removal. (a)-(c) three phase-shifted fringe patterns; (d) fringe pattern with skin texture and background illumination removed.

4.3.3 Fourier spectra of fringe image

The fringe pattern shown in Fig. 4.2(d) can not be directly used for face recognition in that the resultant pattern's horizontal position shifts between different images of the same subject. For example, the nose tip may appear in the dark part of the fringe in one image while in the bright part in another image of the same person.

The 3-D shape information encoded in a distorted fringe pattern can be extracted in the spatial frequency domain [40]. This principle has been adopted by the Fourier transform methods for optical 3-D shape measurement. Here, we utilize this principle to obtain the 3-D face information in the form of Fourier spectra, which can be further processed by existing pattern recognition algorithms. Applying Euler's formula, Eq. 4.9 can be rewritten in the following form:

$$I_f(x,y) = c(x,y)e^{i2\pi f_0 x} + c^*(x,y)e^{-i2\pi f_0 x}\,, \tag{4.11}$$

where $c(x,y) = 1/2e^{i\phi(x,y)}$. Taking 1-D Fourier transform of Eq. 4.11 with respect to x, we have

$$G(f_x,y) = C^*(f+f_0,y) + C(f-f_0,y)\,. \tag{4.12}$$

The Fourier spectra and the band-pass filter are shown in Fig. 4.3. The spectra containing the phase term $\phi(x,y)$ concentrate around the carrier frequency $(f_0,-f_0)$, and are symmetrical in the frequency domain. Either of the conjugate terms $C^*(f+f_0,y)$ or $C(f-f_0,y)$ can be employed. Fig. 4.4 is the frequency spectrum of the fringe image shown in Fig. 4.2(d). In order to reduce the data size for further computation, the spectra around f_0 is extracted

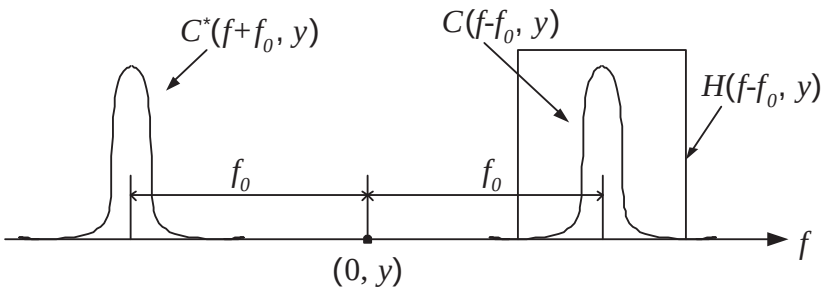

Figure 4.3: Fourier spectra ($|G(f_x, y)|$) of the processed fringe pattern.

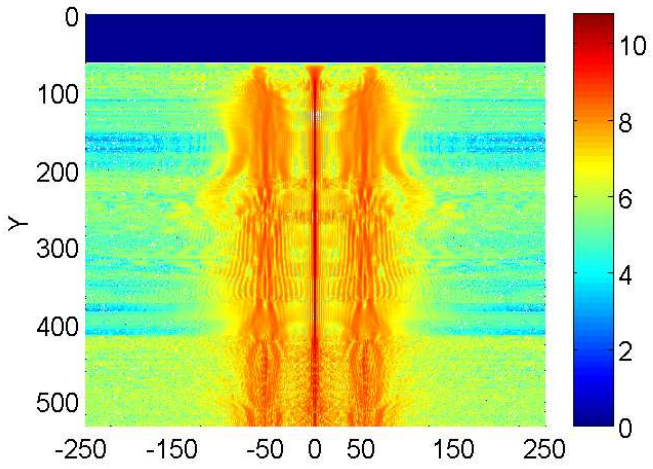

Figure 4.4: Fourier spectra of Fig. 4.8(c)

by a band-pass filter. Theoretically, there should be no zero frequency component in the spatial frequency domain since the background illumination term $I'(x, y)$ has been removed. However, zero frequency components exist as a result of the low reflectivity areas filled with zeros, especially the non-face background in the image. Therefore, a band-pass filter is necessary. Because only half of the spectra is enough to represent the 3-D face information, the data size is greatly reduced.

4.4 Face Image Normalization

A 2-D face image without fringe can be obtained by averaging three phase-shifted fringe patterns in Eq. 4.4∼Eq. 4.6. The centers of eyes, mouth and the face area are detected in the face image by using the Viola-Jones method [103]. Based on the eye centers and the face area detected, the fringe patterns are cropped to keep only the face area aligned by the eye positions. The normalization is applied to the face fringe pattern shown in Fig. 4.2. Face area detection result is shown in Fig. 4.5(a). The 1-D Fourier transform is performed on Fig. 4.5(b). The filtered Fourier spectra are shown in Fig. 4.5. The size of the Fourier spectra shown is a 336×50 array, which is much smaller than the original 2-D fringe image's size 532×500 pixels.

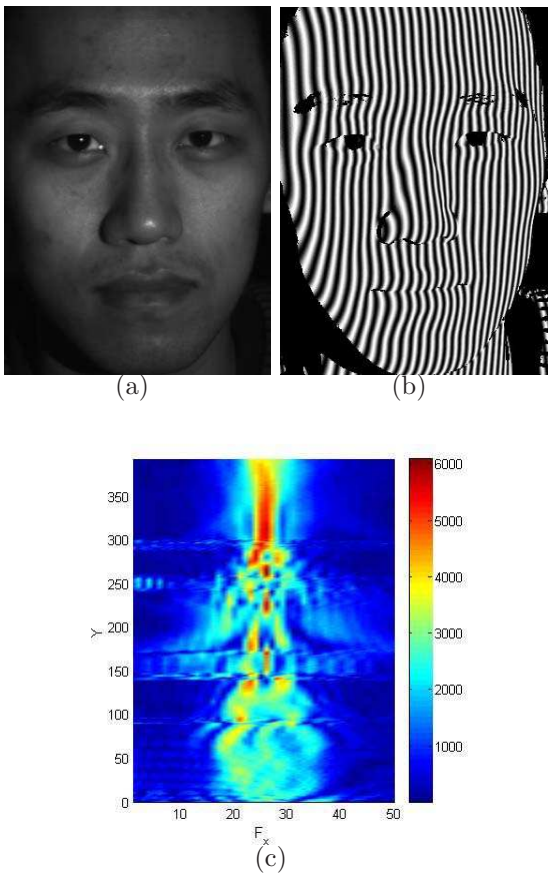

Figure 4.5: Face fringe pattern normalized.(a)Detected face area; (b)Cropped fringe pattern; (c)Filtered Fourier spectra.

4.5 Principal Component Analysis of the Fourier Spectra

Among the face recognition algorithms, principal component analysis (PCA), also known as "eigenfaces", has been extensively studied and widely used as a baseline algorithm [85, 104]. In this paper, eigenface algorithm is applied to the Fourier spectra of the normalized face fringe patterns to accomplish the recognition task. The face spectra obtained from the previous Section is saved as data files, and is sent to the algorithm as inputs. The proposed face recognition process is illustrated in Fig. 4.6.

Eigenface algorithm takes the face spectra gallery as a high-dimension vector space. Each image is represented by a vector X of length N. The training set of M face spectra form a $N \times M$ matrix Φ. The eigen vectors of the covariance matrix of Φ are called the eigenfaces. The eigenfaces are ranked according to their corresponding eigenvalues in descending order. Top eigenfaces, which are the most representative features of the gallery, are chosen to form a subspace. When an unknown face is presented, it is projected onto the eigenfaces, and a set of coordinates are generated. The distances between the coordinates of the unknown face and those of the known persons are calculated. The nearest neighbor is considered as the unknown face's identity.

There are several distance metrics available for the nearest neighbor search such as Euclidean distance, Cityblock distance, and Mahalanobis distance. The Mahalanobis distance is selected as a distance measure. Every dimension in the subspace is weighted by the corresponding eigen value. Compared with Euclidean distance, the advantage of Mahalanobis distance is that no eigenface would dominate the result, and the contribution of each eigenface is balanced and comparable.

4.6 Experiments and Simulation

4.6.1 Experiments

Fringe images used in the experiments are captured by the digital fringe projection system introduced in Section 4.3.1. The resolution of the B/W camera is 532×500 pixels. The projector projects three phase-shifted sinusoidal fringe patterns with the resolution of 1024×768 pixels. The pitch of the projected fringe pattern is 9 pixels/cycle.

In the first experiment, a face's fringe images are captured in different conditions to verify the proposed texture and illumination removal method. First, makeup (white powder) is applied onto the cheeks of the subject. One

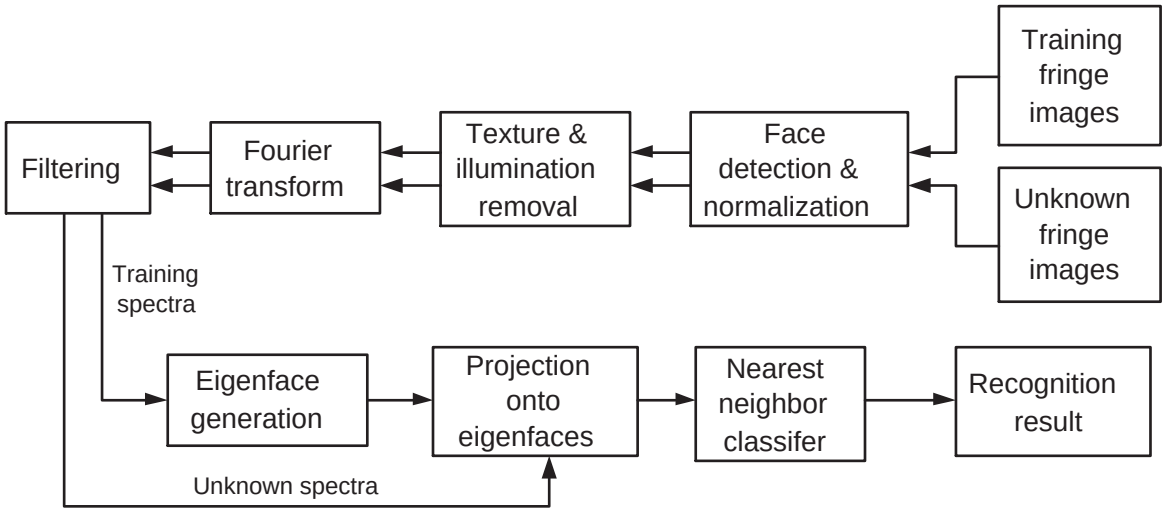

Figure 4.6: Face recognition process by use of PCA.

set of fringe images with makeup is captured. Another set of fringe images of the same face without makeup are captured for comparison. The fringe images, averaged flat images, and the texture removal results are shown in Fig. 4.7. The texture variation caused by the makeup is completely removed in Fig. 4.7(c) and Fig. 4.7(f).

Then, two sets of face fringe images are captured with different background illumination, which result in grayscale intensity variation in the flat images. Fig. 4.8(a) is one of three phase-shifted fringe images captured with normal background illumination. Fig.4.8(b) is generated by averaging three phase-shifted fringe images. Fig. 4.8(c) is the texture and illumination removal result. Fig. 4.8(d) is one of the fringe images captured with less background illumination. The average grayscale intensity of the generated flat image in Fig. 4.8(e) is 78.8% of that of Fig. 4.8(b). The grayscale variation in the flat images is eliminated in the texture and illumination removal results from the above two sets of fringe images.

The second experiment is to evaluate the recognition performance of the proposed method. 165 sets of phase-shifted face fringe patterns were taken from 44 subjects. Subjects were asked to sit at a fixed distance to the fringe projection system. Expressions were avoided during the image capture. At least three sets of fringe patterns for each subject were captured. Face spectrum images are generated from the normalized fringe patterns. Sample face fringe patterns and spectrum images are shown in Fig. 4.9. From the total 165 face spectrum images, 132 are used to form a training set, 3 spectrum

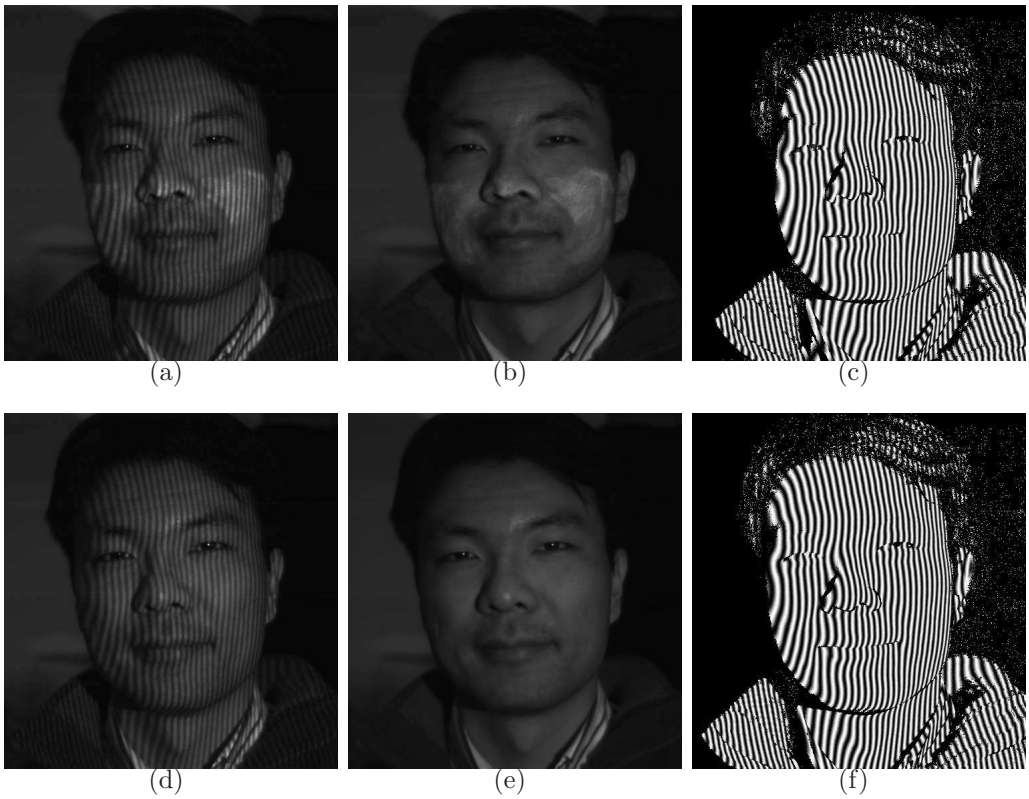

Figure 4.7: Illumination and texture removal result of a face with makeup.

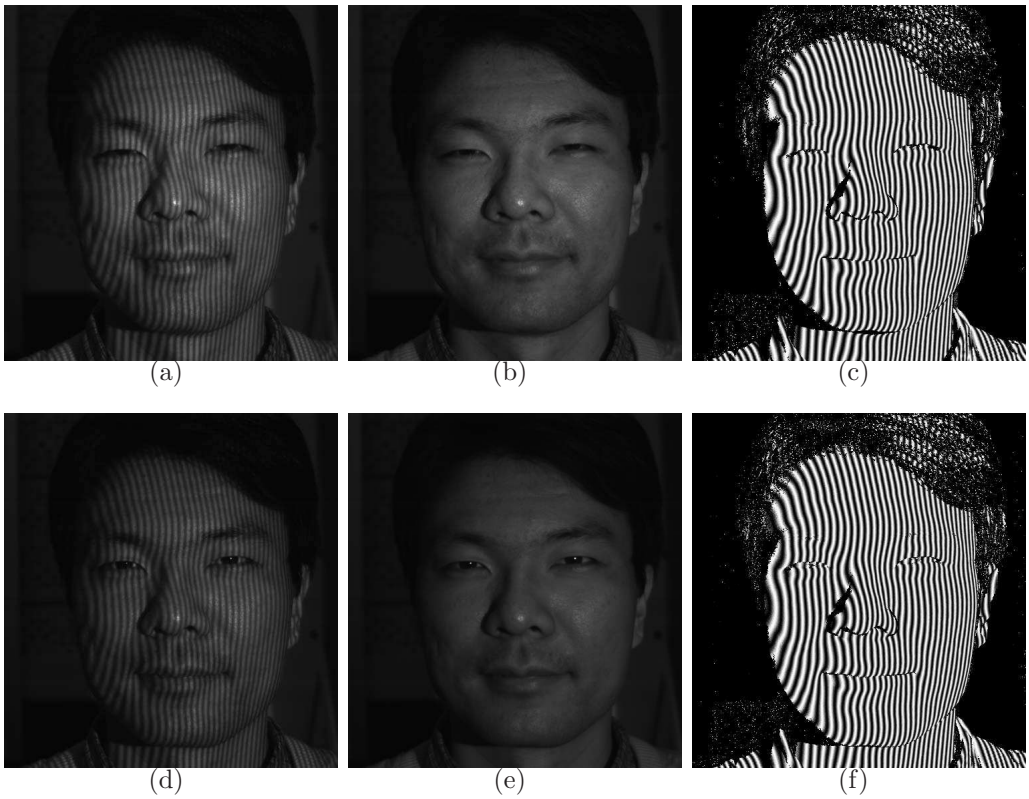

Figure 4.8: Illumination and texture removal result of a face with different background illumination.

images for each person. Top 25 eigenvectors are employed in the eigenface algorithm. The other 33 face spectrum images are used to test the algorithm. The recognition rate is 90.91%. The experimental results indicate that the time for generating a spectrum images is approximately 60% of the time for generating a 3-D face point cloud. The size of the spectrum image is only 10% of the size of the 3-D face point cloud generated from the same fringe patterns.

Flat grayscale images of the subjects are also generated by averaging three fringe patterns. The same PCA algorithm is applied to the corresponding flat grayscale images, and the recognition rate is 87.87%.

The spectrum representation of flat grayscale face image has been shown to be able to effectively reduce data size [105]. The Fourier spectra of the flat grayscale images can be obtained by applying 2D Fourier transform and extract the low frequency band. The same PCa algorithm is applied to the Fourier spectra of the flat grayscale images, and the recognition rate is 93.94%. These preliminary experimental results demonstrated that the proposed method can achieve satisfactory face recognition rate compared with the methods using grayscale images. There is no illumination or skin texture variation in the grayscale images, in that the images of the same subject were captured by our fringe projection system in one session under similar illumination conditions.

4.6.2 Simulation on FRGC2.0 database

The fringe projection process can be simulated by virtual fringe projection on computer, if 3-D face models are available. By use of simulation, we can utilize existing 3D face databases to evaluate the proposed method. Most 3D face databases have corresponding 2D grayscale face images with illumination or certain degree of skin texture variation, in that face images are captured over multiple sessions. The face database of Face Recognition Grand Challenge 2.0 (FRGC2.0) is employed in our simulation [42]. FRGC2.0 provides the 3-D point clouds along with corresponding 2-D intensity images for each person. The 2-D face images in FRGC2.0 are taken with different indoor illumination conditions. The resolution of both 2-D and 3-D face images are 640×480 pixels. Samples of 2-D and 3-D faces are shown in Fig. 4.10(a) and Fig. 4.10(b).

In the simulation program, phase-shifted sinusoidal fringe patterns are virtually projected onto the 3-D face surface to simulate the digital fringe projection system. The virtual projection is enabled by the projective texture technique [106]. The 3-D face mesh generation and virtual fringe projection are implemented using Open Graphic Library (OpenGL) [106]. A sample 3-D face with virtually projected sinusoidal fringe pattern is shown in Fig. 4.10(c). There is no texture variation on the 3-D faces in the database. However, that will not affect the effectiveness of the simulation, since the texture and illu-

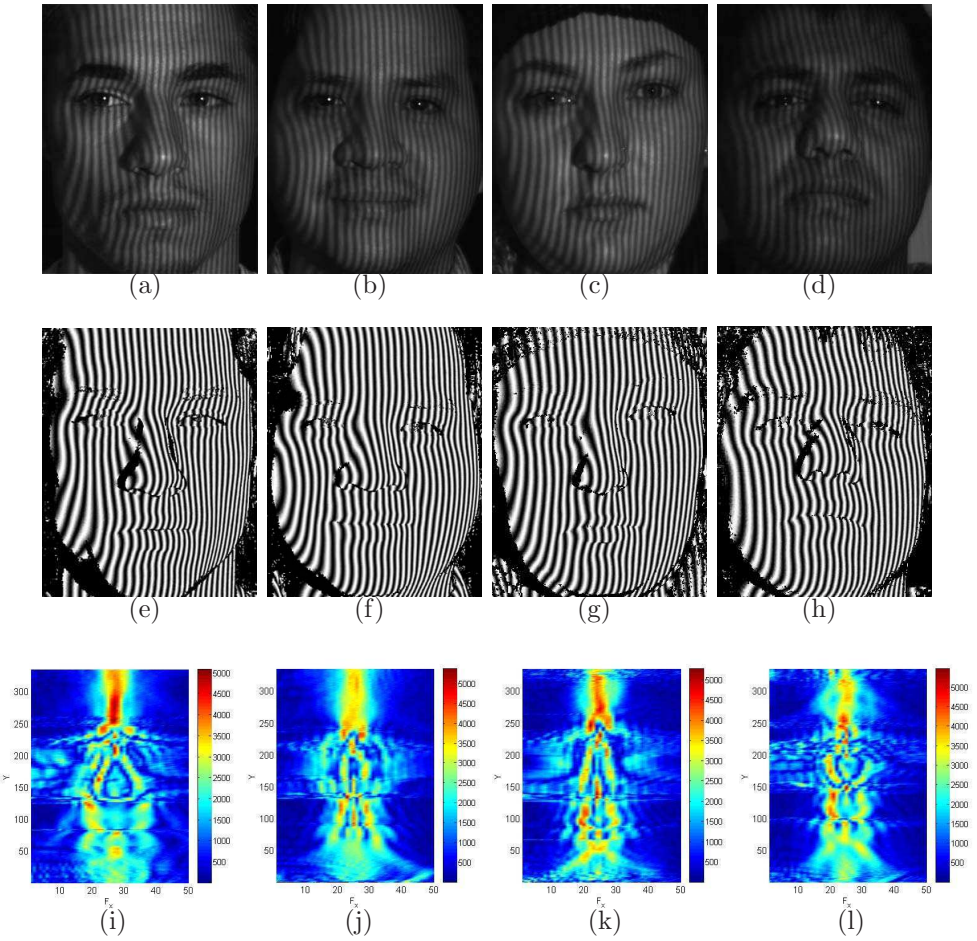

Figure 4.9: Sample face fringe patterns and spetra.

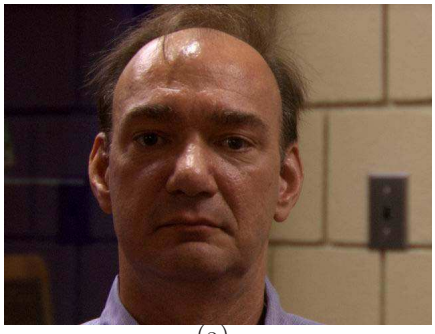

(a)

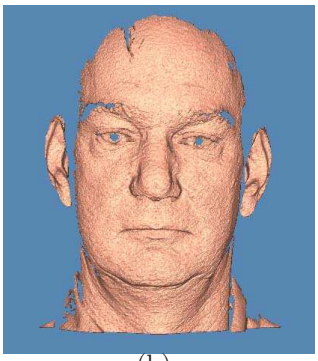

(b)

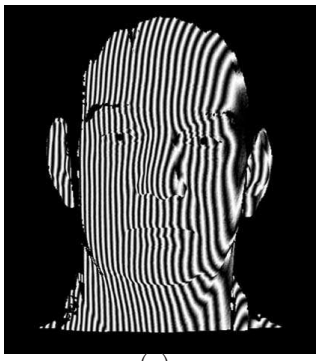

(c)

Figure 4.10: FRGC2.0 face database. (a) 2-D image; (b) 3-D image; (c) 3-D image with virtually projected fringe pattern.

mination removal result has been successfully verified by the experiment in Section 4.6.1.

There are 228 3-D faces of 39 subjects are employed in the the simulation. Face images with exaggerated expressions are excluded. Pose normalization of the 3-D faces is necessary to remove the influence of out-of-plane rotation. The face area and eye and mouth positions are detected in the 2-D intensity images. The corresponding 3-D points are found and used to normalize the pose and scale. Fig. 4.11 shows some samples of the fringe images in the gallery.

The face area is also detected in the 2-D face image and the 3-D points outside of the face area is discarded. Then the phase-shifted fringe patterns are projected onto the normalized 3-D face. The deformed fringe patterns are recorded. Fourier spectra are obtained by applying the proposed method. The 2-D intensity images are also based on the detected features. The scale variation and in-plane-rotation are eliminated by measuring the pixels between eye centers and aligning the line connecting eye centers to the horizontal direction. Histogram equalization is applied to perform illumination normalization.

The proposed method's face recognition performance is compared with the eigenface algorithm using 2-D intensity images. 4 face spectra of each person are used for training. 72 unknown face spectra are used for testing. The same amount of corresponding 2-D intensity images are employed for training and testing. Fig. 4.13 shows that the proposed method achieved a better performance than the eigenface algorithm using 2-D intensity images, when varied number of top eigenfaces are adopted. The result also shows that performances of both methods increase until 30 top eigenfaces are used (approximately 20% of total eigenfaces), which is consistent with the performance analysis in Ref. [104]. When the number of training spectra and 2-D images are varied, the recognition results are shown in Table. 4.1. In both simulation results, the proposed method demonstrated improved recognition performance compared to the eigenface algorithm using 2-D intensity images.

4.7 Summary

We proposed a novel 3-D face recognition method based on the digital fringe projection technique. A high-speed digital fringe projection system projects phase-shifted sinusoidal fringe patterns and captures the deformed fringe patterns of a human face. Two fringe analysis methods are employed. The phase shifting method is used to eliminate the background illumination and facial skin texture variations. The Fourier transform method is applied to generate a Fourier spectra, which represents the 3-D shape of the face. The eigenface

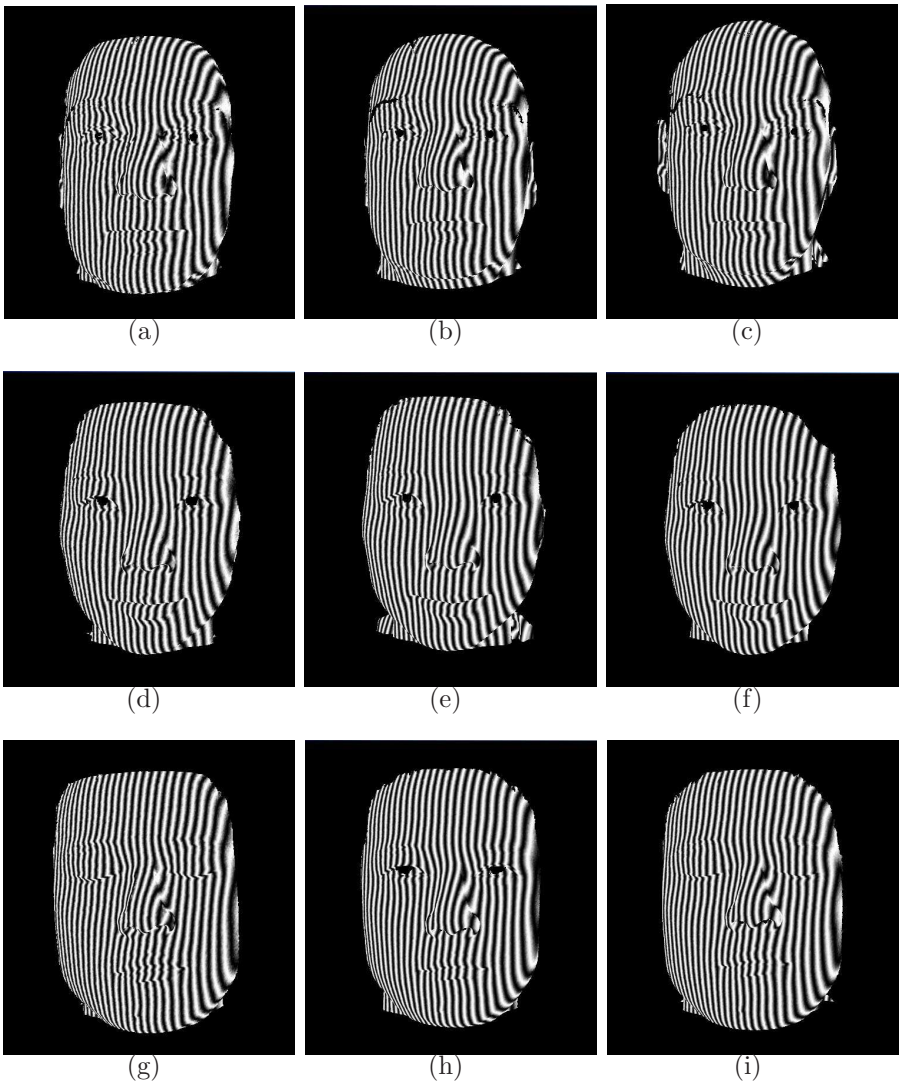

Figure 4.11: Normalized 3-D faces with fringe virtually projected fringe pattern.

Figure 4.12: Normalized 2-D intensity images from FRGC2.0 database.

Table 4.1: Recognition results with different number of training spectra or images.

Input	Training set	Train/person	Eigenfaces	Tests	Recog. rate
Spectra	78	2	16	72	80.6%
	117	3	23	72	84.7%
	156	4	30	72	91.7%
2-D Images	78	2	16	72	73.6%
	117	3	23	72	76.4%
	156	4	30	72	86.1%

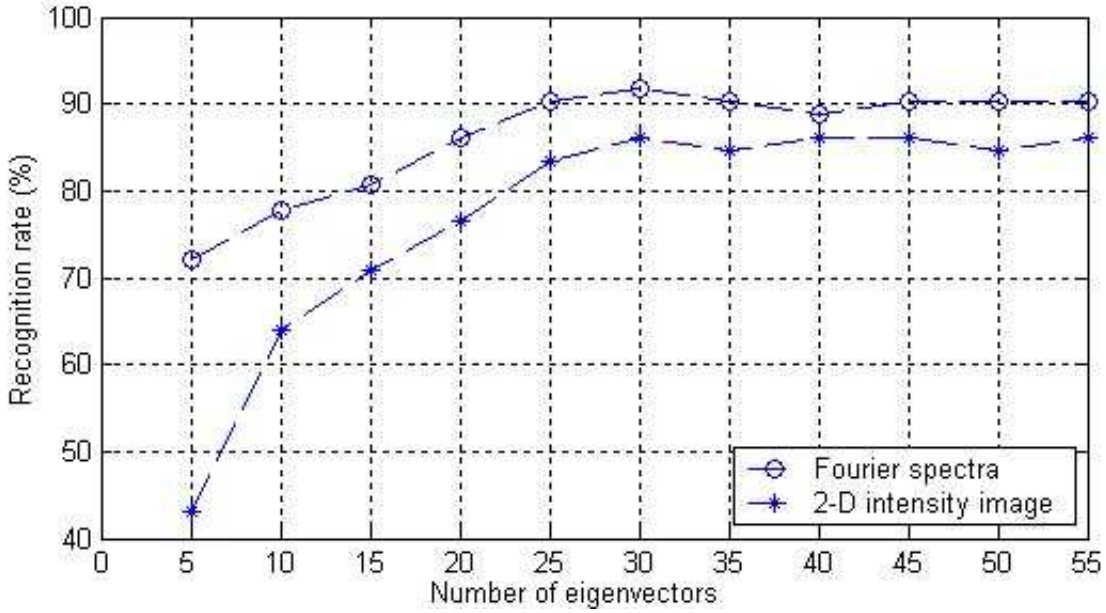

Figure 4.13: Face recognition results with different number of top eigenfaces.

algorithm takes the face spectra as inputs and performs face recognition. The proposed method obtained a spectral representation of the 3-D face without reconstructing the 3-D face geometry. The experimental and simulation results demonstrated satisfactory recognition results and the advantage of reduced storage space and computation load compared to 3-D point clouds.

Chapter 5

Conclusions and Future Work

This chapter concludes this dissertation by summarizing the contributions of this research and discuss possible extensions of this research work in the future.

5.1 Conclusions

This research work developed two 3-D shape measurement techniques and a face recognition method. Fringe analysis methods, Fourier transform method and phase shifting method, played a central role in this research work. The main contributions are summarized as follows:

1. **Developed a modified Fourier method for 3-D shape measurement of dynamic objects**

   A modified Fourier transform method (MFTM) for 3-D shape measurement is developed. The conventional Fourier transform method is improved by acquiring an additional flat image. Based on this idea, two fringe projection schemes are proposed. One scheme directly project a uniform grayscale pattern in addition to the fringe pattern. The other scheme projects three phase-shifted fringe patterns. While both schemes alleviate the spectra overlapping by subtracting a flat image from the fringe image, the former scheme is more suitable for measuring fast moving or changing objects and the latter scheme handles objects with complex shapes better. Spectral leakage reduction is achieved by first extending and then windowing the data before FFT. A binary mask is generated based on the grayscale distribution of the flat image to mask out background and thus to reduce the computation time. A path-following phase unwrapping algorithm is developed by using the fringe visibility as an quality index. Absolute phase retrieval techniques are developed for both fringe projection schemes.

Preliminary experimental result of a free-form workpiece shows that the MFTM has improved performance on measuring objects with complex shapes. A moving cylinder and a face sequence with the subject speaking are captured to demonstrate the MFTM's ability to measure moving or changing object. The MFTM achieved real-time image acquisition, processing, and 3-D display on a high-speed digital fringe projection system. The proposed method has potential applications such as 3-D lip tracking, facial expression capture and online 3-D inspection.

2. **Developed a phase shifting technique for shadow moiré**

   A phase shifting shadow moiré technique by use of the Carré algorithm is developed. The phase shifting is achieved by translating the grating in vertical direction in equal steps to obtain four phase-shifted fringe patterns. The phase shifts in the field of view of the camera are not uniform, while the phase shifts between neighboring grating movements for each pixel are uniform. Carré algorithm is applied to solve the phase map. The grating pattern removal and phase shift step selection are also discussed. The proposed method provides an exact close-form solution for surface height for the first time. The simulation and experimental results verified the principle and demonstrated a satisfactory measurement results.

3. **Developed a face recognition method based on fringe pattern analysis**

   A novel 3-D face recognition method based on the digital fringe projection and analysis is developed. A high-speed digital fringe projection system projects three phase-shifted sinusoidal fringe patterns onto a human face and captures the deformed fringe patterns. Two fringe analysis methods, namely the Fourier transform and phase shifting method, are employed. The phase shifting method is used to eliminate the background illumination and facial skin texture variations. The Fourier transform method is applied to generate a spectrum, which represents the 3-D shape of the face. The eigenface algorithm takes the face spectra as inputs and performs face recognition. The proposed method obtained a spectral representation of the 3-D face without reconstructing the 3-D face geometry. The experimental and simulation results demonstrated satisfactory recognition results compared to 2-D intensity image based technique, and the advantage of reduced storage space and computation load compared to 3-D point clouds.

5.2 Future Work

Further research of this dissertation research is recommended to include:

1. **Automatic filtering the Fourier spectrum** For the MFTM, the extraction of the 3-D shape related terms in the spatial frequency domain is achieved by a band-pass filter. For objects with simple shape, the width and position of the band-pass filter need not to be varied, in that the 3-D shape related terms are well concentrated around the carrier frequency. However, when complex shapes are measured, the carrier frequency will be shifted towards or away from zero frequency. Right now the width and position of the band-pass filter needs to be adjusted based on the overall shape of the spectrum of the object. The filtering affects the phase quality. In the future, an automatic filter adjustment needs be developed in order to achieve better measurement results for different objects without frequently adjusting the filter.

2. **Multiple marker detection and removal for absolute phase retrieval**

   The 3-D reconstruction in the MFTM is based on the retrieval of the absolute phase map, which is built by detecting a embedded marker in the fringe pattern. The robustness of the marker detection can be further improved by employing multiple markers. When a single marker is used, it has to be projected on a relatively flat area to insure the accuracy of marker center detection. If no flat areas are available, the accuracy of the absolute phase map is degraded. Multiple markers provide a possible means to solve the problem. When multiple markers are projected, the chance one of them being projected on a relatively flat area is greatly enhanced. The epipolar geometry can be utilized to help detect the markers. The potential difficulty is that how to determine which marker detection result can be adopted. A strategy needs to be developed to evaluate the marker detection results.

3. **Application of the phase shifting shadow moiré method to 3-D shape measurement by using a SEM**

   Scanning electron microscope (SEM) is a widely used nanometer level 2-D image acquisition tool. The shadow moiré technique can be employed in the SEM setup. Shadow moiré pattern has been successfully observed by placing a grating on top of a small steel ball. Fig. 5.1 shows the moire pattern captured by the back scattered electron (BSE) detector and secondary electron (SE) detector respectively. Introducing phase shifts in a

SEM setup is difficult. Therefore, the complicated approximate uniform phase shifting schemes are not applicable. Our proposed phase shifting method is simple and easy to implement in a SEM shadow moire setup. The standard SEM stage can serve as a phase shifter. In the future, special grating made needs to be manufactured in order to implement the proposed phase shifting shadow moiré method using a SEM.

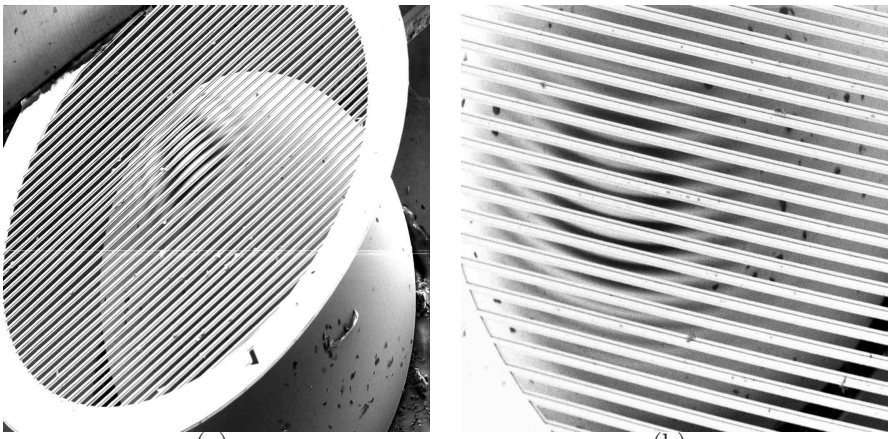

(a) (b)

Figure 5.1: Shadow moiré patterns produced by the SEM.(a) SE detector image; (b) BSE detector image.

4. **Real-time face recognition based on the digital fringe projection system**

   Real-time face image acquisition, processing, and recognition has great application potential. A high-speed fringe projection system is utilized in Chapter 4. The phase-shifted face fringe images are captured at a frame rate of 30 sets/second. In order to achieve real-time face recognition, the face spectra need be obtained in real-time, and a spectral face database has to be built and efficiently managed. Also, the eigenface algorithm needs to be implemented to connect with the face acquisition system and the database.The fringe projection system employed in this research is able to reconstruct 3-D face geometry in real-time. Fringe patterns can be virtually project onto the 3-D face. Due to the pose normalization requirement, the whole frontal face should be captured. Currently more than one shot are needed to obtain a whole frontal face. However, the symmetry of human face can be utilized. The lost part of the face due to occlusion or shadow can be inferred from the available part of the 3-D

face. In this way, the influence of pose variation can be eliminated. The proposed method can build or extend the spectral face database based on existing 3-D database, by using virtual fringe projection technique.

Bibliography

[1] D. K. MacKinnon, V. Aitken, and F. Blais. A comparison of precision and accuracy in triangulation laser range. Proc. IEEE Canadian Conference on Electrical & Computer Engineering, pages 832–837, 2006.

[2] Z. Ji and M. C. Leu. Design of optical triangulation devices. *Opt. Laser Technology*, 21(5):335–338, 1989.

[3] F. Blais. Review of 20 years of range sensor development. *J. Electron. Imaging*, 13(1):231–240, 2004.

[4] John S. Massa, Gerald S. Buller, Andrew C. Walker, Sergio Cova, Manikam Umasuthan, and Andrew M. Wallace. Time of flight optical ranging system based on time-correlated single-photo counting. *Appl. Opt.*, 37(31):7298–7304, 1998.

[5] F. Chen, G. M. Brown, and M Song. Overview of three-dimensional shape measurement using optical method. *Opt. Eng.*, 39(1):10–22, 2000.

[6] D. A. Forsyth and J. Ponce. *Computer vision: a modern approach.* Prentice-Hall, Upper Saddle River, New Jersey, 2002.

[7] R. Hartley and A. Zisserman. *Multiple view geometry in computer vision.* Cambridge University Press, 2000.

[8] Thomas Luhmann, Stuart Robson, Stephen Kyle, and Ian Harleyr). *Close Range Photogrammetry: Principles, Techniques and Applications.* Whittles Publishing, 2006.

[9] Ronald D. Rogus, Robin L. Stern, and Hideo D. Kubo. Accuracy of a photogrammetry-based patient positioning and monitoring system for radiation therapy. *Med. Phys.*, 26(5):721–728, 1999.

[10] J. J. Aguilar, F. Torres, and M. A. Lope. Stereo vision for 3D measurement: accuracy analysis, calibration and industrial applications. *Measurement*, 18(4):193–200, 1996.

[11] S. Malassiotis and M. G. Strintzis. Stereo vision system for precision dimensional inspection of 3D holes. *Machine Vision and Applications*, 15(2):101–113, 2003.

[12] Joaquim Salvi, Jordi Pages, and Joan Batlle. Pattern codification strategies in structured light systems. *Pattern Recognition*, 37(4):827–849, 2004.

[13] Joan Batlle, El Mustapha Mouaddib, and Joaquim Salvi. Recent progress in coded structured light as a technique to solve the correspondence problem: A survey. *Pattern Recognition*, 31(7):963–982, 1998.

[14] Batlle J. Salvi, J. and E. Mouaddib. A robust-coded pattern projection for dynamic 3d scene measurement. *Pattern Recognition Letters*, 19: 1055–1065, 1998.

[15] Z. J. Geng. Rainbow 3-d camera: New concept of high-speed three vision system. *Opt. Eng.*, 35:376–383, 1996.

[16] J. L. Posdamer and M. D. Altschuler. Surface measurement by space-encoded projected beam systems. *Computer Graphics and Image Processing*, 18(1):1–17, 1982.

[17] S. Inokuchi, K. Sato, and F. Matsuda. Range imaging system for 3-d ojbect recognition. *IEEE Proc. of the International Conference on Pattern Recognition*, pages 806–808, 1984.

[18] E. Horn and N. Kiryati. Toward optimal structured light patterns. *Image and Vision Computing*, 17(2):87–89, 1999.

[19] Kiryati N. Caspi, D. and J. Shamir. Range imaging with adaptive color structured light. *IEEE Trans. on Pattern Analysis and Machine Intelligence*, 20(5):470–480, May 1998.

[20] B. Carrihill and R. Hummel. Experiments with the intensity ratio depth sensor. *Computer Vision, Graphics and Image Processing*, 32:337–358, 1985.

[21] Gilia Chazan and Nahum Kiryati. Pyramidal intensity-ratio depth sensor. Technical Report No. 121, Israel Institute of Technology, Technion, Haifa, Israel, Oct. 1995.

[22] Jianhui Pan, Peisen Huang, Song Zhang, and Fu-Pen Chiang. Color n-ary gray code for 3-d shape measurement. In *Proc. 12th Int'l Conference on Experimental Mechanics*, 2004.

[23] K Creath. Phase-shifting interferometry techniques. *Pogress in Optics XXVI*, 26:357–373, 1988.

[24] K. A. Haines and B. P. Hildebrand. Contour generation by wavefront construction. *Phys. Lett.*, 19:10–11, 1965.

[25] K. J. Gåsvik, editor. *Optical Metrology.* John Wiley & Sons, third edition, 2002.

[26] D. Malacara, editor. *Optical Shop Testing.* John Wiley & Sons, second edition, 1992.

[27] Joanna Schmit and Artur Olszak. High-precision shape measurement by white-light interferometry with real-time scanner error correction. *Appl. Opt.*, 41(28):5943–5950, 2002.

[28] J. C. Wyant. Interferometric optical metrology: basic system and principles. *Laser Focus*, page 65:1, 1982.

[29] D. M. Meadows, W. O. Johnson, and J. B. Allen. Generation of surface contours by moiré patterns. *Appl. Opt.*, 9:942–947, 1970.

[30] H. Takasaki. Moiré topography. *Appl. Opt.*, 9(6):1467–1472, 1970.

[31] F. P. Chiang. Moiré methods of strain analysis. In A. S. Kobayashi, editor, *Manual on Experimental Stress Analysis*, pages 51–69, Brookfield Center, CT, 1983. Soc. for Exp. Stress Anal.

[32] G. Mauvoisin, F. Bremand, and A Lagarde. Three-dimensional shape reconstruction by phase-shifting shadow moiré. *Appl. Opt.*, 33(11):2163–2169, 1994.

[33] T. Yoshizawa and T. Tomisawa. Shadow moiré topography by means of the phase-shift method. *Opt. Eng.*, 32(7):1668–1674, 1993.

[34] M. Halioua, R. S. Krishnamurthy, H. Liu, and F. P. Chiang. Projection moiré with moving gratings for automated 3-d topography. *Appl. Opt.*, 22(6):850–855, 1983.

[35] Y. Choi and S. Kim. Phase-shifting grating projection moiré topography. *Opt. Eng.*, 37(3):1005–1010, 1998.

[36] J. A. N. Buytaert and J. J. J. Dirckx. Moiré profilometry using liquid crystals for projection and demodulation. *Optics Express*, 16(1):179–193, 2008.

[37] P. S. Huang, C. Zhang, and F. P. Chiang. High-speed 3-d shape measurement based on digital fringe projection. *Opt. Eng.*, 42(1):163–168, 2003.

[38] D. Doherty and G. Hewlett. Pulse width modulation control in dlp projectors. *Texas Instruments Technical Journal*, 15:115121, 1998.

[39] D. Malacara, editor. *Optical Shop Testing.* John Wiley and Songs, NY, 1992.

[40] M. Takeda, H. Ina, and S. Kobayashi. Fourier-transform method of fringe-pattern analysis for computer-based topography and interferometry. *J. Opt. Soc. Am.*, 72:156–160, 1981.

[41] W. Y. Zhao, R. Chellappa, A. Rosenfeld, and P.J. Phillips. Face recognition: A literature survey. *ACM Computing Surveys*, 35(4):399–458, 2003.

[42] P. J. Phillips, Todd Scruggs, Kevin W. Bowyer, Jin Chang, Kevin Hoffman, Joe Marques, Jaesik Min, and William Worek. Overview of the face recognition grand challenge. volume 1 of *IEEE Computer Society Conference on Computer Vision and Pattern Recognition(CVPR05)*, pages 947–954, 2005.

[43] Andrea F. Abate, Michele Nappi, Daniel Riccio, and Gabriele Sabatino. 2d and 3d face recognition: A survey. *Pattern Recognition Letters*, 28 (14):1885–1906, 2007.

[44] X. Su and W. Chen. Fourier transform profilometry: a review. *Optics and Lasers in Engineering*, 35:263–284, 2001.

[45] M. Takeda and K. Mutoh. Fourier transform profilometry for the automatic measurement of 3-d object shapes. *Applied Optics*, 22(24):3977–3982, 1983.

[46] M. Takeda, M. Kinoshita Q. Gu, H. Takai, and Y. Takahashi. Frequency-multiplex Fourier-transform profilometry: a single-shot three-dimensional shape measurement of objects with large height discontinuities and/or surface isolations. *Applied Optics*, 36(22):5347–5354, 1997.

[47] F. J. Harris. On the use of windows for harmonic analysis with the discrete Fourier transform. volume 66 of *Proc. IEEE*, pages 51–83, 1978.

[48] W. Chen, X. Su, Y. Cao, and L. Xian. Improving fourier transform profilometry based on bicolor fringe pattern. *Opt. Eng.*, 43(1):192–198, 2004.

[49] H. Yue, X. Su, and Y. Liu. Fourier transform profilometry based on composite structured light pattern. *Optics and Laser Technology*, 39: 1170–1175, 2007.

[50] K. Qian. Two-dimensional windowed fourier transform for fringe pattern analysis: principles, applications and implementations. *Optics and Lasers in Engineering*, 45:304–317, 2007.

[51] Dennis C. Ghiglia and Mark D. Pritt. *Two-Dimensional Phase Unwrapping: Theory, Algorithms, and Software*. John Wiley and Sons, Inc, 1998.

[52] R. M. Goldstein, H. A. Zebker, and C. L. Werner. Satellite radar interferometry: two-dimensional phase unwrapping. *Radio Sci.*, 23:713–720, 1988.

[53] J. M. Huntley. Noise-immune phase unwrapping algorithm. *Appl. Opt.*, 28:3268–3270, 1989.

[54] T. J. Flynn. Consistent 2-d phase unwrapping guided by a quality map. Proc. IGARSS'96, pages 2057–2059, Lincoln, NE, 1996.

[55] D. J. Bone. Fourier fringe analysis: the two-dimensional phase unwrapping problem. *Appl. Opt.*, 30:3627–3632, 1991.

[56] Y. Xu and C. Ai. Simple and effective phase unwrapping technique. volume 2003 of *Proc. SPIE*, pages 254–263, 1993.

[57] A. Asundi and Z. Wensen. Fast phase-unwrapping algorithm based on a gray-scale mask and flood fill. *Appl. Opt.*, 37:5416–5420, 1998.

[58] T. J. Flynn. Two-dimensional phase unwrapping with minimum weighted discontinuity. *J. Opt. Soc. Am.*, 14:2692–2701, 1997.

[59] D. C. Ghiglia and L. A. Romero. Minimum l^p-norm two-dimensional phase unwrapping. *J. Opt. Soc. Am. A*, 13:1999–2013, 1996.

[60] J.-J. Chyou, S.-J. Chen, and Y.-K. Chen. Two-dimensional phase unwrapping with a multichannel least-mean-square algorithm. *Appl. Opt.*, 43:5655–5661, 2004.

[61] J. M. Huntley and H. O. Saldner. Temporal phase-unwrapping algorithm for automated interferogram analysis. *Appl. Opt.*, 32:3047–3052, 1993.

[62] David R. Burton and Michael J. Lalor. Multichannel fourier fringe analysis as an aid to automatic phase unwrapping. *Appl. Opt.*, 33(14):2939–2948, 1994.

[63] E. Zappa and G. Busca. Comparison of eight unwrapping algorithms applied to fourier-transform profilometry. *Optics and Lasers in Engineering*, 46:106–116, 2007.

[64] Q. Hu and K. G. Harding. Conversion from phase map to coordinate: Comparison among spatial carrier, fourier transform, and phase shifting methods. *Optics and Lasers in Engineering*, 45:342–348, 2007.

[65] James Cubillo Fiona Berrymana, Paul Pynsent. The effect of windowing in Fourier transform profilometry applied to noisy images. *Optics and Lasers in Engineering*, 41:815825, 2004.

[66] D. J. Bone, H.-A. Bachor, and R. J. Sandeman. Fringe-pattern analysis using a 2-d Fourier transform. *Applied Optics*, 25(10):1653–1660, 1986.

[67] X. Han. *On Improving the Accuracy of a Real-time 3-D Shape Measurement System*. Stony Brook University, Stony Brook, 2006.

[68] Kjell J. Gåsvik. *Optical Metrology*. John Wiley and Sons, Inc, 3rd edition, 2002.

[69] P. S. Huang and X. Han. On improving the accuracy of structured light systems. In P. S. Huang, editor, *Two- and Three-Dimensional Methods for Inspection and Metrology IV*, volume 6382 of *Proc. SPIE*, 2006.

[70] S. Zhang and P. S. Huang. Novel method for structured light system calibration. *Opt. Eng.*, 45(8):083601–1–8, 2006.

[71] M. Frigo and S.G. Johnson. The design and implementation of FFTW 3. *Proceedings of the IEEE*, 93(2):216–231, 2005.

[72] Daniel Malacara, editor. *Optical Shop Testing*. John Wiley and Songs, NY, 1992.

[73] Johannes Schwider, Oliver R. Falkenstoerfer, Horst Schreiber, Andreas Zoeller, and Norbert Streibl. New compensating four-phase algorithm for phase-shift interferometry. *Opt. Eng.*, 32(8):1883–1885, 1993.

[74] P. Hariharan, B. F. Oreb, and T. Eiju. Digital phase-shifting interferometry: a simple error-compensating phase calculation algorithm. *Appl. Opt.*, 26:25042506, 1987.

[75] J. Schwider, R. Burow, K.-E. Elssner, J. Grzanna, R. Spolaczyk, and K. Merkel. Digital wave-front measuring interferometry: some systematic error sources. *Opt. Eng.*, 22:3421 3432, 1983.

[76] P. Carré. Installation et utilisation du comparateur photoelectrique et interferentiel du bureau international des poids de mesures. *Metrologia*, 2:13, 1966.

[77] J. J. J. Dirckx, W. F. Decraemer, and G. Dielis. Phase shift method based on object translation for full field automatic 3-d surface reconstruction from moiré topograms. *Appl. Opt.*, 26(7):1164–1169, 1988.

[78] X. Xie, J. T. Atkinson, M. J. Lalor, and D. R. Burton. Three-map absolute moiré contouring. *Appl. Opt.*, 35(35):6990–6995, 1996.

[79] L. Jin, Y. Kodera, T. Yoshizawa, and Y. Otani. Shadow moiré profilometry using the phase-shifting method. *Opt. Eng.*, 39(8):2119–2123, 2000.

[80] J. Degrieck, W. V. Paepegem, and P. Boone. Application of digital phase-shift shadow moiré to micro deformation measurements of curved surfaces. *Optics and Lasers in Engineering*, 36:29–40, 2001.

[81] J. B. Allen and D. M. Meadows. Removal of unwanted patterns from moiré contour maps by grid translation techniques. *Appl. Opt.*, 10:210–212, 1971.

[82] Q. Kemao, S. Fangjun, and W. Xiaoping. Determination of the best phase step of the Carré algorithm in phase shifting interferometry. *Measurement Science and Technology*, 11(8):1220–3, 2000.

[83] J. van Wingerden, H.J. Frankena, and C. Smorenburg. Linear approximation for measurement errors in phase shifting interferometry. *Applied Optics*, 30(19):2718–2729, 1991.

[84] K. Creath. Phase-measurement interferometry techniques. *Progress in optics*, 26:349–393, 1988.

[85] M. Turk and A. Pentland. Eigenfaces for recognition. *J. Cognitive Neuroscience*, 3(1):71–86, 1991.

[86] V. I. Belhumeur, J. P. Hespanha, and D. J. Kriegman. Eigenfaces vs.fisherfaces: recognition using class specific linear projection. *IEEE-Trans. Patt. Anal. Mach. Intell.*, 19(7):711–720, 1997.

[87] D. L. SWETS and J. WENG. Using discriminant eigenfeatures for image retrieval. *IEEE Trans. Patt. Anal. Mach. Intell.*, 18(8):831–836, 1996.

[88] Kyong I. Chang, Kevin W. Bowyer, and Patrick J. Flynn. Using discriminant eigenfeatures for image retrieval. *IEEE Trans. Patt. Anal. Mach. Intell.*, 27(4):619–624, 2005.

[89] Kevin W. Bowyer, Kyong Chang, and Patrick Flynn. A survey of approaches and challenges in 3D and multi-modal 3D + 2D face recognition. *Computer Vision and Image Understanding*, 101(1):1–15, 2006.

[90] Xiaoguang Lu, Dirk Colbry, and Anil K. Jain. Three-dimensional model based face recognition. Proc. International Conference on Pattern Recognition, pages 362–366, 2004.

[91] S. Malassiotis and M.G. Strintzis. Pose and illumination compensation for 3d face recognition. volume 1 of *International Conference on Image Processing*, pages 91–94, 2004.

[92] Bernard Achermann, Xiaoyi Jiang, and Horst Bunke. Face recognition using range images. Proc. International Conference on Virtual Systems and MultiMedia, page 129, 1997.

[93] Hong Guo and Peisen S. Huang. Absolute phase technique for the fourier transform method. *Optical Engineering*, 48(4):043609, 2009.

[94] A.C. Zimmermann, A.A. Gonçalves Jr, and J.M. Barreto. A 3D Object Extraction and Recognition Method. In *IEEE-Sixth International Conference on Control, Automation, Robotics and Vision-ICARV*. Citeseer, 2000.

[95] Yang Wang, Mohit Gupta, Song Zhang, Sen Wang, Xianfeng Gu, Dimitris Samaras, and Peisen Huang. High resolution tracking of non-rigid motion of densely sampled 3D data using harmonic maps. *Int. J. Comput. Vis.*, 76:283300, 2009.

[96] Xiaoguang Lu, Dirk Colbry, and Anil K. Jain. Three-dimensional model based face recognition. *Pattern Recognition, International Conference on*, 1:362–366, 2004. ISSN 1051-4651.

[97] P. Flynn K. Chang, K. Bowyer. Face recognition using 2D and 3D facial data. Multimodal User Authentication Workshop, page 2532, December 2003.

[98] Chris Boehnen and Patrick Flynn. Accuracy of 3d scanning technologies in a face scanning scenario. In *3DIM '05: Proceedings of the Fifth International Conference on 3-D Digital Imaging and Modeling*, pages 310–317, Washington, DC, USA, 2005. IEEE Computer Society. ISBN 0-7695-2327-7.

[99] C. Beumier and M. Acheroy. Automatic 3D face authentication. *Image and Vision Computing*, 18(4):315–321, 2000.

[100] Chiraz BenAbdelkadera and Paul A. Griffin. Comparing and combining depth and texture cues for face recognition. *Image and Vision Computing*, 23:339–352, 2005.

[101] R. A. Andrade, B. S. Gilbert, D. W. Dawson, C. Hart, S. P. Kozaitis, and J. H. Blatt. Real-time optically processed face recognition system based on arbitrary moiré contours. *Optical Engineering*, 35(9):2534–2540, 1996.

[102] J. J. Esteve-Taboada, D. Mas, and J. García. Three-dimensional object recognition by fourier transform profilometry. *Applied Optics*, 38(22): 4760–4765, 1999.

[103] P. Viola and M. Jones. Robust real-time object detection. *Intl. J. Computer Vision*, 57(2):137–154, 2002.

[104] Hyeonjoon Moon and P. J. Phillips. Computational and performance aspects of pca-based face-recognition algorithms. *Perception*, 30:303–321, 2001.

[105] H. Abdi F. Yang and A. Monopoli. Development of a fast panoramic mosaicking and recognition system. *Opt. Eng.*, 44(8):087005–1–10, 2005.

[106] Cass Everitt. Projective texture mapping, 2001. http://www.nvidia.com/developer.